Selective Hydrogenation of Phenylacetylene on Bimetallic Cu-Pd and Cu-Pt Catalysts

A Thesis

Submitted by

George Cladaras

In partial fulfillment of the requirements

for the degree of

Master of Science

in

Chemical Engineering

TUFTS UNIVERSITY

August 2013

Advisor: Professor Maria Flytzani-Stephanopoulos

Abstract:

The development of selective catalysts has become a key concept in improving the efficiency of processes. Controlling the product distribution of a reaction can result in fewer by-products and reduce energy requirements for process equipment downstream. The selective hydrogenation of alkynes to alkenes is of major importance to industrial polymerization processes where alkyne/diene impurities can poison the polymerization catalyst and have an unwanted inhibiting effect on the growth of the polymer chain. In many circumstances, bimetallic catalysts have proved to have superior catalytic properties such as greater activity, selectivity or stability compared to their monometallic analogs. A study by the Sykes group (Chemistry, Tufts) in collaboaration with our group has shown that in ultra-high vacuum (UHV), the addition of Pd minority species (0.01 ML) onto an otherwise inert Cu(111) single crystal surface can activate the Cu surface for selective hydrogenation reactions. This thesis work is an extension of the surface science study to the preparation of bimetallic catalysts at the nanoscale and their testing in hydrogenation reactions at ambient reaction conditions. The overall aim of this work was to develop single atom alloy Pd-Cu and Pt-Cu catalysts which are highly active and selective for the selective hydrogenation reaction of phenylacetylene to styrene.

The bimetallic catalysts were prepared by a colloidal synthesis of Cu nanoparticles immobilized on γ-alumina support and the precious metals as a minority species were deposited by galvanic replacement. The prepared materials and synthesis technique were characterized with electron microscopy (TEM), UV-Vis spectroscopy, X-Ray diffraction (XRD), temperature programmed reduction (TPR), BET surface area measurements, chemisorption experiments and X-ray photoelectron spectroscopy (XPS). The resulting catalysts can be described as γ-Al_2O_3

supported Cu nanoparticles with a narrow size distribution. The Pt/Pd species are alloyed and well-dispersed on the surface of the nanoparticles.

The bimetallic catalysts were tested for the liquid phase hydrogenation of phenylacetylene and were compared to their monometallic analogs for reactivity and selectivity. Both the Pt-Cu and Pd-Cu bimetallic catalysts display a significant improvement of the selectivity to styrene, especially at high conversions. Based on the rate data, activation energy measurements and the model study done in UHV, it is concluded that the reaction mechanism has been altered in the bimetallic samples. Pt and Pd serve as sites for molecular hydrogen dissociation to hydrogen atoms, which in turn spillover onto the Cu surface where the hydrogenation reaction occurs. In summary, this work has demonstrated how Pd-Cu and Pt-Cu bimetallic catalysts can serve as both active and highly selective hydrogenation catalysts, where the Pd and Pt entities promote the hydrogenation activity of a Cu surface which maintains high selectivity for phenylacetylene hydrogenation to styrene.

Acknowledgements

First and foremost I would like to express deep appreciation to my advisor, Professor Maria Flytzani-Stephanopoulos, for the consistent support and invaluable guidance she has provided me throughout my graduate studies. While writing my thesis and reflecting back on the experiences and discussions I have had working with Professor Flytzani-Stephanopoulos, I can understand how her ingenuity, passion and diligence have all strongly influenced me both as an engineer and as an individual. She has taught me how to critically evaluate research and engineering problems, while shaping me into a more intellectual and resourceful person. These traits and many others will remain with me in my future endeavors, and I feel lucky to have had her as my mentor. I will always be grateful to have had this opportunity.

I would also like to acknowledge Professor Howard Saltsburg for the constructive criticism and spirited discussions throughout this project. The dynamic he brings to the group along with Professor Stephanopoulos creates a fascinating environment for scientific discussion. His knowledge and passion for science are truly admirable and I am fortunate to have been able to gain from his experiences.

Furthermore, I would like to thank my thesis committee, Dr. Charles Krueger for generously providing me with his expertise and guidance in my research endeavors, and Professor Matthew Panzer for his constructive feedback.

I am very thankful to have had such great colleagues while working in the Nano-Catalysis and Energy Laboratory at Tufts. I would especially like to thank Dr. Matthew Boucher, Dr. Branko Zugic and Dr. Yiannis Valsamakis for their mentorship and advice. Thank you to Matt Rutter, Dr. Gautham Sridharan, Jilei Liu, Joseph Lessard, Ming Yang, Chongyang Wang, Tim Lawton and many others. All of these people helped create a positive and enjoyable experience at Tufts.

I would not be here without the loving care of my mother who I can always rely on to encourage and guide me. I would also like to acknowledge all the previous teachers and mentors I have had, especially Professor Michael Stoukides who was an inspirational teacher and helped me be here today. Finally, I would also like to extend my appreciation to my family and friends for their support and genuine interest in my progress and well-being.

Table of Contents

Chapter 1 – Introduction

1.1 Background

The manufacture of many products used in modern society for fuels, chemicals, polymers and pharmaceuticals depends on catalysts. Catalysts are required to facilitate chemical reactions so they can occur at useful rates and with preference to a desired product. Designing catalysts with desirable activity and higher selectivity is of major importance in order to alleviate energy and process requirements for separation and purification.[1] When the rate of the reaction is low, the size of the vessel in which the reaction takes place will be unnecessarily large and expensive. If the product selectivity is low, the reactants are not used efficiently and energy will be needed to separate the desired products. Therefore, it is imperative to design catalysts that can enhance the activity, selectivity of a reaction and be stable over a period of time or regenerative.[2]

By better understanding how catalysts work, opportunities to conserve energy and raw materials are arising through the development of new, more efficient catalyst design strategies. Utilizing the information that is obtained from synthesis and characterization methods at the nanoscale enables the correlation of the structural properties with the physical and chemical properties of the materials.[1] An important aspect of comprehending a catalyst's reactivity is identifying and characterizing the active site for reaction, in order to implement catalyst design strategies that will result in materials with desired structures and properties. Work from our group has emphasized the difference in catalytic properties between bulk gold nanoparticles and atomically dispersed cationic gold species anchored on defect sites of ceria, for the water gas shift (WGS) reaction.[3] Another report by our group has demonstrated the importance of –OH groups at the interface with atomically dispersed Au/TiO_2 as H_2O activation sites for an

exceptionally active and stable WGS catalyst.[4] Highly dispersed, oxidized Pt atoms stabilized by alkali metals which provided interaction with OH groups were also characterized as active sites for the WGS reaction.[5] Investigations of this nature go beyond a simple observation of a system and can provide insight on how to implement design strategies for developing catalytic systems with desired properties.

The rational design of catalysts has extended to model surfaces and single crystals in ultra-high vacuum (UHV) in order to study catalytic systems in a more controlled environment. They can provide an advantage compared to real catalytic processes when there is a need to target the system at the molecular level in order to acquire more information about the surface-adsorbate structures/properties, interfacial/defect phenomena, electronic/geometric properties and much more.[6] This approach can aid the design of catalytic materials in ambient conditions which are tuned to have the desired properties. The combination of two metals in order to develop a catalyst with enhanced properties has attracted much attention and has benefitted significantly from UHV studies which have extracted important information about the interactions between alloyed metal systems.

1.2 Bimetallic Catalysts

Bimetallic or alloy catalysts are prepared by mixing two metal components within a single catalyst. They have been proven to play an important role in promoting the activity, selectivity and stability of numerous catalyst systems.[7] Sinfelt was one of the first to introduce and characterize the properties of bimetallic catalysts used in the petroleum refineries.[8] Since

then, bimetallic catalysts have had an important role in industrial applications as catalysts for reforming[9], hydrogenation/hydrogenolysis,[10,11] oxidation[12] and other types of reactions.

In many cases the properties of bimetallic catalysts are significantly different from their monometallic analogues because of synergistic effects from the alloying of the two metals. Zhang et al.[13] have demonstrated that the modified geometry and electronic properties of the active species on Au/Pd bimetallic nanoparticles greatly increases the activity for aerobic glucose oxidation. Evidence from XPS data and DFT calculations led them to propose that electron transfer from the anionic top Au atoms to O_2 generates a hydroperoxo-like species that plays a crucial role in the oxidation of glucose. He et al.[14] observed a dramatic enhancement in activity and selectivity in the hydrogenation of the nitro group in chloronitrobenzene when adding Pt to a Au/TiO_2 catalyst and attribute this improvement to the synergistic effects of the Au, Pt and TiO_2 species. They propose that the Pt entities are responsible for the dissociative activation of H_2 molecules that spill over to Au sites at the support interface. Acceleration of the hydrogen spillover process by adding Pt entities to other metals has also been observed in other instances and has improved the conversion and selectivity in selective hydrogenation reactions.[15]

Copper Platinum/Palladium Bimetallic Catalysts

Platinum- based catalysts are widely used for a number of applications in heterogeneous catalysis and fuel cells. Bimetallic Pt-Cu catalysts are used for a number of reactions including hydrodechlorination of 1,2-dichloroethane[16], NO_x reduction[17], dehydrogenation[18] and for applications in electrocatalysis[19]. Palladium- based bimetallic catalysts have also been

extensively used in heterogeneous catalysis for reactions such as hydrogenation and dehydrogenation,[20,21] WGS,[22] CO_2 reforming of methane,[23] and many others. In many of these instances both Pt and Pd have been combined with Cu in order to perturb the electronic and geometric structure of the catalyst in the hope of enhancing its catalytic properties.

Lonergan et al.[24] investigated the low temperature 1,3-butadiene hydrogenation over supported Pt-Cu/γ-Al_2O_3 in a batch reactor system and found it was more selective to butenes than monometallic Pt/γ-Al_2O_3 and the other Pt-Co,Ni,Pt/γ-Al_2O_3 alloys that were examined. In this case, the bimetallic catalysts were prepared by co-impregnation of the metal precursors onto the metal oxide support. Conventionally, co-impregnation followed by calcination and reduction treatments is a simple and common method for the synthesis for both Pt-Cu and Pd-Cu alloy catalysts. [16,17,18,22,25,26] However, the disadvantages of this method are that the surface composition is uncontrollable, the exclusive formation of bimetallic entities is not guaranteed and it often leads to a non-uniform size distributions[16]. New synthesis methods that can overcome these disadvantages and lead to well-controlled chemical compositions and particle sizes are attracting more interest. For example, Wei et al.[16] employed a two-step method based on grafting-adsorption-reduction procedure to synthesize silica supported Pt-Cu bimetallic nanoparticles and have achieved better control over particle size, structure, composition and stability. In another example, Zhou et al.[17] have used a polyol reduction method to synthesize Pt-Cu core-shell and alloy nanoparticles and found that the Cu@Pt core-shell nanoparticles had a similar activity to monometallic Pt catalyst but a significantly higher selectivity to N_2 in the NO_x reduction. Muhler and coworkers used a sonication- facilitated method to prepare supported bimetallic Pt-Cu and Pd-Cu nanoparticles by galvanic replacement on nitrogen-doped carbon nanotubes. The prepared bimetallic nanoparticles were well dispersed with high uniformity in

size and composition with enhanced electrocatalytic activity in the oxygen reduction reaction compared to commercial Pt/C catalyst.[27] These examples prove that control over the synthesis of the catalyst can lead to materials with the desired properties for a given reaction system.

1.3 Selective Hydrogenation Reactions

When there is a desire to produce a specific product among other compounds that are thermodynamically possible but are undesirable byproducts, then the reaction selectivity becomes of major importance. Developing catalysts for selective hydrogenation reactions of unsaturated hydrocarbons, in the presence of less unsaturated hydrocarbons has been a heavily studied topic because of its importance for industrial processes. Highly selective catalysts are preferred to help reduce the energy consumption required for product separation and waste disposal processes in chemical industries. There has been a lot of focus in identifying the molecular factors that control the selectivity and hence the product distribution of a given reaction system.[28] There are many factors that can contribute the selectivity of a reaction such as surface structure,[29] metal/metal oxide interactions,[30] charge transfer,[31] oxidation states,[32] and others. In the context of examining bimetallic catalytic systems, one factor that can heavily influence the selectivity is the surface composition of the two metals. An example of how the surface composition can have an effect on the selectivity of a reaction was recently reported by our group.[33] Very low concentrations of Pd atoms on Cu(111) were demonstrated to act as sites for hydrogen dissociation which spilled over and populated the Cu surface where the hydrogenation reaction occurred.[33] Higher concentrations (1-ML) of Pd on the Cu surface dramatically lowered the selectivity of the process. Somorjai and co-workers[32] have

demonstrated that they can tune the reactivity of colloidal Rh/Pt nanoparticles for CO oxidation by adjusting the surface composition of the nanoparticles. It was observed that under the oxidizing conditions of the reaction, Rh atoms are pulled to the surface with moderate surface segregation of the Rh and overall re-arrangement of the surface composition hence transforming the activity and product distribution of the reaction.

A general scheme for the hydrogenation C-C multiple bonds of unsaturated hydrocarbons is presented in **Figure 1**.[34] The selective formation of an alkene can be defined in terms of *mechanistic selectivity* or *thermodynamic selectivity* depending on the nature of the catalytic system. In mechanistic terms, when $k_2 >> k_4$ (**Figure 1**) the production of the intermediate alkene product is favorable due to the large difference in the kinetics of the system. In terms of thermodynamics, when there is competitive adsorption between the alkyne and alkene on the surface of the catalyst and the adsorption of the alkyne molecule is much stronger than that of the alkene ($k_1/k_{-1} >> k_3/k_{-3}$), then the dominant adsorption of the alkyne prevents the consecutive hydrogenation towards the saturated hydrocarbon.[34,35,36] Palladium has been found to be the most active and selective hydrogenation catalyst. Its selectivity has been attributed to the stronger adsorption of the diene/alkyne compared to that of the alkene which is formed.[34,37,38] UHV studies by Lambert and co-workers[39] of acetylene and ethylene on Pd(111) found that acetylene adsorbs more strongly than ethylene. It has been proposed that the alkyne either displaces or blocks alkene adsorption, resulting in high surface coverage of alkyne and hence preferential hydrogenation. Platinum which has been shown to be a less active hydrogenation catalyst than Pd, also shows a relatively high selectivity which has also been attributed to higher heats of adsorption of the alkynes/dienes compared to alkenes.[35] It is important to note that even though there is a preferential hydrogenation of alkynes during competitive hydrogenations, as individual

species the alkyne rate of hydrogenation is lower than that of alkenes. [40] Based on all of the previous evidence, it can be concluded that the dominant phenomenon of the selective hydrogenation of unsaturated hydrocarbons on Pd and Pt species is the surface adsorption of the competing molecules, which is of thermodynamic nature and could be classified as *thermodynamic selectivity*.

Phenylacetylene Hydrogenation

The catalytic hydrogenation of phenylacetylene is both of industrial and scientific interest. In industry, styrene is used as a monomer for the manufacture of polystyrene, foamed polystyrene and different copolymers such as acrylonitrile-butadiene-styrene, styrene-acrylonitrile and styrene-butadiene rubbers.[41] During the preparation of polystyrene, phenylacetylene as an impurity can poison the catalyst even in low concentrations and has an uncontrolled inhibiting effect on the growth of the polymer chain. The result of this effect can lead to degradation of the polystyrene quality; hence the phenylacetylene needs to be removed before polymerization occurs.[41,42] From a scientific viewpoint, the catalytic hydrogenation reaction of phenylacetylene can be used as a model system for evaluating the activity and selectivity of catalytic materials for alkyne hydrogenation.

Palladium on different supports is the industrial standard used for hydrogenation reactions, including phenylacetylene.[41] Kinetic models for the step-wise hydrogenation of phenylacetylene to styrene and to ethylbenzene over a Pd/Al_2O_3 catalyst were proposed in 1986 by Chaudhari et al.[43] and on Pd/C in 1996 by Jackson et al.[44] for the same chain reaction system. In both cases, it was reported that the rate of styrene hydrogenation in the presence of

phenylacetylene was much slower than that obtained for pure styrene and that only after phenylacetylene was completely converted did the reaction rate of styrene increase significantly. This effect has generally been attributed to the competitive adsorption between pheynlacetylene and styrene on the catalyst surface. Duca et al.[45] also studied the kinetics of liquid phase phenylacetylene hydrogenation on pumice supported Pd catalysts and found that the electron density transfer from the support to the metal species can have a positive effect on the catalytic activity which is shown to increase with the dispersion. The alloying of the palladium surface atoms with Cu metal on a pumice support was reported to increase the selectivity of phenylacetylene to styrene by Guczi et al.[46] who attributed the behavior to electronic effects of the alloy and the ensemble size variation.

1.4 Thesis Motivation

A recent surface science report by Sykes and co-workers in collaboration with our group, has demonstrated the advantages of bimetallic catalysis by investigating a Cu(111) crystal surface with atomically dispersed Pd sites. It was demonstrated how the Pd atoms serve as hosts for hydrogen dissociation and spillover onto the Cu surface where the hydrogen is weakly bound and effective for hydrogenation. In other words, the addition of minority Pd atoms (0.01 ML) activated an otherwise inert Cu(111) single crystal, creating a bi-functional surface which is an active and selective hydrogenation catalyst.[33]

Inspired by the results of the surface science study, the aim of this thesis was to investigate the extension of the information obtained on a single crystal Cu(111) surface to a real

catalytic system. The target was to develop single atom surface alloy bimetallic catalysts which are highly active and selective hydrogenation catalysts and investigate the feasibility of H_2 spillover in ambient reaction conditions. Initially the goal was to prepare Cu nanoparticles with the majority of Cu(111) (low index surface) and deposit Pd atoms onto the Cu nanoparticles. After the preparation and characterization of the catalytic material, the aim was the testing of the material for hydrogenation of highly unsaturated hydrocarbons under ambient temperature and pressure, and examination of its selectivity compared to a monometallic Pd catalyst. Spillover of H_2 onto the Cu surface was to be investigated as well, based on the experimental data. Another goal was to extend this work to a different metal, platinum, which could also act as an activation site for hydrogen dissociation on a Cu substrate, and investigate the effect of this metal in activating copper for the selective hydrogenation reaction of phenylacetylene.

1.5 References

1. Li, Y. & Somorjai, G. a. Nanoscale advances in catalysis and energy applications. *Nano letters* **10,** 2289–95 (2010).

2. U.S. Department of Energy. Catalysis for Energy. (2007).

3. Fu, Q., Saltsburg, H. & Flytzani-Stephanopoulos, M. Active nonmetallic Au and Pt species on ceria-based water-gas shift catalysts. *Science (New York, N.Y.)* **301,** 935–8 (2003).

4. Yang, M., Allard, L. F. & Flytzani-Stephanopoulos, M. Atomically Dispersed Au−(OH).expand to include the jourmal etc. (2013).

5. Zhai, Y. *et al.* Alkali-stabilized Pt-OHx species catalyze low-temperature water-gas shift reactions. *Science* **329,** 1633–6 (2010).

6. Somorjai, G. a & Li, Y. Impact of surface chemistry. *Proceedings of the National Academy of Sciences of the United States of America* **108,** 917–24 (2011).

7. Sankar, M. *et al.* Designing bimetallic catalysts for a green and sustainable future. *Chemical Society Reviews* **41,** 8099–139 (2012).

8. Sinfelt, J. H. *Bimetallic Catalysts: Discoveries, Concepts, and Applications (Exxon Monograph)*. (Wiley: New York, 1983).

9. Catalysis, ??? Platinum-Tin Reforming Catalysts. **359,** 348–359 (1981).

10. Ru, N. *et al.* Solvent-Free, Low-Temperature, Selective Hydrogenation of Polyenes Using a Bimetallic Nanoparticle Ru-Sn Catalyst. *Angewandte Chemie (International ed. in English)* **40,** 1211–1215 (2001).

11. Ruppert, A. M., Weinberg, K. & Palkovits, R. Hydrogenolysis goes bio: from carbohydrates and sugar alcohols to platform chemicals. *Angewandte Chemie International Ed.***51,** 2564–601 (2012).

12. Murahashi, S. & Hirai, N. Aerobic Oxidation of Alcohols with Ru-Co Bimetallic Catalysts in the Presence of Aldehydes. *Journal of Organic Chemistry* 7318–7319 (1993).

13. Zhang, H., Watanabe, T., Okumura, M., Haruta, M. & Toshima, N. Catalytically highly active top gold atom on palladium nanocluster. *Nature Materials* **10,** 1–4 (2011).

14. He, D., Jiao, X., Jiang, P., Wang, J. & Xu, B.-Q. An exceptionally active and selective Pt–Au/TiO2 catalyst for hydrogenation of the nitro group in chloronitrobenzene. *Green Chemistry* **14,** 111 (2012).

15. Liu, R. *et al.* Physically and chemically mixed TiO2-supported Pd and Au catalysts: unexpected synergistic effects on selective hydrogenation of citral in supercritical CO2. *Journal of Catalysis* **269,** 191–200 (2010).

16. Wei, X., Wang, A.-Q., Yang, X.-F., Li, L. & Zhang, T. Synthesis of Pt-Cu/SiO2 catalysts with different structures and their application in hydrodechlorination of 1,2-dichloroethane. *Applied Catalysis B: Environmental* **121-122,** 105–114 (2012).

17. Zhou, S., Varughese, B., Eichhorn, B., Jackson, G. & McIlwrath, K. Pt-Cu core-shell and alloy nanoparticles for heterogeneous NO(x) reduction: anomalous stability and reactivity of a core-shell nanostructure. *Angewandte Chemie (International ed. in English)* **44,** 4539–43 (2005).

18. Veldurthi, S., Shin, C.-H., Joo, O.-S. & Jung, K.-D. Promotional effects of Cu on Pt/Al2O3 and Pd/Al2O3 catalysts during n-butane dehydrogenation. *Catalysis Today* **185,** 88–93 (2012).

19. Neergat, M. & Rahul, R. Unsupported Cu-Pt Core-Shell Nanoparticles: Oxygen Reduction Reaction (ORR) Catalyst with Better Activity and Reduced Precious Metal Content. *Journal of the Electrochemical Society* **159,** F234–F241 (2012).

20. Kolli, N. El, Delannoy, L. & Louis, C. Bimetallic Au–Pd catalysts for selective hydrogenation of butadiene: Influence of the preparation method on catalytic properties. *Journal of Catalysis* **297,** 79–92 (2013).

21. Gu, X., Lu, Z., Jiang, H., Akita, T. & Xu, Q. Synergistic Catalysis of Metal À Organic Framework-Immobilized. 11822–11825 (2011).

22. Kugai, J., Miller, J. T., Guo, N. & Song, C. Oxygen-enhanced water gas shift on ceria-supported Pd–Cu and Pt–Cu bimetallic catalysts. *Journal of Catalysis* **277,** 46–53 (2011).

23. Crisafulli, C. & Scir, S. CO 2 reforming of methane over Ni – Ru and Ni – Pd bimetallic catalysts. **59,** 21–26 (2000).

24. Lonergan, W. W. *et al.* Low-temperature 1,3-butadiene hydrogenation over supported Pt/3d/γ-Al2O3 bimetallic catalysts☆. *Catalysis Today* **160,** 61–69 (2011).

25. Kugai, J., Miller, J. T., Guo, N. & Song, C. Role of metal components in Pd–Cu bimetallic catalysts supported on CeO2 for the oxygen-enhanced water gas shift. *Applied Catalysis B: Environmental* **105,** 306–316 (2011).

26. Xie, H. *et al.* Hydrodechlorination of 1,2-dichloroethane catalyzed by dendrimer-derived Pt–Cu/SiO2 catalysts. *Journal of Catalysis* **259,** 111–122 (2008).

27. EnyuSun, Z. *et al.* Rapid and Surfactant-Free Synthesis of Bimetallic Pt−Cu Nanoparticles Simply via Ultrasound-Assisted Redox Replacement. (2012).

28. Somorjai, G. a & Park, J. Y. Molecular factors of catalytic selectivity. *Angewandte Chemie (International ed. in English)* **47,** 9212–28 (2008).

29. Somorjai, G. a, York, R. L., Butcher, D. & Park, J. Y. The evolution of model catalytic systems; studies of structure, bonding and dynamics from single crystal metal surfaces to nanoparticles, and from low pressure (<10(-3) Torr) to high pressure (>10(-3) Torr) to liquid interfaces. *Physical chemistry chemical physics : PCCP* **9,** 3500–13 (2007).

30. Schwab, G. M. Boundary Layer Catalysis. *Angewandte Chemie (International ed. in English)* **6,** 375– (1967).

31. Somorjai, G. a, Bratlie, K. M., Montano, M. O. & Park, J. Y. Dynamics of surface catalyzed reactions; the roles of surface defects, surface diffusion, and hot electrons. *The journal of physical chemistry. B* **110,** 20014–22 (2006).

32. Park, J. Y., Zhang, Y., Grass, M., Zhang, T. & Somorjai, G. a. Tuning of catalytic CO oxidation by changing composition of Rh-Pt bimetallic nanoparticles. *Nano letters* **8,** 673–7 (2008).

33. Kyriakou, G. *et al.* Isolated metal atom geometries as a strategy for selective heterogeneous hydrogenations. *Science (New York, N.Y.)* **335,** 1209–12 (2012).

34. Guo, X.-C. & Madix, R. J. Selective Hydrogenation and H-D Exchange of Unsaturated Hydrocarbons on Pd(100)-p(1x1)-H(D). *Journal of Catalysis* 336–344 (1995).

35. Chemistry, S. Hydrogenation of carbon – carbon multiple bonds : **173,** 185–221 (2010).

36. Bond, G. C., Dowden, D. a. & Mackenzie, N. The selective hydrogenation of acetylene. *Transactions of the Faraday Society* **54,** 1537 (1958).

37. Ouchaib, T. Competitive hydrogenation of butadiene and butene on palladium and platinum catalysts. *Journal of Catalysis* **119,** 517–520 (1989).

38. Sautet, P. & Paul, J. Low Temperature Adsorption of Ethylene and Butadiene on Platinum and Palladium Surfaces. *Catalysis Letters* **9,** 245–260 (1991).

39. Tysoe, W. T., Nyberg, G. L. & Lambert, R. M. Low temperature catalytic chemistry of the Pd(111) surface: benzene and ethylene from acetylene. *Journal of the Chemical Society, Chemical Communications* 623 (1983). doi:10.1039/c39830000623

40. Marvell, E. N. & Li, T. *Catalytic Semihydrogenation of the Triple Bond*. (1973).

41. Basimova, R. a. *et al.* Selective hydrogenation on palladium-containing catalysts of byproduct phenylacetylene present in industrial fractions of styrene. *Petroleum Chemistry* **49,** 360–365 (2009).

42. Huang, X., Wilhite, B., McCready, M. J. & Varma, a. Phenylacetylene hydrogenation in a three-phase catalytic packed-bed reactor: experiments and model. *Chemical Engineering Science* **58,** 3465–3471 (2003).

43. Chaudhari, R. V *et al.* KINETIC REACTION MODELLING OF A COMPLEX CONSECUTIVE IN A SLURRY REACTOR : HYDROGENATION ACETYLENE OF. (1986).

44. Jackson, S. D. & Shaw, L. A. and styrene on a palladium / carbon catalyst. **134,** 91–99 (1996).

45. Selective hydrogenation of phenylacetylene on pumice supported Pd catalysts.pdf.

46. Guczi, L. *et al.* Pumice-Supported Cu – Pd Catalysts : Influence of Copper on the Activity and Selectivity of Palladium in the Hydrogenation of Phenylacetylene and But-1-ene. **462,** 456–462 (1999).

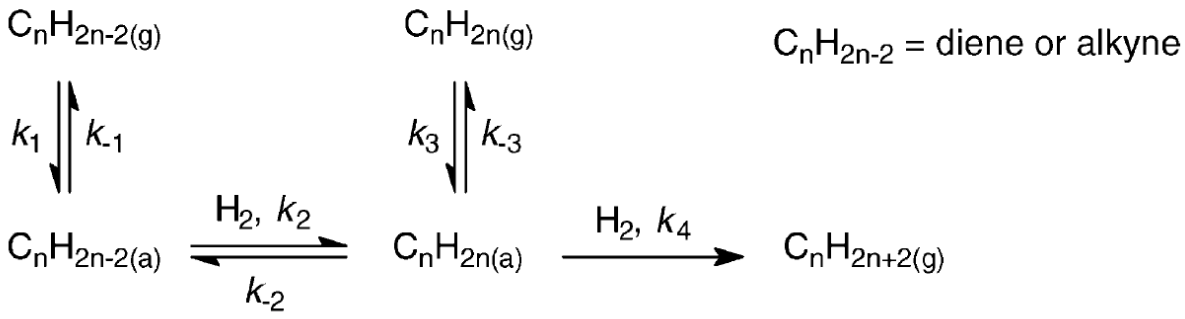

Figure 1 General reaction pathways for the hydrogenation of unsaturated hydrocarbons

Chapter 2 – Materials and Methods

2.1 Catalyst Preparation

This section describes the materials and preparation methods used to prepare the different mono and bimetallic catalysts used in this work. Copper nanoparticles were prepared by a colloidal nanoparticle synthesis method, immobilized on γ-alumina and deposition of Pt or Pd was achieved through the galvanic replacement (GR) reaction. These catalysts were compared to

monometallic catalysts synthesized by incipient wetness impregnation. The results of activity testing and analysis of these materials are presented in subsequent chapters.

2.1.1 Materials

The chemicals and reagents used in this work are listed in **Table 2.1**. All materials were used as provided by suppliers without further purification.

2.1.2 Synthesis of Copper Nanoparticles

The supported Cu nanoparticles are prepared by immobilization of a colloidal suspension of the Cu nanoparticles. Colloidal metal particles are commonly synthesized by reduction of dissolved metal precursor salts in the presence of capping agents (CA) such as surfactants (e.g. citrate) or polymeric ligands (e.g. polyvinylpyrrolidone (PVP)). PVP which was used in this work, has a polar amide group in its monomer unit which interacts favorably with the salt precursor and creates a barrier to stabilize the metal seed formation while preventing agglomeration of the metal cluster during reduction and colloid formation.[1] The capping agents are also used to control the growth of the initially formed nanoclusters by varying the metal:CA ratio.[2] Using this type of a preparation method allows the formation of nanoparticles with tunable size control and narrow particle size distributions.

The synthesis procedure followed to prepare the Cu nanoparticles was adapted from methods reported by the Somorjai group[3] and Chunwei et al.[4], with slight modifications. In order

to prepare 1 g total of γ-alumina supported Cu nanoparticles (10 wt%), the synthesis procedure is as follows:

(i) 200 cc of deionized (DI) water is poured into an Erlenmeyer flask, with 100% N_2 gas bubbling through a sparger and under constant magnetic stirring for approximately 20 min to ensure that the water has been de-aerated.

(ii) 0.38 g of $Cu(NO_3)_2 \cdot 3H_2O$ and 0.38 g of polyvinylpyrrolidone (PVP MW of 40,000 g/mol) are gradually added under constant vigorous stirring to achieve a 200:1 molar ratio of Cu:PVP

(iii) Once fully dissolved, a 0.1 M solution of ascorbic acid is gradually added as an antioxidant agent until the color of the solution changes from a transparent light blue to a transparent light red.

(iv) In a separate Erlenmeyer flash 0.14 g of $NaBH_4$ are added to 40 cc of DI water and stirred until fully dissolved. The solution of $NaBH_4$ is added dropwise to the solution containing the Cu precursor and PVP until the color gradually changes from a light red to black. The excess amount of $NaBH_4$ added is designed to achieve a 2:1 molar ratio of Na:Cu to ensure complete reduction of the Cu species in solution.

(v) After stirring for 15 min, this solution is added dropwise to 0.9g of γ-Al_2O_3 suspended in 100 cc of DI water under constant stirring. Once the colloidal solution has been added to the support mixture, the suspension is stirred for 30min and filtered and washed with 500 cc of DI water.

(vi) After allowed to dry in vacuum for 12 hr, the powder is calcined at 300 ^oC for 4 hr to remove the PVP capping agent from the Cu nanoparticles.

2.1.3 Deposition of Pt and Pd by galvanic replacement

The galvanic replacement (GR) reaction occurs spontaneously and irreversibly when atoms of a host metal react with ions of another metal which have a higher reduction potential in solution. The outcome is the exchange of host metal atoms which become oxidized and released into solution as ions, while the metal ion species are reduced and plated onto the host metal surface. As the deposition of the metal ions onto the host metal surface takes place, interdiffusion across the interface of the metals leads to alloy formation.[5] Overall, GR provides a simple and versatile route to prepare bimetallic metal clusters with high tunability of the surface composition.

In order to prepare bimetallic nanoparticles of Pt-Cu and Pd-Cu the electrochemical or redox potentials for these elements must be examined in order to determine the feasibility of this preparation. **Table 2.2** has the standard redox potentials of Cu, Pt, and Pd to the standard hydrogen electrode for ideal reaction conditions at 25 ^{o}C and 1 atm. It is important to note that different temperatures, presence of ions and other non-standard conditions can affect the values of the redox potentials.[6] Since Cu has a lower redox potential (Cu^{2+}/Cu, E^{0}=+0.340 V) than both Pt (Pt^{2+}/Pt, E^{0}=+1.188 V) and Pd (Pd^{2+}/Pd, E^{0}=+0.915 V), it is favorable that both the Pt and Pd ions will exchange with the Cu host metal via the following reactions:

$$Cu + Pt^{2+} \rightarrow Cu^{2+} + Pt \ (\Delta E^{0} = +0.575 \text{ V})$$

$$Cu + Pd^{2+} \rightarrow Cu^{2+} + Pd \ (\Delta E^{0} = +0.848 \text{ V})$$

The propensity of Cu to oxidation (both bulk and surface) is a significant barrier to the synthesis of Pt/Pd-Cu bimetallic nanoparticles by GR. Even though the Cu^{2+}/Cu redox couple has a higher redox potential than H^{+}/H_2 in the electrochemical series, Cu nanoparticles formed by reduction of Cu^{2+} are susceptible to oxidation due to the alkalinity of the $NaBH_4$ solution.[7] The L-ascorbic acid and the nitrogen protection during the preparation process prevent formation of bulk copper oxide during the formation of the Cu nanoparticles.

The Cu nanoparticles were reduced to 250 ^{o}C for 2 hr before GR to ensure that the Cu nanoparticles were fully reduced and in their metallic state. Further characterization of the reduction and oxidation state of the Cu nanoparticles is discussed in **Chapter 3**.

In the case of preparing Pd-Cu/Al_2O_3 catalyst, a procedure developed by Muhler and co-workers[8] was followed, using high-intensity ultrasound to facilitate the GR reaction. The Cu/Al_2O_3 was transferred to an aqueous solution after the reduction treatment, under nitrogen protection and constant stirring. The desired amount of $Pd(NO_3)_2$ was added to the solution and a sonicating tip was immersed into the suspension to enhance the rate of the GR reaction.[9] After 15 min, the suspension filtered and washed with 500 cc of DI water, and dried in vacuum for 12 hr.

In the case of the Pt-Cu/Al_2O_3 catalysts, after following the previous procedure with thermal reduction treatment in H_2, it was observed by UV-Vis that not all of the Pt species were exchanging onto the surface of the Cu. In order to ensure the complete uptake of the Pt onto the Cu host, a different approach was applied following a procedure developed by Wei et al.,[10] with slight modifications. After thermal reduction in H_2, the Cu/Al_2O_3 was re-dispersed in an aqueous solution under nitrogen protection and vigorous stirring. A solution of 0.2 M $NaBH_4$ was added dropwise until the color of the suspension turned from a dark red to a bright red, and there was

no more evident color change with additional $NaBH_4$. After stirring for 15 min, a certain amount of 2 wt% HCl was added dropwise until there were no more bubbles produced, ensuring the exhaustion of excess $NaBH_4$ in the solution. The desired amount of $(NH_4)_4Pt(II)(NO_3)_2$ solution was added to the suspension and allowed to stir for 1 hr for the GR reaction to take place. The suspension was filtered and the recovered solid was dried under vacuum for 12 hr.

An explanation for this difference in preparation procedures between Pd and Pt could be related to various factors. One main reason could be the surface oxidation of the Cu nanoparticles once added in the aqueous solution. Pacioni et al.[11] used spectroscopic methods to quantify the uptake of oxygen on unprotected Cu nanoparticles and demonstrated that within 2 hours the surface of the nanoparticles is fully oxidized. Brief exposure to air or even under N_2 protection, there could still be oxygen species dissolved in the aqueous solution which would result in partial oxidation of the surface Cu. This factor in combination with the coordination of the two different metal precursors in solution could be enough to create a barrier for complete uptake of Pt when the sodium borohydride is not used to reduce the Cu surface.

Also, it is important to note that the resulting catalyst in this case required thorough washing with DI water in order to remove any adsorbed chloride species. In order to detect the chlorides in the filtered solution, a small amount of silver nitrate ($AgNO_3$) was added and stirred by hand. When the chlorides were still present, the solution turned to an opaque light beige color. The catalyst was washed with warm DI water until the filtrate solution was clear after the addition of $AgNO_3$. The chloride species not only can poison the Pt catalyst, [12] but they also create problems with the gas chromatograph by corroding the flame ionization detector's (FID) inner surfaces resulting in electrical leakage and a highly noisy baseline.[13] In order to solve this

problem, the FID (unlit) as well as the GC column temperature must be raised to high temperatures (250-275 ^{o}C).

2.1.4 Incipient Wetness Impregnation

Impregnation is a widely used technique for preparing precious metal-based catalysts. The properties of the metal solution (e.g. volume, pH, temperature) used for impregnation can influence the catalyst properties such as dispersion and morphology.[14] There are two common types of impregnation procedures; impregnation with excess solution and incipient wetness impregnation (IWI). The latter is done in one step, where a measured amount of aqueous solution (equal to the pore volume of the oxide support) containing the desired concentration of the precious metal ion is added dropwise to the oxide support, to fill the pore volume of the solid. The advantage of this technique is that the desired amount of precious metal is all being deposited onto the oxide support, but it could lead to non-uniformity of the particle size and structures.[14]

IWI was used to prepare Pt/Al_2O_3 and Pd/Al_2O_3 catalysts. The commercial γ-Al_2O_3 support used has a pore volume of 0.55 cc/g and a surface area of 210 m^2/g. The impregnation was done by gradually injecting 0.55 cc of a solution containing the amount of metal precursor in order to obtain the desired weight loading of catalyst, into 1 g of γ-Al_2O_3. After every few drops, the solid was crushed and mixed until all of the metal solution was added. The resulting wet powder was dried under vacuum for 12 hr and calcined at 400 ^{o}C for 4 h.

2.2 Catalytic Activity Measurements

2.2.1 Liquid Batch Reactor

The reactions were carried out in a 50 cc liquid Parr reactor which can be seen in **Figure 2.1**. There are inlet/outlet lines for the hydrogen gas flow and separate lines for the cooling water which is used to chill the magnet which controls the stirring rod inside the reactor. There is an injection port on the reactor head, controlled with an open-close valve, which is used to inject the liquids (reactant and solvent) through a septum which does not allow the leakage of gases either in or out of the reactor. Also, there is a sampling port which has a syringe filter at the end which is used to separate the liquids from the solid catalyst. Finally, there is a heating jacket around the reactor attached to a temperature controller used to regulate the temperature of the reactor system.

In a typical reaction experiment, the catalyst sample was placed at the bottom of the reactor and the reactor was sealed. After the gas and cooling water line were connected and the heating jacket was in place, 100% H_2 gas was used to purge the system. To begin the reduction treatment, while the H_2 gas was flowing, the temperature was set to the desired value (400 ^oC for Pt and 250 ^oC for Pd) and the reactor was heated at a ramp rate of 5 ^oC/min and held at temperature to ensure complete reduction of the samples. Once the reactor was cooled, de-aerated phenylacetylene dissolved in n-hexane was injected into the Parr reactor under H_2 flow. The reactor was then pressurized to 100 psi under 100% H_2 while the reactant mixture was stirred continuously. Liquid samples were drawn from the reactor by opening the valve controlling the sampling port, and filtered ex-situ so that the reactant:catalyst ratio remained constant during the experiment. To check for the absence of diffusion control in the reactor,

experiments were done at 50, 70 and 90% of the total rotational speed the motor can achieve. In all cases an identical rate of reaction was measured confirming the absence of external diffusion limitations.

2.2.2 Analysis

The liquid samples were analyzed in a HP 5890 gas chromatograph (GC) equipped with a flame ionization detector (FID) and a capillary column capable of separating phenylacetylene, styrene, ethyl benzene and ethyl cyclohexane. The GC column used was a 30 m Restek Rxi-5ms (diphenyl dimethyl polysiloxane) with a 0.25 mm ID and 1.00 μm d_f (film thickness). The concentration of the liquid samples was 50-200 ppm (diluted in n-hexane) and 10 μL of each sample was injected manually into the column. The ramping procedure was a 2 min hold at 50 ^{o}C, followed by a linear ramping to 175 ^{o}C, and a 2 min hold there. The column head pressure was maintained at 15 psig with He flow at all times.

Calibration of the GC was done by injecting samples with known ppm concentrations of the different species of interest. Specifically, the three known concentrations prepared were 200, 500 and 1000 ppm of each species, and each sample was injected three times and the average peak area was used. The calibration was calculated based on the relationship:

$$(Calibration) = \frac{(PeakArea)}{(PPM)}$$

by plotting the average peak area measured against the known ppm concentration of each species in each sample. The different calibrations are equal to the slope of each linear fit which is illustrated in **Figure 2.2**.

The equations used in order to calculate the conversion and selectivity are the following:

$$(conversion)\% = \frac{(PA)_{initial} - (PA)_{final}}{(PA)_{initial}}$$

$$(selectivity)\% = \frac{(Styrene)_{final}}{(PA)_{initial} - (PA)_{final}}$$

2.3 Catalyst Characterization Methods

2.3.1 BET Surface AreaBET surface area measurements were conducted using a Micromeritics AutoChem 2920 equipped with a thermal conductivity detector (TCD). The BET surface area was determined by single-point N_2 adsorption/desorption cycles. In a typical experiment, 0.2 g of the sample were loaded into the reactor between beds of quartz wool and pretreated in 100% He to 250 ^oC at a rate of 10 ^oC/min and held for 30 min to remove any adsorbed species (i.e. H_2O) from the catalyst surface. The analysis gas was switched to 30% N_2 – He and the sample was immersed into a liquid nitrogen bath to measure the adsorbed species and then into a water bath to measure the desorption peak. BET calibration was applied to correlate and quantify the amount of N_2 adsorbed/desorbed and hence the surface area of the sample.

2.3.2 Temperature Programmed Reduction

Temperature programmed reduction (TPR) is a technique in which the surface reduction of an oxide is monitored while the temperature of the sample is linearly ramped with time. This type of

an analysis can yield information about the quantity, adsorption/bond strength or the types of oxygen groups present on the catalyst surface.

The H_2-TPR measurements were carried out in a Micromeritics AutoChem 2920 equipped with TCD. The loaded samples were pretreated in 20% O_2 – He to 300 ^oC at a ramp rate of 10^oC/min in order to oxidize the active metal species on the catalyst surface. After cooling to room temperature, the samples were exposed to 20% H_2 – Ar at 30 cc/min while linearly ramping the temperature to 400 ^oC with a ramp rate of 10^oC/min. The process was monitored by TCD and the H_2 calibration was applied in order to quantify the amount of oxygen species removed from the catalyst.

The CO-TPR experiment was carried out in a Micromeritics AutoChem 2920, and the process was monitored by an online quadrupole mass spectrometer (SRS residual gas analyzer). The sample was purged at room temperature in He for 30 min and the flow was switched to 10% CO – He (30 cc/min) and the temperature was linearly ramped to 400 ^oC at a ramp rate of 10^oC/min. The quadropole mass spectrometer was used to monitor the species being produced from the interaction of the CO with the catalyst surface, in order to determine the types of oxygen groups.

2.3.3 CO Chemisorption

CO can be used as a probe molecule which selectively adsorbs onto a metal species (i.e. Pt, Pd). A specific volume of CO is pulsed over the sample and the amount of CO adsorbed can be quantified and used to estimate the surface area, dispersion and particle size of a specific metal species on the catalyst surface.

CO chemisorption measurements were conducted using the Micromeritics AutoChem 2920 equipped with a TCD. In a typical experiment, the samples were first pretreated in 20% H_2 – Ar to 250 ^oC at a rate of 10^oC/min and held for 2 hr. After the sample was cooled in He to room temperature, 10% CO – He was pulsed over the sample until the discretely injected gas volumes were determined unchanged by the TCD. The difference in the total amount of CO injected and the amount measured in the gas effluent were used to calculate dispersion of the active metal species using a stoichiometry of metal:CO (1:1).

2.3.4 High Resolution Transmission Electron Microscopy (HR-TEM)

Electron microscopy is generally used to resolve nanometer scale images. In this work, HRTEM was used to estimate the particle size, distribution and lattice spacing of the nanoparticles. The samples used for imaging were prepared by sonicating a small amount of catalyst in ethanol, which was then deposited onto a lacey carbon, 200 mesh copper grid. HRTEM was performed at the Harvard Center for Nanoscale Systems on a JEOL 2100 electron microscope operated with a lanthanum hexaboride source at 200 kV.

2.3.5 UV-Vis Spectroscopy (UV-Vis)

UV-Vis is a characterization technique that is used to examine the electronic transitions of metals based on the absorption intensity of varying wavelengths in the range of 200 – 800 nm. The UV-

Vis samples were prepared by injecting the desired solutions into cuvettes and shaking well before measurements. The UV-Vis instrument used was an Evolution^{TM} 300 UV-Vis Spectrophotometer (Thermo Scientific).

2.3.6 X –Ray Diffraction (XRD)

XRD is a bulk analysis technique used to determine the crystalline phases present in a sample. The XRD measurements were performed at MIT on a Rigaku RU300 Cr-source powder diffractometer. Cr radiation was used with a power setting of 50 kV and 250 mA. A scan rate of 1 degree/min with a 0.02 degree step size was used. The XRD samples were prepared by adding approximately 0.5 g of catalyst powder into a sample holder.

2.3.7 X-Ray Photoelectron Spectroscopy (XPS)

XPS is a surface analysis technique that is used to characterize the composition, chemical shifts and oxidation states of a material. In XPS, the X-ray beam irradiates the sample causing the release of core-level electrons. These electrons are collected and analyzed for their number and kinetic energy, which is correlated to their binding energy. Since each element's electrons have a distinct binding energy, the resulting spectrum of intensity plotted against binding energy can be used to determine the relative composition of a sample, along with the oxidation state of its components from shifted peaks. Additionally, since the photoelectrons excited and released in

this technique have an escape depth of a few nanometers, this provides a method to determine the near-surface composition and oxidation state of the sample.

The XPS measurements were performed at the Harvard Center for Nanoscale Systems on a Thermo Scientific K-Alpha system equipped with an Al source and 180^{o} double focusing hemispherical analyzer and 128-channel detector. High resolution XPS spectra were obtained at a pass energy of 40 – 50 eV. The XPS samples were prepared by adhesion of dried powder samples onto a copper tape supported by a carbon double-sided tape backing. The results were analyzed using CasaXPS software and all of the spectra were aligned during the analysis to the C 1s peak at 284.5 eV.

2.4 References

1. Bönnemann, H. & Richards, R. M. Nanoscopic Metal Particles Synthetic Methods and Potential Applications. 2455–2480 (2001).

2. Ferrando, R., Jellinek, J. & Johnston, R. L. Nanoalloys: from theory to applications of alloy clusters and nanoparticles. *Chemical reviews* **108,** 845–910 (2008).

3. Tsung, C.-K. *et al.* Sub-10 nm platinum nanocrystals with size and shape control: catalytic study for ethylene and pyrrole hydrogenation. *Journal of the American Chemical Society* **131,** 5816–22 (2009).

4. Wu, C., Mosher, B. P. & Zeng, T. One-step green route to narrowly dispersed copper nanocrystals. *Journal of Nanoparticle Research* **8,** 965–969 (2006).

5. Cobley, C. M. & Xia, Y. Engineering the Properties of Metal Nanostructures via Galvanic Replacement Reactions. *Materials science & engineering. R, Reports : a review journal* **70,** 44–62 (2010).

6. Dursun, a., Pugh, D. V. & Corcoran, S. G. Dealloying of Ag-Au Alloys in Halide-Containing Electrolytes. *Journal of The Electrochemical Society* **150,** B355 (2003).

7. Sarkar, a. & Manthiram, a. Synthesis of Pt@Cu Core−Shell Nanoparticles by Galvanic Displacement of Cu by Pt 4+ Ions and Their Application as Electrocatalysts for Oxygen Reduction Reaction in Fuel Cells. *The Journal of Physical Chemistry C* **114,** 4725–4732 (2010).

8. EnyuSun, Z. *et al.* Rapid and Surfactant-Free Synthesis of Bimetallic Pt−Cu Nanoparticles Simply via Ultrasound-Assisted Redox Replacement. (2012).

9. Mohl, M. *et al.* Formation of CuPd and CuPt Bimetallic Nanotubes by Galvanic Replacement Reaction. *Mechanical Engineering* 9403–9409 (2011).

10. Wei, X., Wang, A.-Q., Yang, X.-F., Li, L. & Zhang, T. Synthesis of Pt-Cu/SiO2 catalysts with different structures and their application in hydrodechlorination of 1,2-dichloroethane. *Applied Catalysis B: Environmental* **121-122,** 105–114 (2012).

11. Pacioni, N. L., Filippenko, V., Presseau, N. & Scaiano, J. C. Oxidation of copper nanoparticles in water: mechanistic insights revealed by oxygen uptake and spectroscopic methods. *Dalton transactions (Cambridge, England : 2003)* **42,** 5832–8 (2013).

12. Gracia, F., Wolf, E. E., Miller, J. T. & Kropf, A. J. EXAFS Studies of the Poisoning Effect of Cl on Pt / Al 2 O 3 Catalysts during Oxidation Reactions. 1–2

13. Hinshaw, J. V. The Flame Ionization Detector. *LCGC North America* Volume 23, Issue12 (2005).

14. Regalbuto, J. *Catalyst Preparation: Science and Engineering*. (2006).

Table 2.1 Precursors and reagents

Element or Compound	Precursor	Source

Cu	Copper nitrate trihexahydrate, 99.99%	Johnson Matthey
Pt	Tetraamine platinum(II) nitrate, 99.995%	Sigma Aldrich
Pd	Palladium nitrate hydrate, 99.9%	Sigma Aldrich
γ-Al_2O_3	Aluminum oxide, ultra-pure grade, 99.99%	Inframat Advanced Materials
PVP	Poly(vinylpyrrolidone) MW=40,000-80,000	Alfa Aesar
$NaBH_4$	Sodium Borohydride, ≥98%	Sigma Aldrich
C_6H_8O	L-ascorbic acid, reagent grade	Sigma Aldrich
$AgNO_3$	Silver nitrate, ACS reagent, 99.0%	Sigma Aldrich
$CH_3(CH_2)_4CH_3$	n-hexane, anhydrous, 95%	Sigma Aldrich
C_6H_5CCH	Phenylacetylene, 98%	Sigma Aldrich

Table 2.2 Redox potentials of relevant species to the standard hydrogen electrode (SHE)

Half Reaction	**E^0 (V) vs SHE[(a)]**
$Cu^{2+} + 2e^- \leftrightarrow Cu_{(s)}$	+0.340

$Pt^{2+} + 2e^- \leftrightarrow Pt_{(s)}$	+1.188
$Pd^{2+} + 2e^- \leftrightarrow Pd_{(s)}$	+0.915

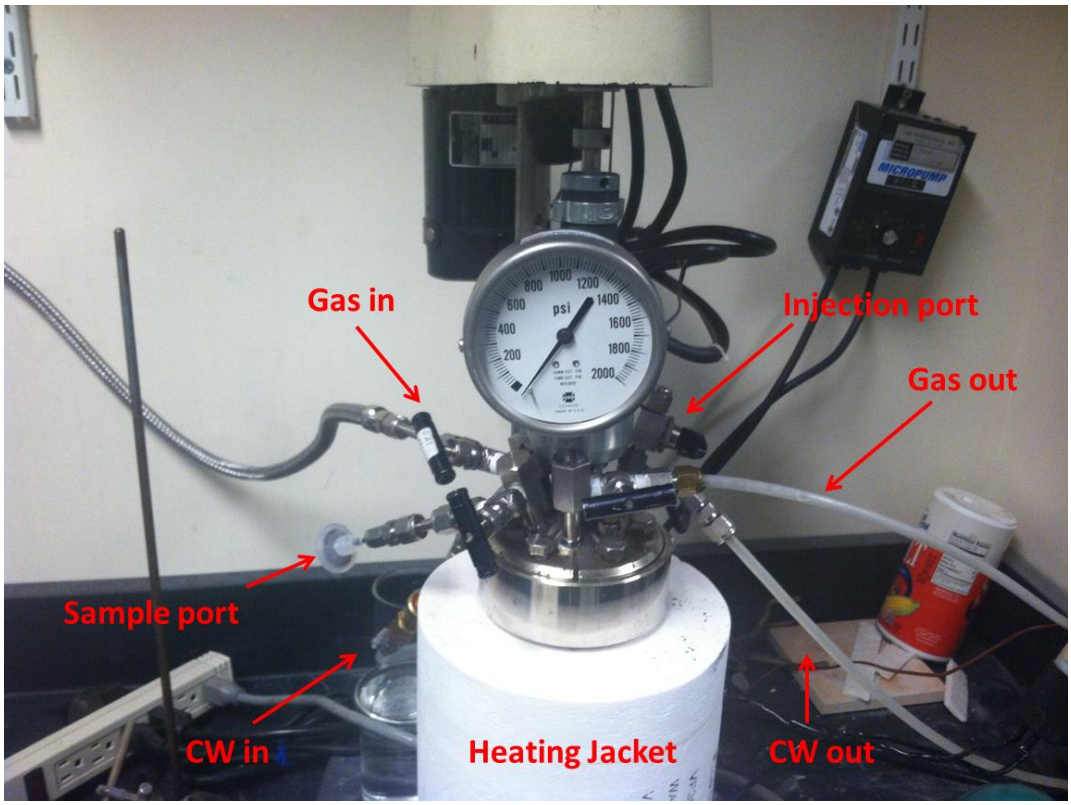

Figure 2.1 High pressure liquid batch reactor system

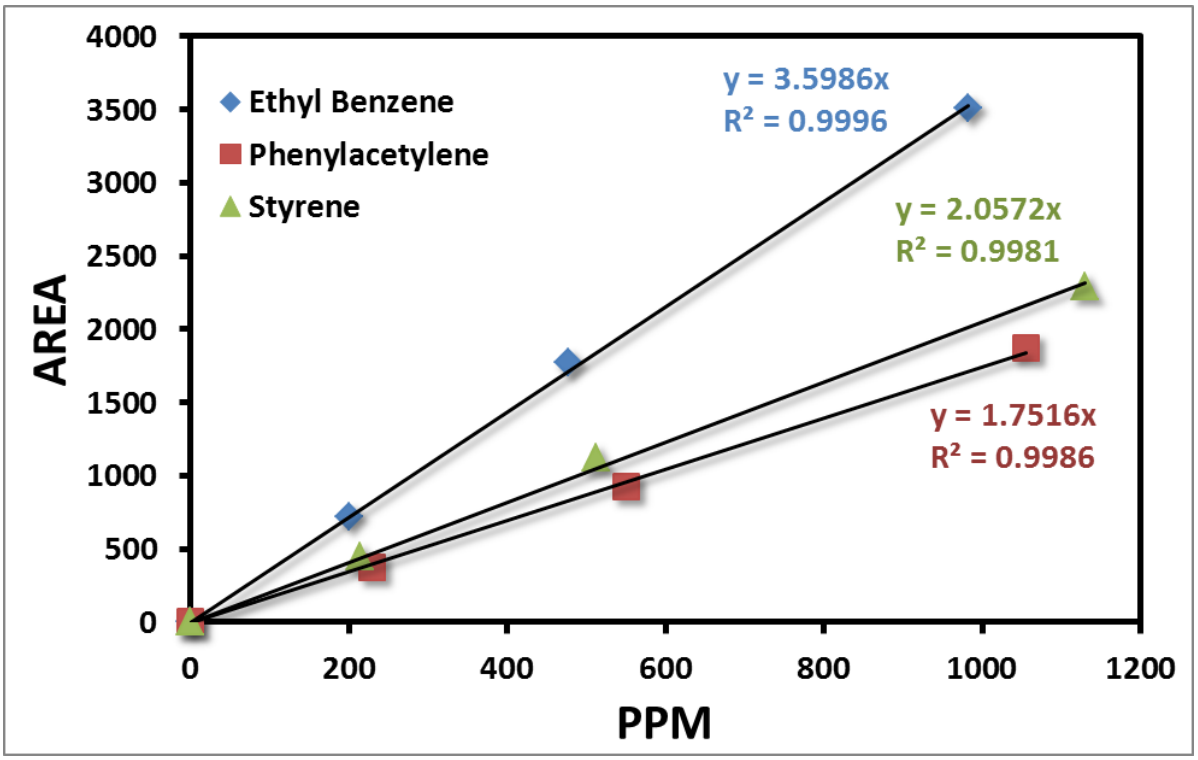

Figure 2.2 GC calibration curves for phenylacetylene, styrene and ethyl benzene. The slope of each line is equal to the calibration used.

Chapter 3 – Characterization of Materials

3.1 Choice of preparation technique

A simple and widely used method to prepare bimetallic alloy catalysts of Pt-Cu and Pd-Cu is through co-impregnation followed by reduction treatment.[1,2,3] However, this method does not allow control over the surface composition/structure and leads to non-uniform particle size distribution. Therefore, the choice of synthesis method is of great importance in order to design the final structure of a bimetallic catalyst which will determine its electronic/geometric properties, and hence its catalytic activity and selectivity.

The fabrication of metal nanoparticles in the 1-10nm regime through colloidal chemistry, is a versatile method used to control the size and shape of the nanoparticles. This is also identical to the sizes of the heterogeneous metal catalysts used in industry. Advances in nanoscience allow the extension of model studies on single crystal metal surfaces to nanoparticles with controlled shape and sizes hence "bridging the gap" between crystal surfaces and the nanomaterials that are used in industry.[4,5]

The copper nanoparticles were prepared in the absence of the Al_2O_3 support in order to avoid any electrostatic interactions between the organometallic precursor and the support.[6] After immobilization of the colloidal nanoparticles onto the support, the material was calcined in air to burn off the organic ligands. However, this step resulted in the surface oxidation of the Cu which

in turn had to be reduced to its metallic state. After reduction of the nanoparticles, GR was determined to be an appropriate technique to deposit the precious metal onto the copper surface without having to undergo severe heat treatments in air. Since GR is based on the reduction potential of the metal/metal ion, the exchange reaction occurs in a stochastic fashion, meaning that the Pt/Pd species are most likely well dispersed.

3.2 Particle size and distribution

The as-prepared PVP encapsulated Cu colloidal nanoparticles before immobilization onto the Al_2O_3 support are shown in **Figure 3.1**. A portion of the colloidal solution was directly deposited onto a TEM grid and imaged. The average particle size was measured to be approximately 3.4 +/- 0.9 nm, with a narrow size distribution from a total count of 300 particles, as shown in **Figure 3.2**. Lattice resolved images were obtained for the Cu nanoparticles of **Figure 3.1** which can be seen in **Figure 3.3**. The lattice spacing of the Cu nanoparticle (d=0.21 nm) was calculated from the high resolution images and corresponds to the interplanar spacing of the low-index Cu(111) surface.[7]

The alumina supported Cu nanoparticles are shown in **Figure 3.4**. Some of the supported Cu nanoparticles that are distinguishable from the support are outlined in the figure. The supported Cu nanoparticles were approximately 5.1 +/- 1.2 nm with a narrow size distribution as shown in **Figure 3.4**. Comparison of the nanoparticles formed in solution and the ones immobilized and dried shows that there was almost no change in the particle size after the

immobilization and drying step. Due to the low *z*-contrast of Cu, atomically resolved images were not obtained for the supported nanoparticles.

3.3 Reducibility of copper nanoparticles and sintering

The oxidation state of the Cu nanoparticles was also taken into consideration, to ensure that the Cu nanoparticles were in their metallic state during reaction conditions and before GR. Temperature programmed reduction (TPR) of the nanoparticles was done under H_2 and CO flow monitored by a thermal conductivity detector (TCD) and by mass spectroscopy.

In **Figure 3.5(a)** is the H_2 TPR of the Cu nanoparticles supported on alumina and the signal corresponds to the reduction of oxygen species and formation of H_2O monitored by TCD. From the plot it is evident that the reduction peaked at 180 ^oC and complete reduction of the Cu nanoparticles occured at 210 ^oC. As described in Chapter 2, the copper precursor was reduced in excess of $NaBH_4$ with ascorbic acid which should prevent the formation of bulk CuO nanoparticles and it has also been reported that bulk CuO reduces at temperatures above 200 ^oC.[8] This is evidence to conclude that bulk CuO nanoparticles were not formed but rather that this reduction feature is due to the formation of CuO during the calcination step. The formation of oxygen species was verified by CO-TPR which is shown in **Figure 3.5(b)**; the signal in this case corresponds to CO_2 formation which was monitored by mass spectroscopy. The reduction in this case peaks at 150 ^oC which could be due to the small difference in reduction potential between H_2 and CO. There was no formation of H_2 or H_2O which would be indicative of activated bound

OH species on the surface of the support. Based on these results, the reduction temperature of the nanoparticles was set at 250 ^{o}C to ensure complete reduction of the Cu species.

Another method used to characterize the reducibility and oxidation state of the copper nanoparticles was XRD which is shown in **Figure 3.6**. The red line corresponds to the diffraction peaks after calcination of the Cu nanoparticles and the blue line shows them after being reduced to 250 ^{o}C for 1 hr. The XRD data confirm the Cu nanoparticles are in their metallic state after reduction treatment in H_2. This is evident from **Figure 3.6(a)** where there is formation of Cu(111) and Cu(200) peaks at 2θ = 66.5 and 78.7 respectively, after the sample is reduced. These results further confirm there is no formation of bulk CuO nanoparticles and that there is no bulk phase CuO present in the pre-reduced sample after storage for several days in vacuum. **Figure 3.6(b)** emphasizes the reduction of CuO to Cu, and the difference between the CuO and Al_2O_3 at peaks 2θ = 53.6 and 53.2 respectively.

To obtain an estimation of the Cu nanoparticle size after thermal treatment in air to 300 ^{o}C to remove the PVP, the Scherrer formula was applied to the XRD data. In a diffractogram, the Scherrer equation relates the width of a peak at half maximum height, to the nano crystallite size.[9] It is applicable to nano-scale particles under 100 nm with a narrow size distribution for approximating the particle size,[10] and the equation is shown below:

$$D = \frac{K \cdot \lambda}{\beta \cdot \cos\theta}$$

where D is the average particle size, K is a constant related to the crystallite shape, λ is the X-ray wavelength in nm, β is the peak width of the diffraction peak profile at half maximum height in radians. From the Scherrer equation an average particle size of approximately 13 nm

was calculated from the diffractogram in **Figure 3.6(b)** for the CuO nanoparticles. To confirm this result, CO chemisorption measurements were done on the same sample assuming a stoichiometry of CO:Cu = 1. The resulting dispersion was 6.5% corresponding to a nanoparticle size of 15nm. From these calculations, it is evident that there was an increase in the Cu nanoparticle size due to the calcination of the sample.

In order to quantify the amount of CuO species that are reduced during the TPR, the peak in **Figure 3.5(a)** is integrated based on the TCD calibration of the Autochem Analyzer for H_2. The measured amount of H_2 is equal to 1.455 cc for 0.1 g of sample that was used in STP conditions. By converting the mol of H_2 into mol of O_2 by a ratio of H_2:O_2 = 0.5, the total amount of oxygen removed from the surface is calculated. Assuming a particle size of 15 nm and spherical geometry for the shape of the nanoparticles, it is estimated that approximately 41% of the copper on the surface is present as CuO.

3.4 Deposition of Pt and Pd by galvanic replacement (GR)

The UV-Vis data confirms the success of the GR preparation in order to synthesize the bimetallic nanoparticle catalysts. After reduction treatment, the Cu nanoparticles were in their metallic state, Pt and Pd were exchanged onto the surface of the nanoparticles through GR which was described in the experimental section. For the UV-Vis experiments, standard solutions of Pt, Pd and Cu were prepared with the same concentration as the filtrate solution that was obtained after GR. UV-Vis spectra were obtained for these three solutions (GR filtrate, Pt/Pd standard, Cu standard) in both preparations with Pt and Pd. On **Figure 3.7(a)** are the results for the Pt-Cu

system and the different solutions are noted on the figure. From this figure it is evident that complete uptake of Pt occurred which by the disappearance of the Pt^{2+} shoulder at around 300 nm. Muhler and co-workers[11] who also prepared Pt-Cu nanoparticles by GR, observed Cu ions released in the filtrate solution after GR. Typically, aqueous solutions containing Cu^{2+} species have a characteristic broad adsorption band in the range of 600-800 nm.[12] The concentration of $(NH_4)_4Pt(II)(NO_3)_2$ in the filtrate solution was expected to be 5.5 10^{-3} M which was the concentration prepared for the Pt^{2+} and Cu^{2+} standard solutions. The inset on **Figure 3.7(a)** shows the normalized absorption bands of the GR filtrate and the Cu^{2+} standard in order to compare the two samples. There is a measurable amount of Cu^{2+} in the filtrate solution which confirms that GR is occurring. It is important to note that the relative intensity of the Cu^{2+} absorption band of the GR filtrate is lower than that of the Cu^{2+} standard solution. This lower intensity could be attributed to Cu species re-adsorbing onto the metal nanoparticles. An experiment was done with the Pt precursor in solution with the γ-alumina support in order to confirm that there was no uptake onto the support. Since there is complete uptake of Pt observed by the signal at 300 nm, this lower intensity could be attributed to Cu species re-adsorbing.

The same experiment was done with Pd-based catalyst and the results can be seen in **Figure 3.7(b)**. The preparation of the $Pd_{0.18}Cu_{15}/Al_2O_3$ sample was done in a larger amount of solution, hence the concentrations of the Pd^{2+} and Cu^{2+} species in solution were much lower (3.75 10^{-4} M). For this reason the Cu^{2+} was not visible in the filtrate solution. In this case, the concentrations of the active metals used for GR are lower than the concentrations used by Muhler and co-workers[11] which may make them harder to detect in the GR filtrate by UV-Vis. To confirm the adequacy of GR, the concentration of Pd in solution before GR was increased by a factor of 5, corresponding to 1.875 10^{-3} M of Cu^{2+}, and the preparation was repeated to

examine if the exchange reaction occurs. From the inset on **Figure 3.7(b)**, the normalized absorption bands from the Cu^{2+} standard solution and the GR filtrate are shown and compared for the higher concentration. Again in this case it was confirmed that there was no uptake of Pd onto the alumina support and the smaller intensity of Cu^{2+} ions in solution could be from re-adsorption of Cu. An overall lower intensity of the GR filtrate was also observed by Muhler and co-workers. [REF]

In both cases it is evident that there is complete uptake of Pt/Pd by disappearance of the corresponding absorbance band. The Cu^{2+} ions released in solution indicate that the exchange reaction occurred successfully.

3.5 Characterization of Bimetallic Catalysts

3.5.1 Surface Characterization of Pt-Cu

The XPS results for $Pt_{0.25}Cu_{15}/Al_2O_3$ and $Pt_{0.25}/Al_2O_3$ are shown in **Figure 3.8**. All of the samples were pre-reduced at 400 ^oC for 6 hr in 100% H_2 flow and then deposited onto the copper foil for analysis. It is most common for Pt samples that the $4f_{7/2}$ lines are examined in XPS but there is an overlap with the Al 2p lines at those binding energies. Especially at low Pt loadings the interference does not allow the accurate measurements in this region. Therefore, the Pt $4d_{5/2}$ was measured to evaluate the chemical states of Pt in the samples.

In **Figure 3.8** the blue line corresponds to signal from the $Pt_{0.25}Cu_{15}/Al_2O_3$ bimetallic sample and the black line is representative of the impregnated $Pt_{0.25}/Al_2O_3$. It is interesting to

note that the peak of $Pt_{0.25}/Al_2O_3$ has a binding energy of 315.3 eV which corresponds to Pt^{2+}.[13] A lot of work and discussion has stemmed from the effort to understand the interaction of Pt/Al_2O_3 as well as with other oxide supports. In the case of $Pt/\gamma\text{-}Al_2O_3$, Kwak et al.[14] have suggested that coordinatively unsaturated Al^{3+} centers on the surface of $\gamma\text{-}Al_2O_3$ served as anchoring sites for the formation of PtO based structures. They also concluded that this strong interaction between PtO and the Al^{3+} centers retains the Pt atomically dispersed for low loadings (<1wt%). Other reports have also concluded that low loadings of $Pt/\gamma\text{-}Al_2O_3$ exhibit different/unusual properties than those of bulk Pt. Supported $Pt/\gamma\text{-}Al_2O_3$ nanoclusters were studied by Vila et al.,[15] through DFT, molecular dynamics (MD) and X-ray spectroscopy. They theoretically evaluated fluctuating cluster-substrate interactions and charge transfer phenomena which were correlated to positive energy shifts experimentally observed with decreasing nanoparticle size and temperature. Another report by Behafarid et al.[16] examined the electronic properties and charge transfer effects of different Pt nanoparticles on $\gamma\text{-}Al_2O_3$ with XANES and also detected positive energy shifts. The Pt nanoparticles were prepared with different shapes (2D, 3D structures) and sizes (0.8 – 5.4 nm) in order to independently asses the influence of H_2 adsorbates and nanoparticle-support interactions with the electronic properties of the Pt particles. Specifically, larger positive energy shifts were observed for the smallest particles with the highest contact area with the support. All of these analyses converge to the same conclusion that highly dispersed Pt supported on $\gamma\text{-}Al_2O_3$ has a positive energy shift due to interaction with the support. To verify the dispersion of the $Pt_{0.25}/\gamma\text{-}Al_2O_3$ sample, CO chemisorption was conducted after pre-treatment in H_2 to 400 ^oC and 100% dispersion was measured which is equivalent to a particle size of less than 1 nm. These references in combination with the dispersion measurement provide justification to the fact that the impregnated monometallic Pt sample is shifted to higher

binding energy which in this case overlaps with the Pt^{2+} binding energy which could be attributed to a PtO bond.

The XPS peak of the $Pt_{0.25}Cu_{15}/Al_2O_3$ bimetallic sample lines up exactly to the binding energy of the Pt foil at 314.2 eV.[13] Previous XPS studies by Lee et al.[17] on Cu-Pt alloys with various Cu:Pt ratios show practically zero core-level peak shift for Pt $4f_{7/2}$ as a function of Pt concentration. The analysis also indicates that there is no charge transfer into the Pt d-band of Cu-Pt alloys, which they suggest may be main reason why Pt does not display a measureable core-level shift. Other spectroscopy done by Cho et al.[18] also found a negligible shift in the Pt $4f_{7/2}$ peak for Cu-Pt alloys with varying concentrations. Even though the observed peak in this case is Pt $4f_{7/2}$ the trend should be the same for the $4d_{5/2}$. In another report by Liao et al.[19] where γ-alumina supported bimetallic Cu-Pt catalysts are prepared by co-impregnation, they observe no measureable shifts for the Pt $4d_{5/2}$ peak and suggest that Pt species are present in their metallic state. A different study by Neergat and Rahul[20] on unsupported core-shell Cu-Pt nanoparticles reported a shift in binding energy to lower values compared to a Pt standard. They attribute this shift to lower binding energy to electronic modification of the surface Pt by the inner Cu core. The fact that the Pt $4d_{5/2}$ peak is located at the position of metallic Pt and furthermore does not overlap with the peak observed for the monometallic sample is strong indication of alloy formation on the surface of the nanoparticles. It is important to note that the Cu-Pt particles were indeed core-shell structures having a much larger surface concentration of Pt compared to the sample in this work and which could display different electronic properties due to the different structure. In our case, the Pt species on the surface of the nanoparticles have replaced the Cu species and are most likely embedded into the Cu lattice forming a bimetallic surface alloy.

Further evidence of alloy formation could be derived by examination of the Cu 2p XPS spectra shown in **Figure 3.9**. It has been shown by various sources that there is a negative shift in the Cu 2p binding energy in Cu-Pt alloys. Specifically, for a surface concentration of approximately 10% Pt there should be an observable negative energy shift by 0.3 to 0.4 eV, to lower binding energies.[17,18] In **Figure 3.9** the black dotted line corresponds to the peak of the bimetallic $Pt_{0.25}Cu_{15}/Al_2O_3$ sample and the blue dotted line corresponds to the peak for metallic Cu. By carefully examining the peak, there is an evident shift of approximately -0.4 eV which can be attributed to this surface alloy formation of Cu-Pt. It is also important to note that there is a presence of CuO species on the bimetallic sample which are measured through the XPS. This is most likely due to the brief exposure of the sample to air.

From the survey scan of the XPS data on the $Pt_{0.25}Cu_{15}/Al_2O_3$ sample it is found that the atomic ratio of Cu:Pt equals 9:1 on the surface of the nanoparticels, which is equivalent to 11.11at.??% surface content of Pt. While XPS is a surface technique, the signal can be representative of several atomic layers beneath the surface.[10,21,22] At the binding energy of Cu $2p_{3/2}$, the escape distance (λ), corresponding to the inelastic mean free path of an electron from Cu, is approximately 1 nm.[21,22] Based on the UV-Vis measurements presented in **Figure 3.7(a)**, which demonstrate complete uptake of the Pt and by assuming that all of the Pt is on the surface of the nanoparticle with a surface ratio of 9:1 (Cu:Pt), an estimation can be made for the size of the nanoparticles. By using simple spherical geometry for the shape of the Cu nanoparticles, **Figure 3.10** shows the Pt loading as a function of particle size. At a weight loading of 0.01 g of which corresponds to a total 0.25 at% and assuming that the XPS signal is representative of 3 Cu atomic layers deep, the average particle size is estimated to be ~12.5 nm. There is a small difference of 2.5 nm between this result and the particle size calculated by the Scherrer analysis.

These calculations are subject to an error in approximating the particle size but given the proximity of the two results, the conclusion can be made that there is certainly an increase in particle size after heat treatment. This calculation also confirms that all of the Pt species are detectable by XPS meaning that they are all present on the surface and most likely well dispersed. If a residual amount of Pt species (undetectable by UV-Vis) was left in solution after GR meaning that the actual loading was slightly lower than the expected there would be an increase in particle size based on this theoretical calculation, better justifying the result derived from the Scherrer equation.

3.5.2 Surface Characterization of Pd-Cu

The XPS results for $Pd_{0.18}Cu_{15}/Al_2O_3$ and $Pt_{0.18}/Al_2O_3$ are shown in **Figure 3.11**. All of the samples were pre-reduced at 250 ^oC for 2 h in 100% H_2 flow and then deposited onto the copper foil for the analysis. In **Figure 3.11**, the characteristic doublet peaks corresponding to Pd^0 (Pd $3d_{5/2}$ at 334.9 eV)[23] for the monometallic $Pd_{0.18}/Al_2O_3$ sample are in black color while the spectra for the bimetallic $Pd_{0.18}Cu_{15}/Al_2O_3$ are shifted to higher binding energies (Pd $3d_{5/2}$ at 335.6 eV) in blue. Pumice supported $Cu_{0.05}Pd_{1.5}$ bimetallic catalysts prepared by Guczi et al.[23] had the same observed positive energy shift as with the bimetallic catalyst in this work, after H_2 treatment at 298 K. However, after H_2 treatment to 623 K they observed a shift to a Pd 3d binding energy of 334.8 eV. This difference in binding energy is attributed to the partial oxidation of the Pd species by CuO prior to reduction and the interaction with the pumice support after reduction. Another XPS and TPR study of γ-alumina supported Pd-Cu catalysts reported by Batista et al.[24] concluded that both monometallic Pd and bimetallic Pd-Cu catalysts were present on the catalyst surface in their metallic state. An important observation made by

Batista et al.[24] in the same study, is that even after reduction treatment, Cu species on the surface of the catalyst become rapidly oxidized to CuO when exposed to air even for short time intervals. It is important to note that the oxidation of Cu nanoparticles exposed to air has also been observed in several other instances.[25] This means that exposure of the catalyst in air after H_2 reduction treatment would result in the partial oxidation of the coppersurface. The formation of CuO species would cause a partial oxidation of the Pd and hence a shift to slightly higher binding energies. This hypothesis can be supported by examining the Cu 2p XPS spectra for the bimetallic sample shown in **Figure 3.12**. Deconvolution of the Cu $2p_{3/2}$ peak into Cu^0 and Cu^{2+} was done by considering that the ratio of the satellite peak (943.3 eV) to the CuO contribution (934.6 eV) from the Cu $2p_{3/2}$ peak should be 0.4.[26] This results in approximately 40% of the Cu measured by XPS present as CuO while the remaining 60% is present as metallic Cu^0 (Cu 2p at 932.7 eV). The relative amount of CuO measured by XPS corresponds to a surface oxide for a 13 nm Cu nanoparticle. [21,22] These results are in agreement with those reported by Guczi et al.[23] for the pumice supported Pd-Cu catalysts and by Strohmeier et al.[26] for Cu/Al_2O_3. In conclusion, the shift in binding energy of the Pd $3d_{5/2}$ peak for $Pd_{0.18}Cu_{15}/Al_2O_3$ shown in **Figure 3.11** can be attributed to the partial oxidation of the Pd species by CuO and more importantly establish the fact that the Pd is alloyed with the Cu.

From the XPS survey scan an atomic ratio of 20:1 (Cu:Pd) on the surface of the nanoparticles is calculated. Similarly to the previous analysis for the Cu-Pt catalyst, calculations are done to estimate the nanoparticle size based on the assumptions that (i) the XPS signal is representative of about three Cu atomic layers, (ii) based on the UV-Vis measurements, there has been complete uptake of Pd onto the Cu, (iii) there is a 5% Pd surface coverage, and (iv) the nanoparticles are spherical. In **Figure 3.13**, the Pd loading is plotted as a function of nanoparticle

size, hence based on these calculations the nanoparticles should be approximately 16nm. Considering the proximity of this value to the nanoparticle size determined by the Scherrer equation it can be concluded that the Pd species exist on the surface of the copper nanoparticles and are well dispersed.

3.6 Summary

The successful preparation of surface alloy bimetallic Pt-Cu and Pd-Cu catalysts was demonstrated in this chapter. The PVP-encapsulated colloidal nanoparticles that were prepared and immobilized onto γ-Al_2O_3 support had a narrow size distribution of 5.1 +/- 1.2 nm. Lattice resolved images of the Cu nanoparticles have inferred that the surface of the nanoparticles in solution was predominately Cu(111). After immobilization, the Cu nanoparticles were calcined at 300 ^{o}C for 4 h to remove the organic ligand and the reducibility of the Cu was measured by TPR. XRD spectroscopy proved that after this calcination there were CuO species formed which after reduction disappeared. By applying the Scherrer equation to the diffractogram, an estimation of the sintering of the Cu nanoparticles was obtained. After reduction treatment, GR was employed as a method to synthesize bimetallic Cu-Pt and Cu-Pd surface alloy nanoparticles. To examine the success of the technique, UV-Vis measurements were used on the filtrate of the GR along with standard solutions of the precursors, which proved that the Pt and Pd exchanged with the Cu host metal in solution. In order to characterize the bimetallic nanoparticles XPS measurements were performed which yielded results about the successful alloy formation and the surface compositions. In order to confirm that the precious metal species were well dispersed onto the Cu host, theoretical calculations were applied using the surface composition measured

by XPS, and predicted that as a function of nanoparticle size, the Pt/Pd species were present on the surface of the nanoparticles in well-dispersed, possibly atomic state

3.7 References

1. Zheng, R. *et al.* Controlling hydrogenation of CO and CC bonds in cinnamaldehyde using silica supported Co-Pt and Cu-Pt bimetallic catalysts. *Applied Catalysis A: General* **419-420,** 126–132 (2012).

2. Veldurthi, S., Shin, C.-H., Joo, O.-S. & Jung, K.-D. Promotional effects of Cu on Pt/Al2O3 and Pd/Al2O3 catalysts during n-butane dehydrogenation. *Catalysis Today* **185,** 88–93 (2012).

3. Kugai, J., Miller, J. T., Guo, N. & Song, C. Oxygen-enhanced water gas shift on ceria-supported Pd–Cu and Pt–Cu bimetallic catalysts. *Journal of Catalysis* **277,** 46–53 (2011).

4. Somorjai, G. a, York, R. L., Butcher, D. & Park, J. Y. The evolution of model catalytic systems; studies of structure, bonding and dynamics from single crystal metal surfaces to nanoparticles, and from low pressure (<10(-3) Torr) to high pressure (>10(-3) Torr) to liquid interfaces. *PCCP* **9,** 3500–13 (2007).

5. Somorjai, G. a & Park, J. Y. Molecular factors of catalytic selectivity. *Angewandte Chemie (International ed. in English)* **47,** 9212–28 (2008).

6. Regalbuto, J. *Catalyst Preparation: Science and Engineering*. (2006).

7. Hansen, P. L. *et al.* Atom-resolved imaging of dynamic shape changes in supported copper nanocrystals. *Science* **295,** 2053–5 (2002).

8. Kundakovic, L. & Flytzani-Stephanopoulos, M. Reduction characteristics of copper oxide in cerium and zirconium oxide systems. *Applied Catalysis A: General* **171,** 13–29 (1998).

9. Singh, A. K. *Advanced X-ray Techniques in Research and Industry*. 594 (IOSPress, 2005).

10. Bergeret, G. & Gallezot, P. Handbook of Heterogeneous Catalysis, Chapter 3. 738–765 (2002).

11. EnyuSun, Z. *et al.* Rapid and Surfactant-Free Synthesis of Bimetallic Pt−Cu Nanoparticles Simply via Ultrasound-Assisted Redox Replacement. (2012).

12. Lacroix, L. B. *et al.* Electronic Structure of the Perturbed Blue Copper Site in Nitrite Reductase : Spectroscopic Properties , Bonding , and Implications for the Entatic / Rack State. **7863,** 7755–7768 (1996).

13. Shyo, J. Z. & Otto, K. IDENTIFICATION OF PLATINUM PHASES ON γ-ALUMINA BY XPS. *Applied Surface Science* **32,** 246–252 (1988).

14. Kwak, J. H. *et al.* Coordinatively unsaturated Al3+ centers as binding sites for active catalyst phases of platinum on gamma-Al2O3. *Science (New York, N.Y.)* **325,** 1670–3 (2009).

15. Vila, F., Rehr, J. J., Kas, J., Nuzzo, R. G. & Frenkel, A. I. Dynamic structure in supported Pt nanoclusters : Real-time density functional theory and x-ray spectroscopy simulations. 3–6 (2008). doi:10.1103/PhysRevB.78.121404

16. Behafarid, F. *et al.* Electronic properties and charge transfer phenomena in Pt nanoparticles on γ-Al2O3: size, shape, support, and adsorbate effects. *Physical chemistry chemical physics : PCCP* **14,** 11766–79 (2012).

17. Lee, Y., Lim, K., Chung, Y., Whang, C. & Jeon, Y. XPS core-level shifts and XANES studies of Cu – Pt and Co – Pt alloys. **478,** 475–478 (2000).

18. Cho, E. Unoccupied States and the Charge Transfer in Cu-Pt Alloys Studied by Bremsstrahlung Isochromat Spectroscopy and X-ray Photoelectron Spectroscopy. **31,** 323–328 (1997).

19. Liao, P. C. Activity and XPS Studies Catalysts Bimetallic. **316,** 307–316 (1982).

20. Neergat, M. & Rahul, R. Unsupported Cu-Pt Core-Shell Nanoparticles: Oxygen Reduction Reaction (ORR) Catalyst with Better Activity and Reduced Precious Metal Content. *Journal of the Electrochemical Society* **159,** F234–F241 (2012).

21. Cumpson, P. J. & Seah, M. P. Elastic Scattering Corrections in AES and XPS . II . Estimating Attenuation Lengths and Conditions Required for their Valid Use in Overlayer / Substrate Experimentss. **25,** 430–446 (1997).

22. Seah, M. P. & Dench, W. A. Quantitative Electron Spectroscopy of Surfaces: A standard database for electron inelastic mean free paths in solids. Vol. 1 (1979).

23. Guczi, L. *et al.* Pumice-Supported Cu – Pd Catalysts : Influence of Copper on the Activity and Selectivity of Palladium in the Hydrogenation of Phenylacetylene and But-1-ene. **462,** 456–462 (1999).

24. Batista, J., Pintar, A., Mandrino, D., Jenko, M. & Martin, V. XPS and TPR examinations of □ -alumina-supported Pd-Cu catalysts. **206,** 113–124 (2001).

25. Pacioni, N. L., Filippenko, V., Presseau, N. & Scaiano, J. C. Oxidation of copper nanoparticles in water: mechanistic insights revealed by oxygen uptake and spectroscopic methods. *Dalton transactions (Cambridge, England : 2003)* **42,** 5832–8 (2013).

26. Strohmeier, B. R., Leyden, D. E. & Field, R. S. Surface Spectroscopic Characterization of Cu / A1203 Catalysts. **530,** 514–530 (1985).

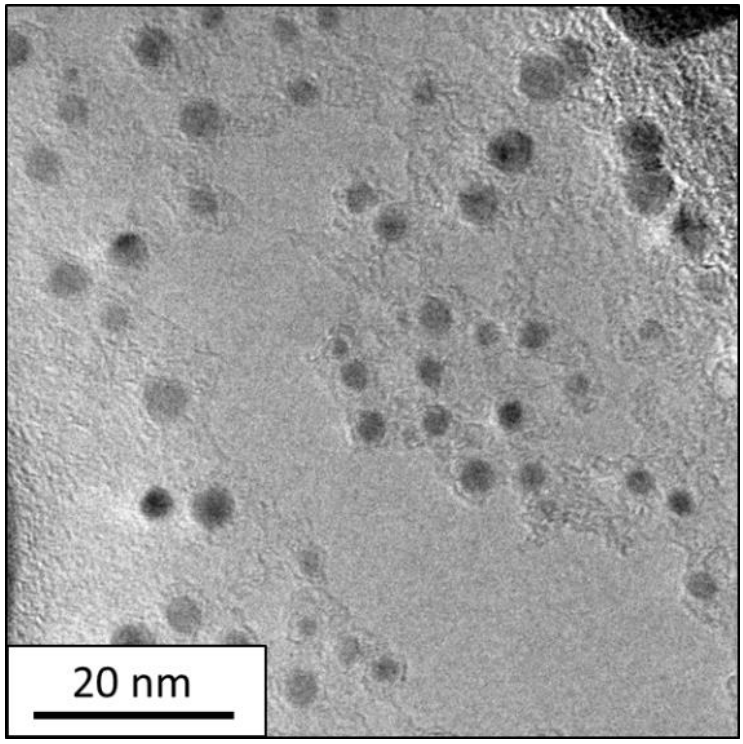

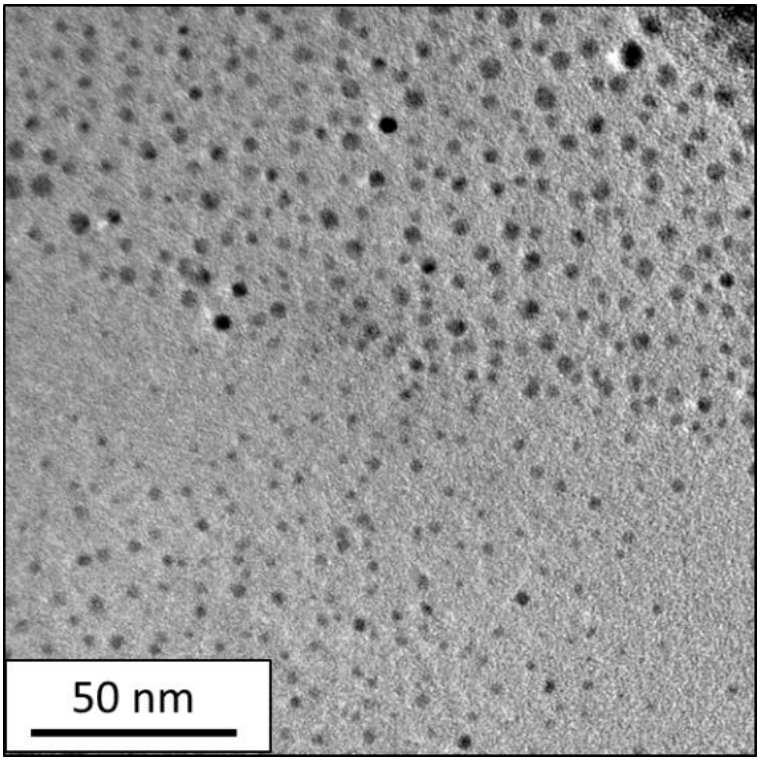

Figure 3.1 TEM images of PVP encapsulated Cu nanoparticles suspended in aqueous solution

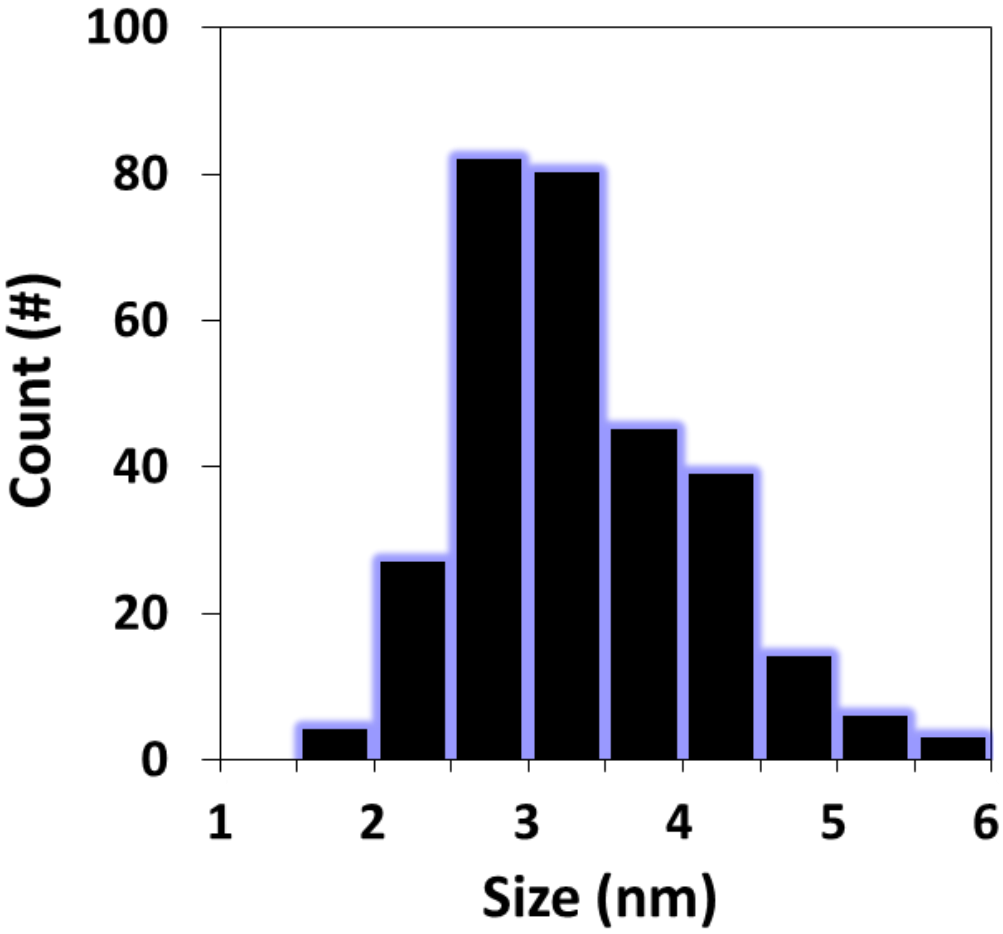

Figure 3.2 Particle size distribution for the PVP encapsulated Cu nanoparticles

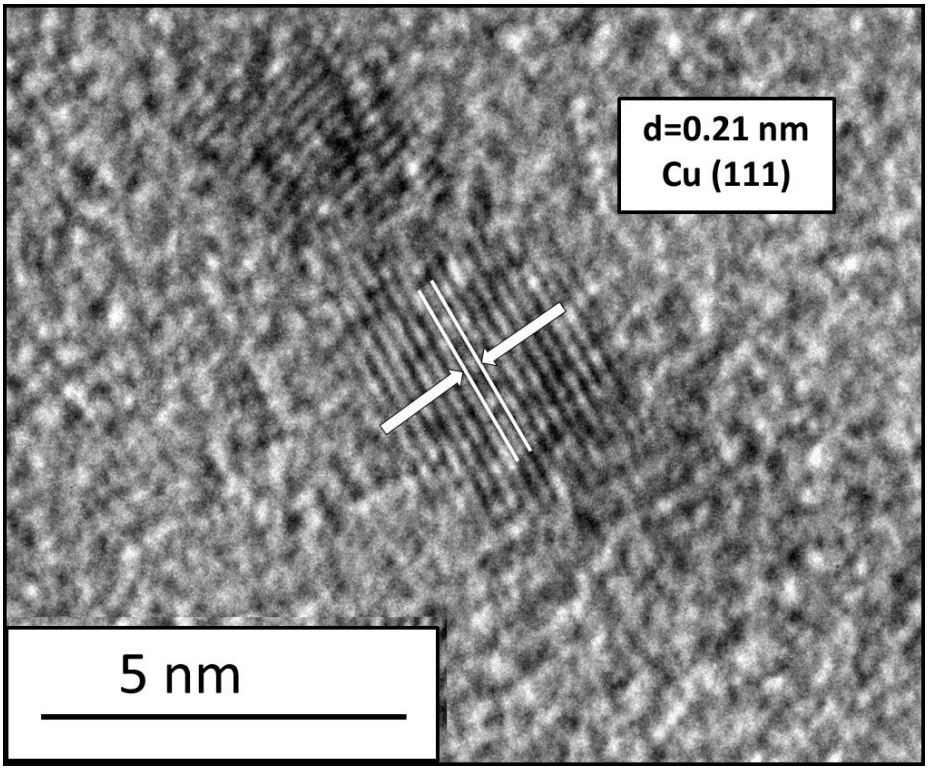

Figure 3.3 Lattice resolved image of Cu nanoparticles in solution by HR-TEM

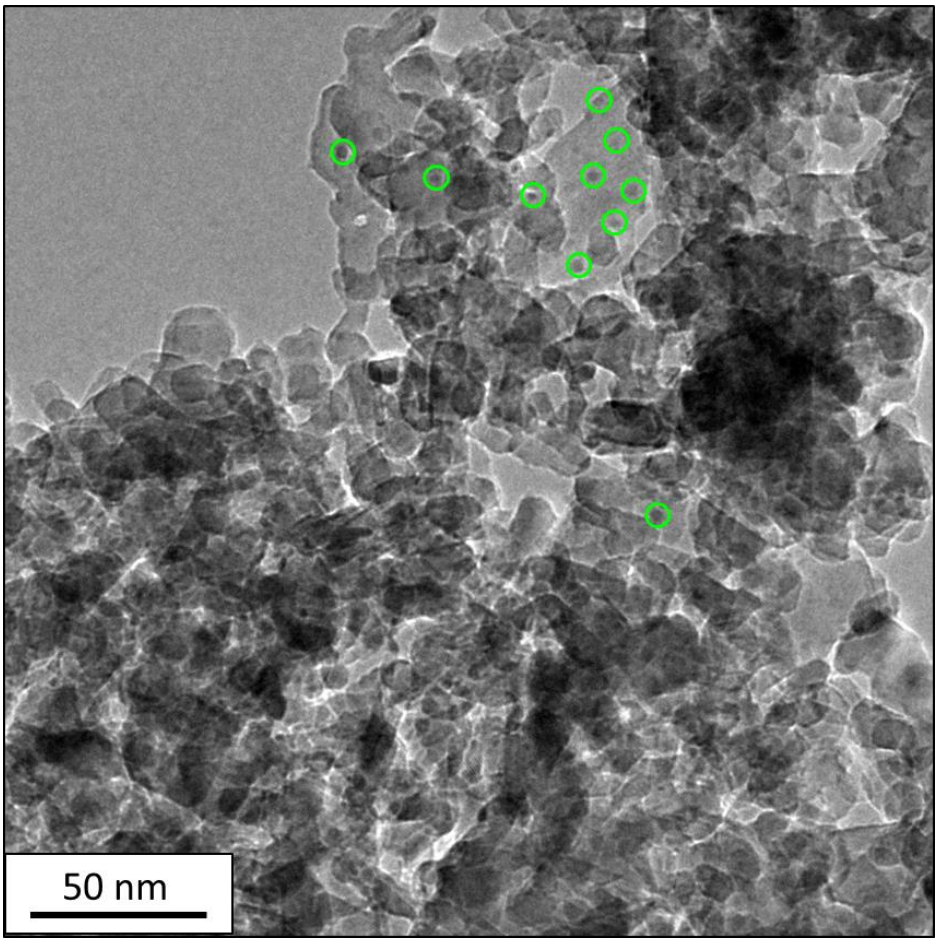

Figure 3.4 TEM image of alumina supported, PVP encapsulated Cu nanoparticles

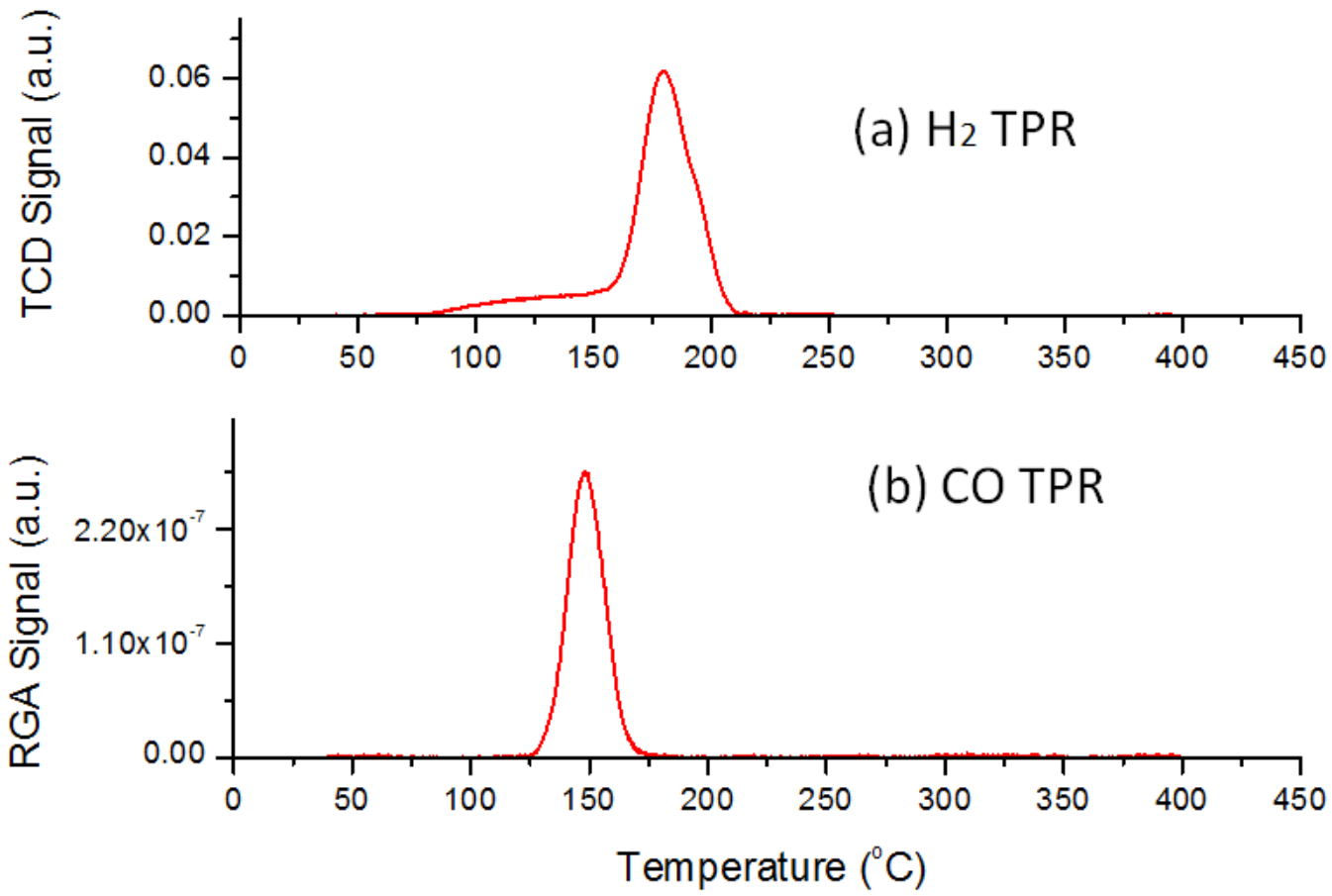

Figure 3.5 (a) H_2-TPR (b) CO-TPR of Cu nanoparticles

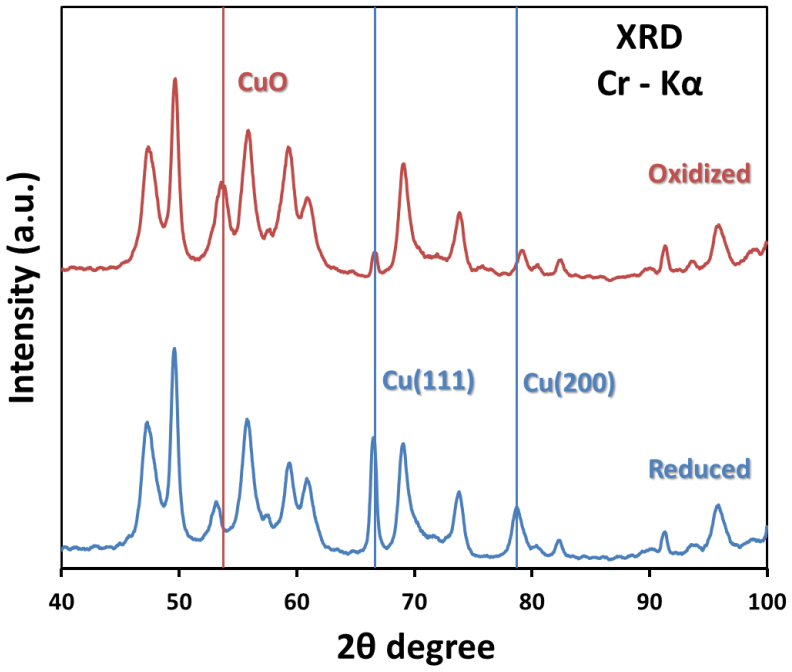

Figure 3.6(a): XRD data of Cu nanoparticles before and after reduction treatment

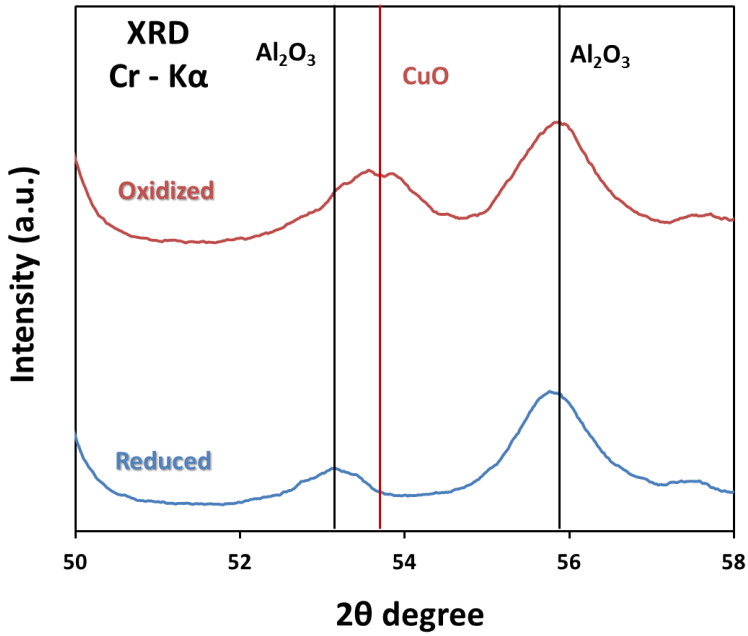

Figure 3.6(b): XRD data emphasizing the reduction of CuO species

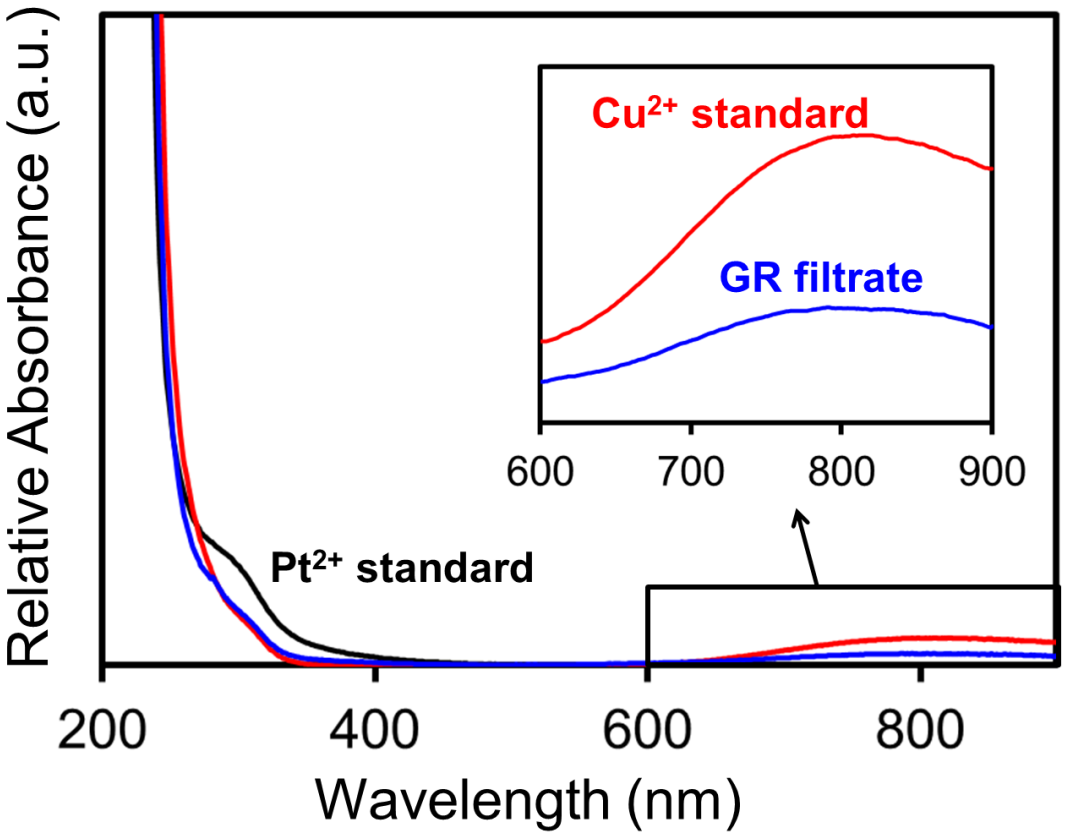

Figure 3.7(a): UV-Vis data of GR reaction with Pt

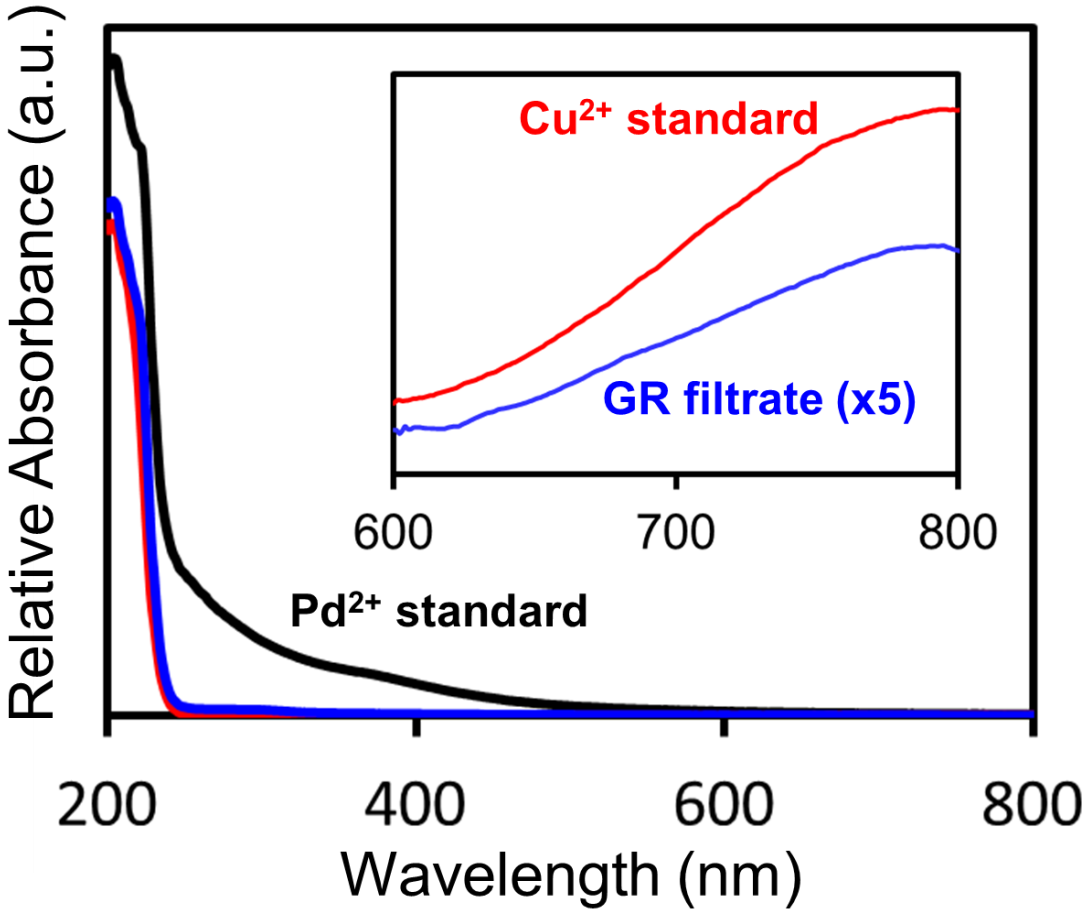

Figure 3.7(b): UV-Vis data of GR reaction with Pd

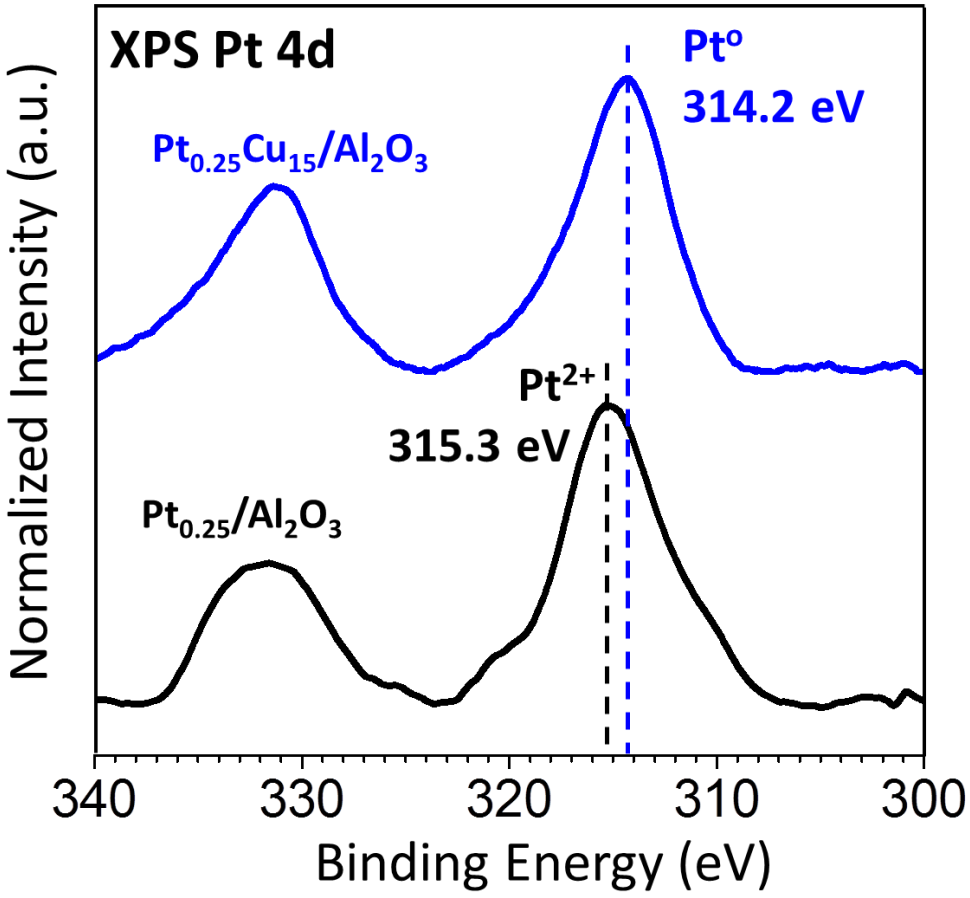

Figure 3.8 XPS spectra of Pt 4d for mono- and bimetallic samples

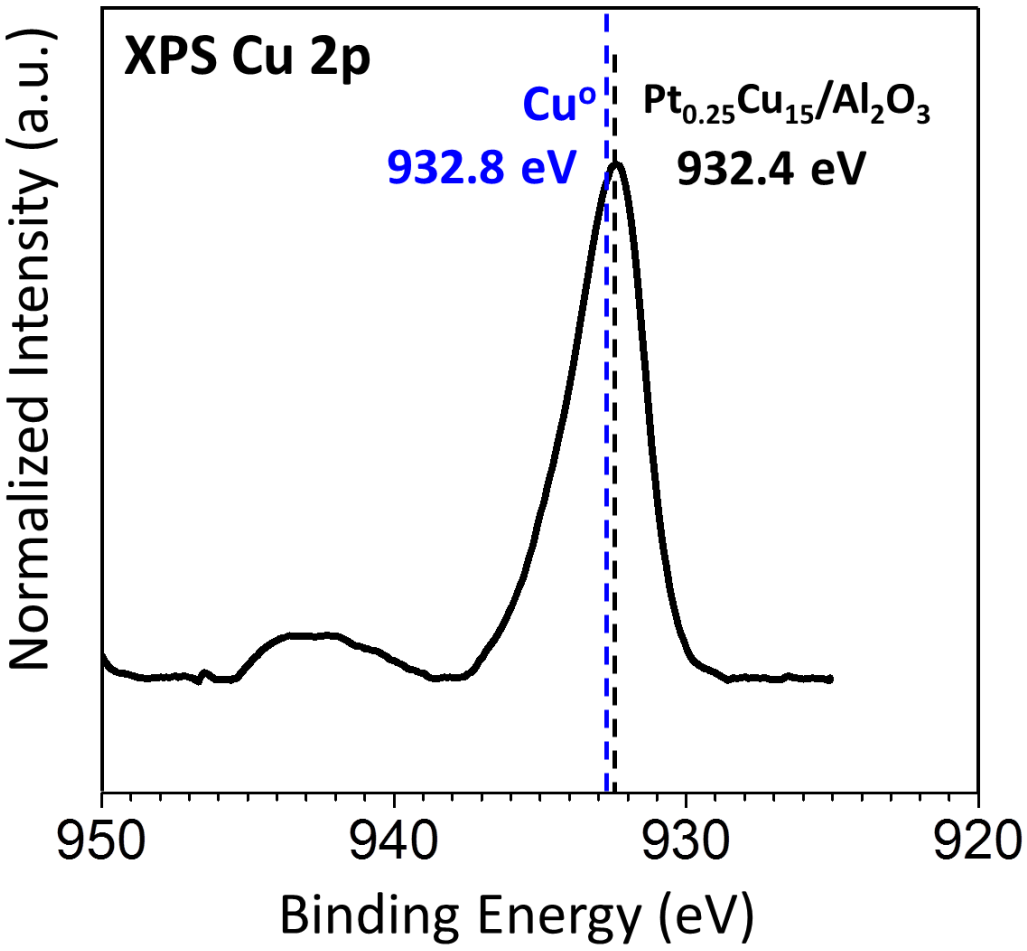

Figure 3.9 XPS spectra of Cu 2p of $Pt_{0.25}Cu_{15}/Al_2O_3$ sample

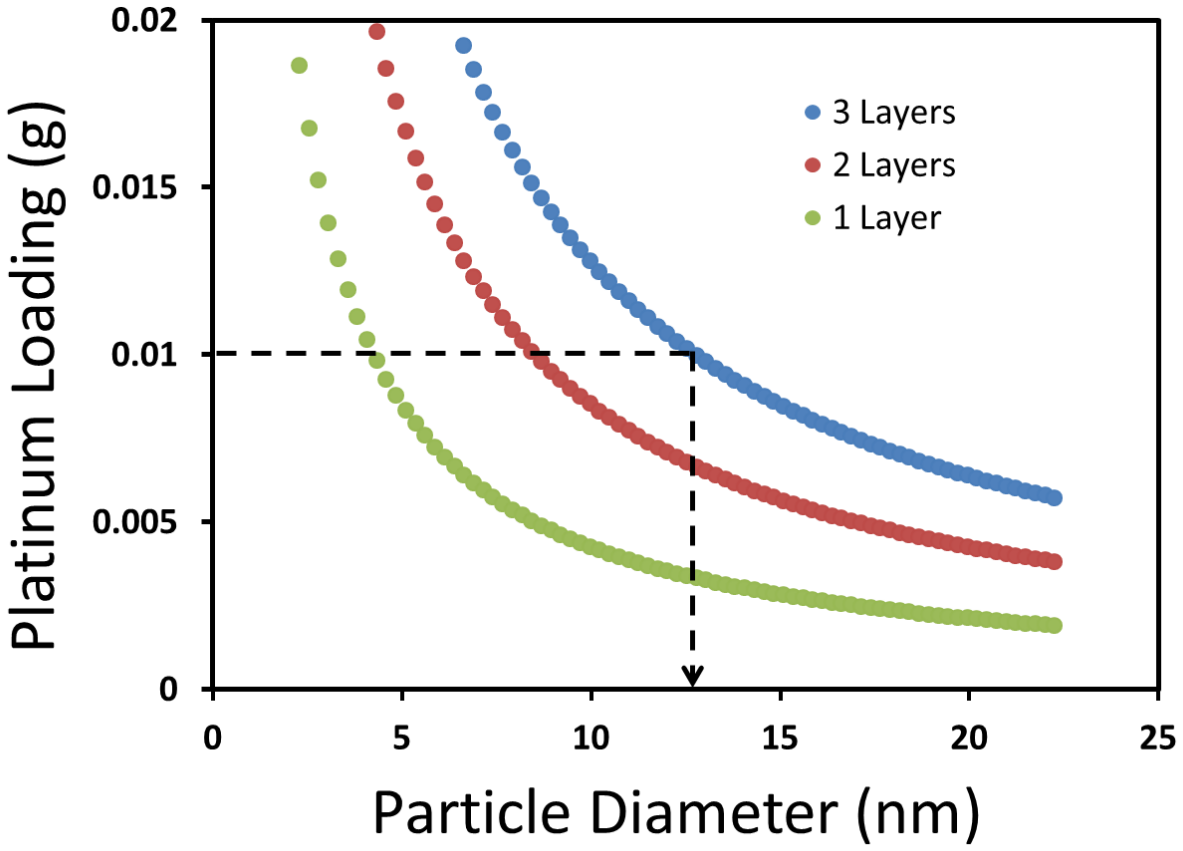

Figure 3.10 Pt loading as a function of nanoparticle size assuming a spherical geometry for Cu and 11% surface coverage of Pt

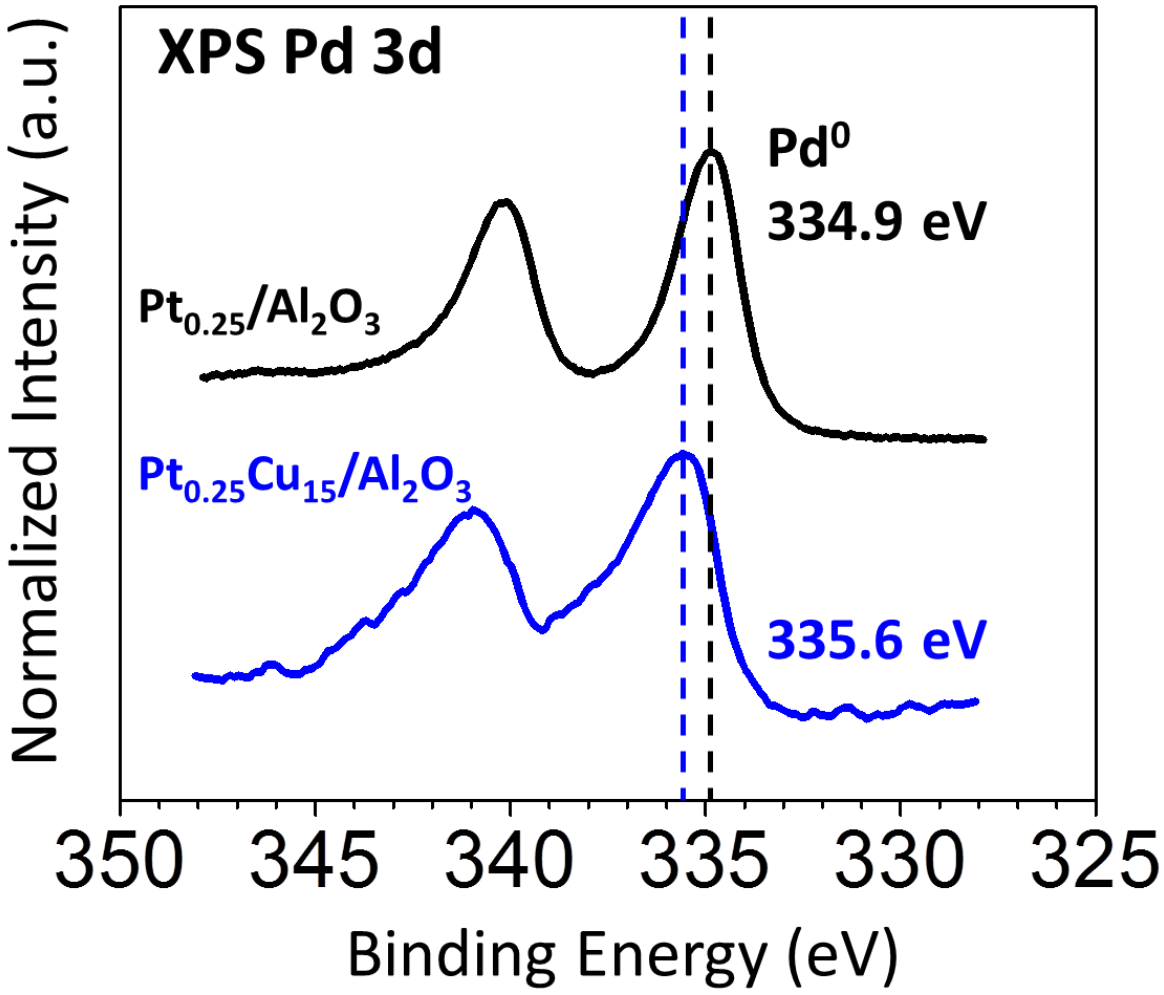

Figure 3.11 XPS spectra for Pd 3d for mono- and bimetallic samples

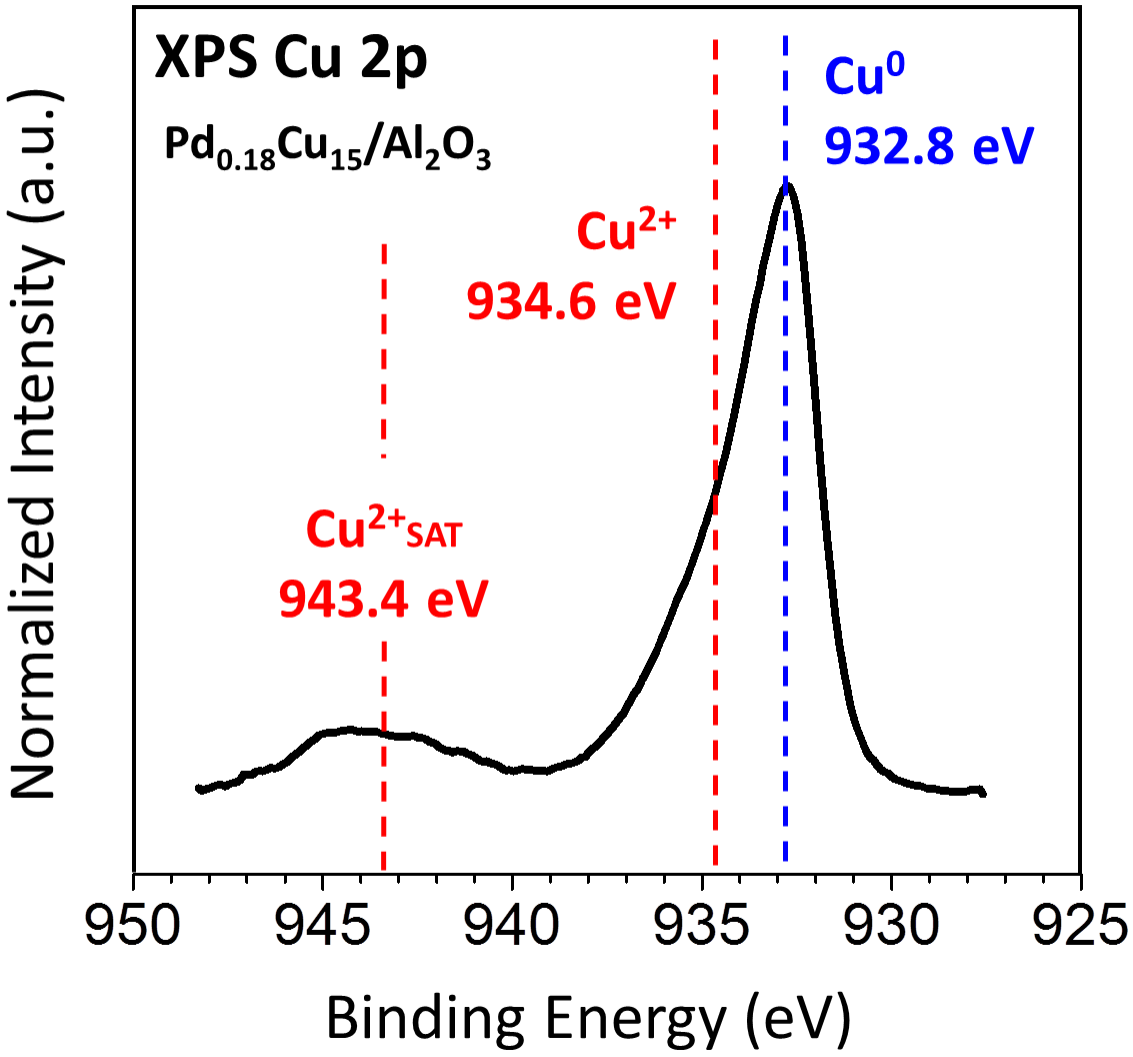

Figure 3.12 XPS for Cu 2p for $Pd_{0.18}Cu_{15}/Al_2O_3$ bimetallic sample

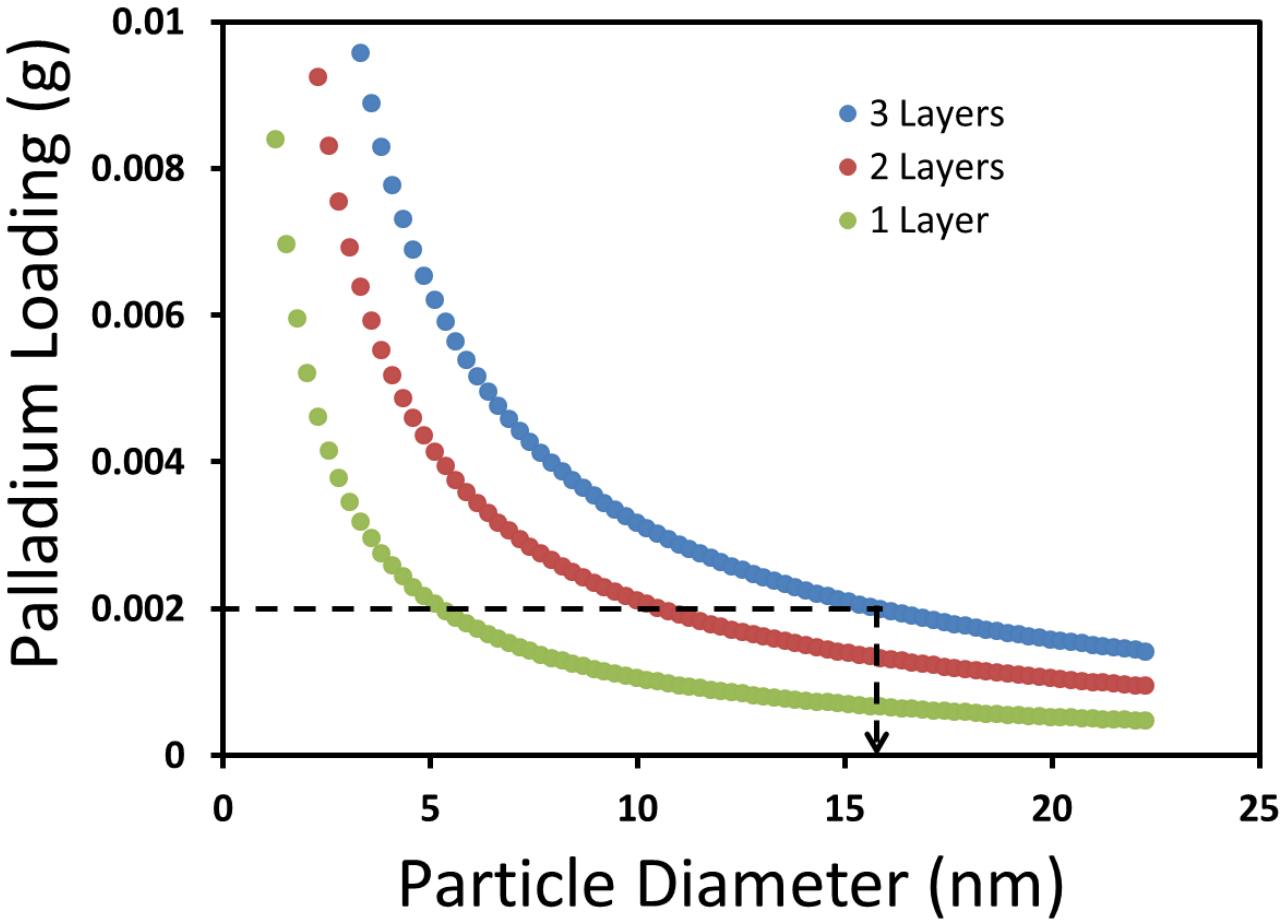

Figure 3.13 Pd loading as a function of nanoparticle size assuming a spherical geometry for Cu and 5% surface coverage of Pd

Chapter 4 – Catalytic Activity & Selectivity Measurements for Phenylacetylene Hydrogenation

4.1 Catalytic activity and selectivity measurements

4.1.1 Pt-Cu Catalysts

The Pt-based catalysts were all reduced in 100% H_2 flow at 400 ^oC for 6 hr, *in situ* prior to reaction. The amount of catalyst used was 0.3 g and the reaction mixture was 0.5 cc of phenylacetylene in 30 cc of n-hexane. In **Figure 4.1** the batch reactor data at 25 ^oC and 100 psi H_2 head pressure for phenylacetylene conversion and styrene selectivity are plotted as a function of time for the monometallic $Pt_{0.25}/Al_2O_3$ prepared by IWI. It is evident that the selectivity of Pt towards styrene is poor especially at high conversions. **Figure 4.2** shows the conversion and selectivity of the bimetallic $Pt_{0.25}Cu_{15}/Al_2O_3$ catalyst prepared by GR which is much more selective than the monometallic Pt catalyst. At 95% conversion the bimetallic $Pt_{0.25}Cu_{15}/Al_2O_3$ catalyst is at 77% selectivity while the monometallic Pt sample is at 45% selectivity for the same conversion. **Figure 4.3** is a time-independent plot of the selectivity as a function of conversion for the two samples. The comparison of selectivity at different conversions is more distinct between the two samples in this plot.

The hydrogenation of phenylacetylene on a commercial $Pt_{0.25}/\gamma\text{-}Al_2O_3$ has previously been investigated by Wilhite et al.,[1] over a range of temperatures, pressures and initial phenylacetylene concentrations. In order to make a comparison between our work and theirs, the initial rate of PA consumption is calculated at 100 psi and 45 ^oC with the same catalyst to

reactant ratio (0.5:1). Furthermore, the dispersion of the catalyst used by Wilhite et al. was measured to be 80 ± 5 % by H_2 chemisorption and was taken into account for normalizing the rate data. The initial rates were calculated and normalized by the surface Pt on each sample and are presented in **Table 4.1**. There is good agreement between the two rates, in our work the calculated result is $5.50\frac{mmol}{g_{Pt,surface}\cdot s}$ and the rate found by Wilhite et al. is equal to $5.00\frac{mmol}{g_{Pt,surface}\cdot s}$. The fact that these results are in such close proximity is a good indication that the results presented are reproducible.

4.1.2 Pd-Cu Catalysts

The Pd-based catalysts were all reduced in 100% H_2 flow at 250 ^oC for 2 hr, *in situ* prior to reaction. The amount of catalyst used was 0.1 g and the reaction mixture was 1 cc of phenylacetylene in 30 cc of n-hexane. **Figure 4.4** shows the time resolved batch reactor data at 25 ^oC and 100 psi H_2 of the the monometallic $Pd_{0.18}/Al_2O_3$ prepared by IWI and **Figure 4.5** has the bimetallic $Pd_{0.18}Cu_{15}/Al_2O_3$ prepared by GR. The monometallic $Pd_{0.18}/Al_2O_3$ has poor selectivity towards styrene, especially at high conversions the product distribution consists primarily of ethyl benzene. On the other hand, the bimetallic $Pd_{0.18}Cu_{15}/Al_2O_3$ catalyst maintains high selectivity towards styrene at all times; it has approximately 94% styrene selectivity at 90% conversion in comparison to $Pd_{0.18}/Al_2O_3$ with 62% selectivity at the same conversion. Hence, the $Pd_{0.18}Cu_{15}/Al_2O_3$ catalyst demonstrates a high selectivity towards styrene at high conversions. In **Figure 4.6** a time-independent plot, shows the selectivity as a function of conversion for the two catalysts.

Several Pd and Pd-based catalysts have been investigated for this reaction system. The initial rates per gram of catalyst in this case are comparable to previous reports for highly dispersed Pd catalysts. By utilizing the data measured by Jackson et al.[2] on a 1 wt% Pd/C catalyst prepared by IWI, in a liquid batch reactor at 20 ^{o}C and 29 psi hydrogen; the initial rate per gram Pd was calculated to be $13.56\frac{mmol}{g_{Pd}\cdot s}$. The initial rate per gram Pd calculated in our work for monometallic $Pd_{0.18}/Al_2O_3$ is $7.75\frac{mmol}{g_{Pd}\cdot s}$; hence these two normalized rate values are very similar. The 1 wt% Pd/C catalyst displays a slightly higher activity and a slightly higher selectivity (~83%) than the $Pd_{0.18}/Al_2O_3$ catalyst at 90% conversion. This could be attributed to the metal/support interaction of Pd/C since it is likely that there is a H_2 spillover effect from Pd onto the C surface which could be contributing the overall activity/selectivity of the material.[3] Furthermore, by comparison of the initial rates, normalized by g_{Pd}, between the bimetallic $Pd_{0.18}Cu_{15}/Al_2O_3$ with a $Pd_{0.6}Cu_{0.05}$/pumice catalyst have similar values as well. The values and the conditions for the initial rates from this work and others are comparable and are summarized in **Table 4.1**.

4.1.3 Discussion

From the results presented, it is clear that there is a marked improvement in the activity of Cu/Al_2O_3 for the hydrogenation of phenylacetylene with the addition of Pt or Pd to the nanoparticles. The bimetallic catalysts in both cases (Pt, Pd) show a significantly higher selectivity to styrene than their monometallic analogs at comparative conversions. These catalysts though ($Pt_{0.25}Cu_{15}/Al_2O_3$ and $Pd_{0.18}Cu_{15}/Al_2O_3$) also have a lower initial rate per gram

of precious metal compared to the monometallic catalysts. A loss in activity was also observed by Guczi et al.[4] for pumice supported $Pd_{1.5}Cu_{0.025}$, $Pd_{0.6}Cu_{0.05}$ compared to monometallic Pd catalysts; this decrease in activity was attributed to the dilution of Pd by Cu, while increased selectivity was claimed to be a result of the decrease in ensemble size needed for multiple (alkylidene) species. Similarly, Lonergan et al.[5] measured a lower rate for $Pt_{0.9}Cu_{8.1}/Al_2O_3$ prepared by IWI compared to $Pt_{0.9}/Al_2O_3$ for the hydrogenation of 1,3 butadiene in a flow reactor. They attempt to correlate the Pt/Cu surface and subsurface structures to the segregation and diffusion of surface atoms which might adsorb "surface species". Despite the lower activity, the bimetallic $Pt_{0.9}Cu_{8.1}/Al_2O_3$ in this work displays enhanced selectivity to produce butenes. In our case where Pt, Pd are the minority species on a Cu surface, and based on the model catalyst study by our group[6], it is expected that Pt and Pd act as sites for the uptake, dissociation and spillover of H_2 onto the Cu host, where the selective hydrogenation occurs. Consequently, a lower rate of phenylacetylene hydrogenation is anticipated compared to a catalyst where the hydrogenation takes place predominantly on the precious metal species.

There is a significant decrease in the rate and selectivity of $Pt_{0.25}/Al_2O_3$ catalyst compared to $Pd_{0.18}/Al_2O_3$ as well as for their corresponding bimetallic counterparts. From previous reports it has been well documented that Pd is a superior hydrogenation catalyst for unsaturated hydrocarbons compared to Pt in terms of activity and selectivity,[7,8] and specifically for the semihydrogenation of phenylacetylene.[9] The decrease in Pt selectivity compared to Pd, has been attributed to the strength of the Pt-alkene bond which is greater than that of the Pd-alkene bond, therefore the formed alkene intermediates are more stable increasing the probability of complete hydrogenation.[8,9] Basically, Pt has a smaller difference in the free energy of adsorption between alkynes and alkenes compared to Pd, allowing for the hydrogenation of both species. Despite the

lower rate and selectivity of the Pt based catalysts compared to Pd, the bimetallic $Pt_{0.25}Cu_{15}/Al_2O_3$ displays a significant increase in selectivity towards styrene compared to $Pt_{0.25}/Al_2O_3$ which can be attributed again to the H_2 spillover effect and reaction on the Cu.

4.2 Kinetic analysis

Obtaining information about the kinetics of the reaction system could reveal more insight about the active sites and other differences of the mono- and bimetallic catalysts. Reaction experiments were carried out for each material in the temperature range of 0 – 60 ^{o}C. Previous reports have suggested that the reaction order for this reaction at low conversion regimes (below 60%) is zero order.[2,10] This means that the initial rates are equal to the rate constant *k* at low conversions. The initial rates were calculated by plotting the mols of phenylacetylene consumed versus time (min), and the slope of the regressed line is equal to the initial rate. By utilizing the Arrhenious equation and linearizing:

$$k = Ae^{-\frac{E_a}{RT}} \Rightarrow \ln(k) = \ln A - \left(\frac{E_a}{R}\right)\frac{1}{T}$$

The apparent activation energy can be calculated from the slope by plotting ln(*k*) as a function of 1000/T with multiplication of the slope by the gas constant *R* and they are expressed in kJ mol^{-1}. These plots are shown in **Figure 4.7** for the Pt catalysts and in **Figure 4.8** for the Pd catalysts.

The apparent activation energy for the hydrogenation of phenylacetylene to styrene for the $Pt_{0.25}/Al_2O_3$ catalyst is equal to 31.2 kJ mol^{-1}. Wilhite et al.[1] calculated an activation energy of 33.9 kJ mol^{-1} on the same catalyst for the same reaction system through theoretical modeling

of the system with Langmuir-Hinshelwood kinetics. These values are relatively similar which provides validation between the two works. The bimetallic $Pt_{0.25}Cu_{15}/Al_2O_3$ catalyst was calculated to have an activation energy of 40.5 kJ mol^{-1} which is an increase of 9.3 kJ mol^{-1} compared to the monometallic Pt.

The calculated value for the monometallic $Pd_{0.18}/Al_2O_3$ is equal to $E_{a,app}$=22.3 kJ mol^{-1}. Previous reports where apparent activation energies have been estimated for the same reaction system are in relatively good comparison to this value. In a study by Mironova et al.[11] an activation energy value of 22.3 kJ mol^{-1} was measured over a $Pd(acac)_2PPh_3$ catalyst, which is exactly the same as the value calculated in this work. Duca et al.,[12] prepared pumice supported Pd catalysts and measured activation energy values of 18.5 kJ mol^{-1} for 0.05% Pd loading and 16.9 kJ mol^{-1} for 0.37% Pd. Another value reported by Jackson et al.[2] over a carbon supported Pd catalyst prepared by IWI, had an activation energy of 26±2 kJ mol^{-1}, and Terasawa et al. found 29 kJ mol^{-1} for a polymer supported Pd complex. All of these values are within a close range considering the different support-metal interaction and dispersion of these catalysts. The apparent activation energy was also measured for the bimetallic $Pd_{0.18}Cu_{15}/Al_2O_3$ catalyst in the same temperature range. The activation energy plot for this catalyst can also be viewed in **Figure 4.8** and the calculated value is $E_{a,app}$=29.1 kJ mol^{-1}. Between the mono- and bimetallic Pd-Cu catalysts, there is increase in activation energy by 6.8 kJ mol^{-1}.

In general, the activation energy for the formation of a product can be reflected through the potential-energy barrier that the reactant must overcome. An increase in the apparent activation energy means that there is a larger activation barrier and would intuitively imply an overall deceleration in the observed rates.[13] This is in agreement with our results; $Pd_{0.18}/Al_2O_3$

has a rate of $7.75\frac{mmol}{g_{Pd}\cdot s}$ which is higher compared to $Pd_{0.18}Cu_{15}/Al_2O_3$ catalyst which has a rate of $4.34\frac{mmol}{g_{Pd}\cdot s}$. The same trend applies between the mono- and bimetallic Pt-based catalysts, which have a larger difference in rates which is also reflected by a larger difference in activation energies. The Pt catalysts also have a larger activation energy compared to the Pd-based materials which have greater reactivity. This increase in the apparent activation energy is evidence of a difference in the active site and/or reaction mechanism for the bimetallic sample. Specifically, since Cu/Al_2O_3 has a much lower rate for the hydrogenation reaction it would be expected that if the reaction is occurring on the Cu surface of the nanoparticles that there would be an increase in the apparent activation energy of the bimetallic samples. These results support the hypothesis that there is dissociation and spillover of H_2 from the Pd to the Cu host metal surface where the reaction occurs. Finally, considering that the activation energies of the bimetallic samples are within close range of 11.4 kJ mol^{-1} and taking into account the statistical error of these measurements, it is safe to assume that the activation energies of the bimetallic samples are similar and representative of this phenomenon.

In the case of product selectivity, the absolute value of the energy-barrier is not important but rather the relative difference compared to the energy value of the undesirable products.[14,15] Zaera and Somorjai have previously discussed that in the case of competitive product formation there are two potential-energy barriers, depicted in **Figure 4.9** (replicated from *Zaera, F., J. Phys. Chem. B 2002, 106, 4043-4052*), and the relative difference between these activation energy barriers will dictate the reaction selectivity. **Figure 4.9** illustrates that small changes (~8.4 kJ mol^{-1}) in the activation barriers of the two competing reactions can completely re-arrange the product distribution of the overall reaction. For the monometallic and bimetallic

catalysts examined in this work, the increase in styrene selectivity that the bimetallic catalysts display, could be explained by a larger activation difference between the two competing reactions (PA → Styrene; Styrene → EB) compared to that of the monometallic sample.

There are numerous factors that could contribute to the observed increase in selectivity such as the nature of the active site, which can also be linked with chemical bonding between reactants and site, including the adsorption geometry, electronic interactions and spatial distributions.[14] Considering that the active sites are different between the mono- and bimetallic catalysts; Pd is the site for $Pd_{0.18}/Al_2O_3$ and Cu for $Pd_{0.18}Cu_{15}/Al_2O_3$, two potential explanations are proposed for the reaction selectivity. The first explanation is related to the adsorption strength of the metal site. Surface science studies with phenylacetylene were done on Cu(111) by Sohn et al.[16] and it was determined by TPD that the most intense desorption peak for phenylacetylene was observed at 410K while styrene desorbed at ~275K. There are no reported TPD measurements for this system on Pd, but if there desorption temperature difference is larger for these molecules on Pd, that would imply a larger relative energy barrier for the two competing reactions. Finally, another possible scenario could be related to the adsorption geometry of phenylacetylene on Cu compared to Pd. In the same study by Sohn et al.[16] it was concluded that hydrogenation of cross-bridged adsorbed phenylacetylene, which was the majority species on the surface, resulted in the formation of styrene. A surface science study of this reaction system on a Pd crystal could provide more insight to fully explain the observed phenomena.

4.3 Langmuir-Hinshelwood analysis

In order to gain further insight regarding the performance and selectivity of the bimetallic catalysts prepared in this work, prediction and comparison of the rate constants was obtained for this chain reaction system by assuming a Langmuir-Hinshelwood (L-H) reaction mechanism. From the reaction data it is evident that there is competitive adsorption between phenylacetylene and styrene on the catalyst surface since the hydrogenation of styrene begins at high phenylacetylene conversions. Previous reports on the hydrogenation of phenylacetylene to styrene have also shown competitive adsorption behavior between the two molecules.[2,17] To begin the L-H analysis the following chain reaction system is followed:

$$PA \xrightarrow{+H_2} St \xrightarrow{+H_2} EB$$

Where PA, St, EB correspond to phenyacetylene, styrene and ethyl benzene respectively. This reaction system assumes that PA cannot be directly converted to EB, and at high H_2 pressures the hydrogenation reactions are not reversible. Also, based on the initial hypothesis, that there is hydrogen dissociation and spillover onto the Cu surface, it is assumed that there are two active sites facilitating different steps of the overall reaction. Cu will be designated as the active site where the unsaturated hydrocarbons adsorb and react with weakly bound H_2 (site 1: S_1) which has spilled over from the Pd/Pt ensembles which correspond to the site for hydrogen dissociation/adsorption (site 2: S_2). This assumes that PA, St and EB are not blocking the Pd/Pt sites and that Cu does not contain sites for dissociative adsorption of H_2. Finally, assuming that all the participating molecules adsorb onto the catalyst surface and that the adsorbed species undergo bimolecular reactions, the following mechanism can be proposed:

Adsorption: $PA + S_1 \xleftrightarrow{K_1} [PA \cdot S_1]$

$$St + S_1 \xleftrightarrow{K_2} [St \cdot S_1]$$

$$H_2 + 2S_2 \xleftrightarrow{K_3} 2[H \cdot S_2]$$

Surface Reaction: $[PA \cdot S_1] + 2[H \cdot S_2] \xrightarrow{k_4} [St \cdot S_1] + 2S_2$ ***(RDS)***

Desorption: $[St \cdot S_1] \xleftrightarrow{K_5} St + S_1$

The surface reaction is assumed to be the rate determining step (RDS) and irreversible for the reasons stated above. By assuming quasi equilibrium for the adsorption and desorption processes and solving the site balances for the number of available sites:

Quasi equilibrium: $k_1[PA][S_1] = k_{-1}[PA \cdot S_1] \Rightarrow K_1 = \frac{k_1}{k_{-1}} = \frac{[PA \cdot S_1]}{[PA][S_1]}$

$$k_2[St][S_1] = k_{-1}[St \cdot S_1] \Rightarrow K_2 = \frac{k_2}{k_{-2}} = \frac{[St \cdot S_1]}{[St][S_1]}$$

$$k_3[H_2][S_2]^2 = k_{-3}[H \cdot S_2]^2 \Rightarrow K_3 = \frac{k_3}{k_{-3}} = \frac{[H \cdot S_2]^2}{[H_2][S_2]^2}$$

Site balances: $S_{1,T} = [S_1] + [PA \cdot S_1] + [St \cdot S_1] \Rightarrow S_{1,T} = [S_1] + K_1[PA][S_1] + K_2[St][S_1]$

$$S_{1,T} = [S_1](1 + K_1[PA] + K_2[St]) \Rightarrow [S_1] = \frac{S_{1,T}}{(1 + K_1[PA] + K_2[St])}$$

$$S_{2,T} = [S_2] + [H \cdot S_2] \Rightarrow S_{2,T} = [S_2] + \sqrt{K_3[H_2][S_2]^2}$$

$$S_{2,T} = [S_2]\left(1 + \sqrt{K_3[H_2]}\right) \Rightarrow [S_2] = \frac{S_{2,T}}{\left(1 + \sqrt{K_3[H_2]}\right)}$$

RDS: $$r_4 = k_4[PA \cdot S_1][H \cdot S_2]^2 \Rightarrow r_4 = k_4 K_1 K_3 [PA][H_2][S_1][S_2]^2$$

$$r_4 = \frac{S_{1,T} S_{2,T} k_4 K_1 K_3 [PA][H_2]}{\left(1 + K_1[PA] + K_2[St]\right)\left(1 + \sqrt{K_3[H_2]}\right)} \qquad (1)$$

Equation (1) is the final expression of the rate in terms of the concentrations of PA, St and H_2. The K constants are the equilibrium constants of the adsorption steps, k_4 corresponds to the rate constant of the surface reaction and $S_{1,T}$, $S_{2,T}$ are the total amount of sites (=constant). Based on the relative adsorption strength of PA and St on the Cu surface the following assumption is applied to yield a limiting case for L-H analysis.

$$1 + K_1[PA] >> K_2[St]$$

This assumption states that the adsorption strength of PA is much stronger than that of St or EB on Cu(111) surface and therefore the dominant species. The assumption is justified by the relative desorption energies of PA, St and EB determined by TPD.[16] Application of this assumption simplifies equation (1) into the following form:

$$r_4 = \frac{S_{1,T} S_{2,T} k_4 K_1 K_3 [PA][H_2]}{\left(1 + K_1[PA]\right)\left(1 + \sqrt{K_3[H_2]}\right)} \quad (2)$$

Since there is a 100 psi head pressure of hydrogen applied to the system, the consumed H_2 in the liquid phase is continuously replenished and the concentration of H_2 is considered to be constant. All of the constant terms in equation (2) can be gathered and expressed as an overall apparent rate constant, and the rate expression simplifies into the following:

$$r_4 = k_{app} \frac{[PA]}{\left(1 + K_1[PA]\right)} \quad (3)$$

and the apparent rate constant is: $k_{app} = \frac{S_{1,T} S_{2,T} k_4 K_1 K_3 [H_2]}{\left(1 + \sqrt{K_3 [H_2]}\right)}$

Based on the rate expression derived from the L-H analysis, the batch reactor design equation is:

$$V \frac{d[PA]}{dt} = -k_{app} \frac{[PA]}{\left(1 + K_1 [PA]\right)} V \quad (4)$$

Equation (4) can also be expressed in terms of PA conversion by applying

$$X = \frac{[PA]_o - [PA]}{[PA]_o} \Rightarrow [PA] = [PA]_o (1 - X)$$

The processes is done under a constant volume and yields the following rate expression in terms of conversion:

$$\frac{dX}{dt} = k_{app} [PA]_o \frac{(1 - X)}{1 + K_1 (1 - X)} \quad (5)$$

The parameters to the L-H model (Equation 5) were determined by using a non-linear optimization routine in Matlab (fmincon) to minimize the sum of the residuals squared between the experimental and simulated data, which is the objective function. At each iteration, ode15s in Matlab is used to simulate the trajectory of conversion as a function of time based on the current parameter set in the optimization. The optimization was terminated once a local minimum was reached. If the function has several local minima, the initial guess is important since it might have an effect on the outcome of the final parameters. An initial estimation of the k_{app} and K_1

parameters can be done by applying a simple power law model to the experimental data for the initial rate. Utilizing the batch reactor design equation:

$$V\frac{d[PA]}{dt} = -k_{1,app}[PA]V \Rightarrow \frac{d[PA]}{dt} = -k_{1,app}[PA]$$

Integration of the above and by substituting PA concentration with conversion yields:

$$\frac{d[PA]}{[PA]} = -k_{1,app}dt \Rightarrow \int_{[PA]_o}^{[PA]} \frac{d[PA]}{[PA]} = -k_{1,app}\int_0^t dt \Rightarrow \ln\left(\frac{[PA]}{[PA]_o}\right) = -k_{1,app}t \Rightarrow \ln(1-X) = -k_{1,app}t$$

The plot of–*ln(1-X)* vs *t* plot should be linear, with a slope of $k_{1,app}$. This plot is shown for both of the bimetallic catalysts in **Figure 4.10**, corresponding to the experimental data from **Figure 4.2** and **Figure 4.5**. The concentration of hydrogen in the system (=constant) is lumped within $k_{1,app}$ value calculated from the slope. By using Henry's Law $\left(H(p,x) = \frac{p}{x}\right)$, the concentration of H_2 dissolved in the liquid phase of n-hexane can be calculated. By using the solubility data previously reported by Katayama et al.[18] for hydrogen in n-hexane, the concentration of [H_2] in the liquid phase is calculated (=0.0047 mol fraction of H_2) and applied in order to calculate the apparent rate constants from the assumed power law model. These values are used as initial guesses in Matlab for the two different bimetallic catalysts in order to predict the actual apparent rate constants from the model fit.

The optimization routine in Matlab is applied to experimental data for the two bimetallic catalyst under the same conditions (catalyst:reactant ratio) and the resulting fit and parameter estimation can be viewed in **Figure 4.11** for $Pt_{0.25}Cu_{15}/Al_2O_3$ and **Figure 4.12** for

$Pd_{0.18}Cu_{15}/Al_2O_3$. The initial concentration of PA is lumped into the value calculated from the fit which means that actual value just for the apparent rate constant would be larger. There is a relatively good fit in both cases which implies that the assumptions used to develop the L-H model are accurate in predicting the behavior of the system. The rate constant has a larger value in the case of $Pd_{0.18}Cu_{15}/Al_2O_3$ which is expected since the Pd-based catalysts have a superior rate compared to Pt and this result is also in agreement with the activation energy data.

The adsorption coefficient of PA onto the Cu (K_1) has a value of 1.5 for the Pt data and 0.6 in the case of Pd. These values are expected to be very similar, if not identical, since the adsorption coefficient of PA on Cu should be the same in both samples and they have been calculated in very close range. This small difference could be a result of statistical error in the experimental data. To explain this further, for $Pd_{0.18}Cu_{15}/Al_2O_3$ in **Figure 4.12**, if the 4^{th} data point at 90 min had a value of approximately 0.85 instead of 0.75, which would be in better agreement with the other data points, the K_1 value which accounts for the non-linearity of the simulated data would be higher at approximately 1.5. The same could apply to several data points for $Pt_{0.25}Cu_{15}/Al_2O_3$.

The main point of this exercise is to prove that the assumptions made for the L-H accurately describe the behavior of the system and that the apparent rate constant results follow the same trends that have been previously observed. This means that there are two active sites on our catalyst material, the Pt/Pd which activates hydrogen which in turn occupies the Cu surface where the reaction occurs. In order to achieve complete parameter estimation for the system, with a high level of confidence, multiple replicates should be used at different initial concentrations.

4.4 Stability Tests

The stability or recyclability of the bimetallic catalysts was examined by using a catalyst that was previously reacted. The sample was filtered and dried before reusing and testing it under identical pretreatment and reaction conditions. When the bimetallic $Pt_{0.25}Cu_{15}/Al_2O_3$ was used after one cycle there was a significant increase in the rate of the reaction, very similar to the monometallic Pt catalyst which is shown in **Figure 4.13**. This is most likely due to the reduction treatment at 400 ^{o}C for 6 hours which resulted into agglomeration of the Pt species on the catalyst surface.[19] The creation of larger Pt clusters would lead to the hydrogenation reaction happening on the Pt instead of the Cu surface. This increase in rate is accompanied by a decrease in selectivity from 77% to 51% between the two cycles. The value of 51% selectivity is very similar to that found for the monometallic $Pt_{0.25}/Al_2O_3$ sample which has 45% at high conversion. This could further support the idea that the repeated heat treatment could eventually have an effect on the particle size which would lead to the hydrogenation occurring on the larger Pt clusters.

4.5 Summary

Based on the activity and selectivity measurements, the bimetallic catalysts in both cases demonstrate an improvement in selectivity especially at high conversions. For the case of the Pt based catalysts, $Pt_{0.25}Cu_{15}/Al_2O_3$ has a selectivity of 77%, at 95% conversion, while $Pt_{0.25}/Al_2O_3$ has 45% selectivity. The $Pd_{0.18}Cu_{15}/Al_2O_3$ catalyst maintains a selectivity of 94% at 90% conversion in comparison to $Pd_{0.18}/Al_2O_3$ which has lower selectivity of 62% at the same

conversion. This increase in selectivity is accompanied by a decrease in the overall observed rate of the bimetallic materials compared to their monometallic counterparts in both cases. The decreased rate is suggested to be related with the change of the reaction mechanism.

Furthermore, by examining the activation energies which were calculated for the samples, it is evident that there is a subtle increase in the activation energies of the bimetallic catalysts compared to the monometallic. This is expected since the monometallic samples have a greater rate than their bimetallic counterparts. The change in activation energy for the bimetallic samples is a good indication of a difference in active site for hydrogenation which further supports the hypothesis of hydrogen spillover onto the copper surface.

It has been reported that there is competitive adsorption between phenylacetylene and styrene molecules on Cu surfaces. The preferential adsorption of a certain molecule would also dictate the degree of selectivity towards styrene that the hydrogenation process displays. In order to model this process, a Langmuir-Hinshelwood model was proposed where it was assumed that two different sites were present on the catalyst. The Pt/Pd site is considered to adsorb and dissociate molecular hydrogen which then spills over onto the second site- Cu, where the adsorption and hydrogenation of the hydrocarbons occurs. A rate expression was derived based on this model and was incorporated into the batch reactor design equation to develop a formula for the rate as a function of conversion. By using Matlab ode15s, simulated data were fit to the experimental points generating numbers for the apparent rate constants and adsorption coefficients. There is an adequate fit of the simulated data to the experimental, indicating that the derived model and assumptions are adequate. However, other assumptions should be checked; for example that of unbound hydrogen supply. This was evaluated etc.. etc.. The apparent rate constants for the reaction are in good comparison with the activation energies meaning that

$Pd_{0.18}Cu_{15}/Al_2O_3$ has a higher rate constant than $Pt_{0.25}Cu_{15}/Al_2O_3$. Also, the adsorption coefficient for PA on Cu in both cases is practically the same, which is good indication that the PA adsorption is occurring on the same site which could only be Cu.

The stability or recyclability of the catalyst samples was examined in order to determine if the samples can be reused for multiple batches. After a harsh pre-treatment in hydrogen at 400 oc for 6h, testing of the $Pt_{0.25}Cu_{15}/Al_2O_3$ catalyst found that the rate of reaction increased significantly, almost equal to the rate of $Pt_{0.25}/Al_2O_3$ and the selectivity also decreased to that of the monometallic sample. This infers that there is Pt particle sintering during the reduction treatment which alters the behavior of the catalyst to that of monometallic Pt and most probably means that the hydrogenation reaction in this case occurs on the Pt sites. New compositions with much lower platinum content should be tried to stabilize Pt atoms against migration and cluster/particle formation even in prolonged reducing reaction environments.

4.6 References

1. Wilhite, B. A., Mccready, M. J. & Varma, A. Kinetics of Phenylacetylene Hydrogenation over Pt / γ-Al 2 O 3 Catalyst. 3345–3350 (2002).

2. Jackson, S. D. & Shaw, L. A. and styrene on a palladium / carbon catalyst. **134,** 91–99 (1996).

3. Srinivas, S. T. & Kanta Rao, P. Direct Observation of Hydrogen Spillover on Carbon-Supported Platinum and Its Influence on the Hydrogenation of Benzene. *Journal of Catalysis* **148,** 470–477 (1994).

4. Guczi, L. *et al.* Pumice-Supported Cu – Pd Catalysts : Influence of Copper on the Activity and Selectivity of Palladium in the Hydrogenation of Phenylacetylene and But-1-ene. **462,** 456–462 (1999).

5. Lonergan, W. W. *et al.* Low-temperature 1,3-butadiene hydrogenation over supported Pt/3d/γ-Al2O3 bimetallic catalysts☆. *Catalysis Today* **160,** 61–69 (2011).

6. Kyriakou, G. *et al.* Isolated metal atom geometries as a strategy for selective heterogeneous hydrogenations. *Science (New York, N.Y.)* **335,** 1209–12 (2012).

7. Marvell, E. N. & Li, T. *Catalytic Semihydrogenation of the Triple Bond*. (1973).

8. Chemistry, S. Hydrogenation of carbon – carbon multiple bonds : **173,** 185–221 (2010).

9. Dominguezdominguez, S., Berenguermurcia, a, Cazorlaamoros, D. & Linaressolano, a. Semihydrogenation of phenylacetylene catalyzed by metallic nanoparticles containing noble metals. *Journal of Catalysis* **243,** 74–81 (2006).

10. V, E. S. P. B. *et al.* Optimization of the Selective Semi-Hydrogenation of Phenylacetylene with Supported Palladium Systems. **63,** 375–389 (1990).

11. Mironova, L. V., Belykh, L. B., Usova, I. V. & Shmidt, F. K. Kinetics of hydrogenation of phenylacetylene under the action of a catalyst formed from Pd(AcAc)2PPh3. *Kinetics and Catalysis* **26,** 413–416 (1985).

12. Duca, D., Liotta, L. F. & Deganello, G. Liquid phase hydrogenation of phenylacetylene on pumice supported palladium catalysts. *Catalysis Today* **24,** 15–21 (1995).

13. Laidler, K. J. *Chemical Kinetics*. (Harper & Row, 1987).

14. Zaera, F. Outstanding Mechanistic Questions in Heterogeneous Catalysis. *The Journal of Physical Chemistry B* **106,** 4043–4052 (2002).

15. Somorjai, G. a & Park, J. Y. Molecular factors of catalytic selectivity. *Angewandte Chemie (International ed. in English)* **47,** 9212–28 (2008).

16. Sohn, Y., Wei, W. & White, J. M. Phenylacetylene on Cu(111): Adsorption Geometry, Interfacial Electronic Structures and Thermal Chemistry. *Journal of Physical Chemistry C* **111,** 5101–5110 (2007).

17. Hamilton, C. a, Jackson, S. D., Kelly, G. J., Spence, R. & de Bruin, D. Competitive reactions in alkyne hydrogenation. *Applied Catalysis A: General* **237,** 201–209 (2002).

18. Katayama, T. *et al.* Solubilities of Hydrogen and Nitrogen in Alcohols and n-Hexane. **21,** 194–196 (1976).

19. Bournonville, J. P. & Martino, G. *Sintering of Alumina Supported Platinum*. *Studies in Surface Science and Catalysis* **6,** 159–166 (Elsevier Scientific Publishing Company, 1980).

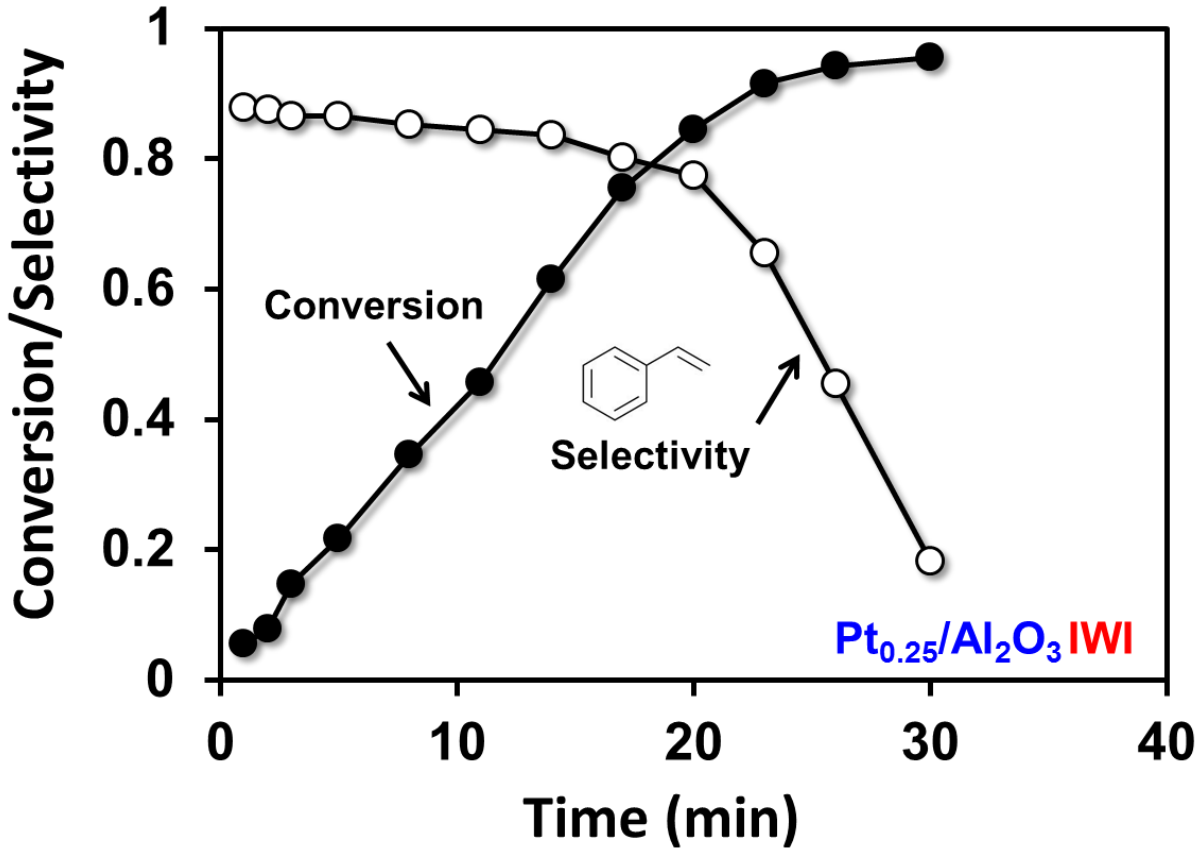

Figure 4.1 Time resolved batch reactor data at 20 ^{o}C for phenylacetylene hydrogenation on $Pt_{0.25}/Al_2O_3$ prepared by IWI

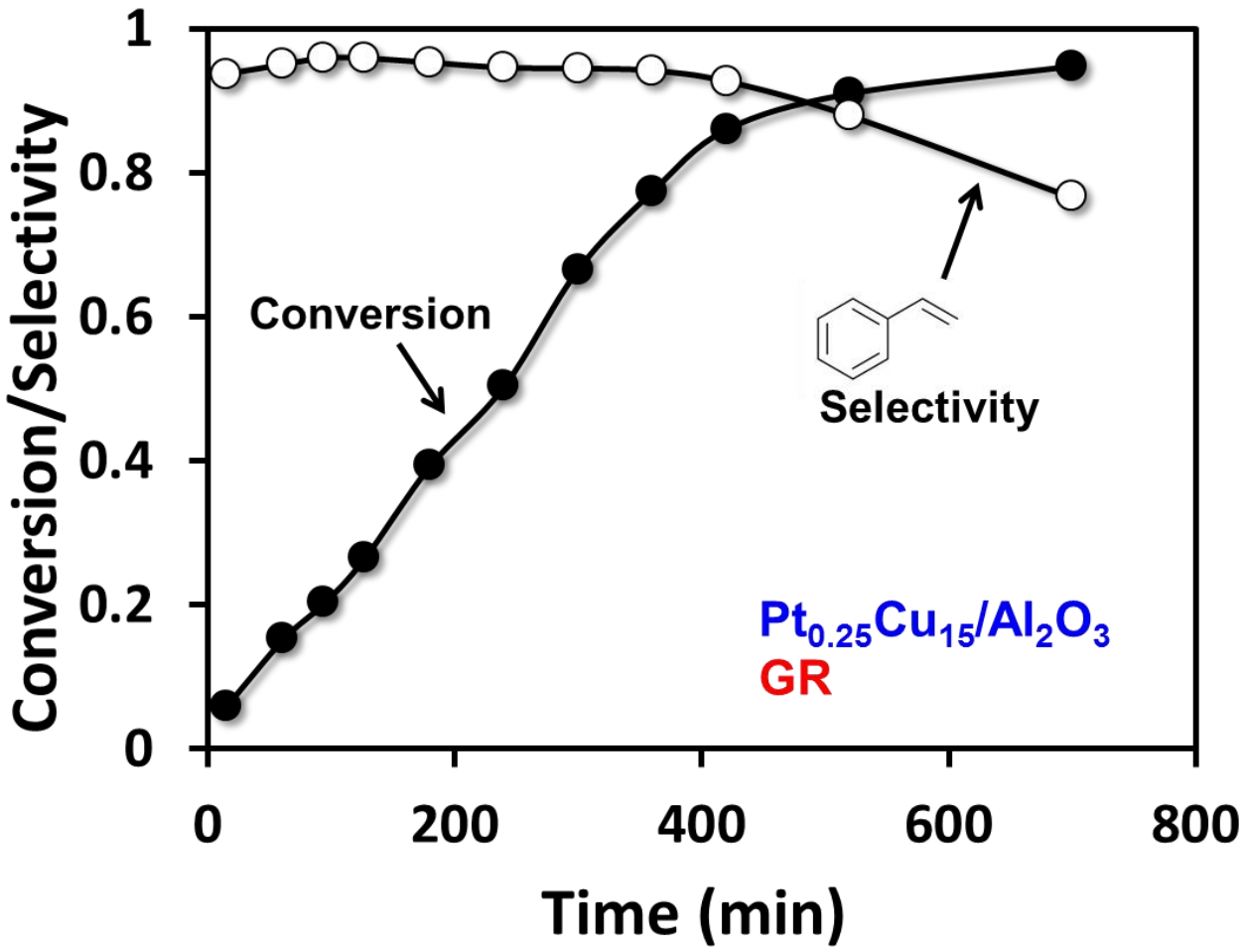

Figure 4.2 Time resolved batch reactor data at 20 ^{o}C for phenylacetylene hydrogenation on $Pt_{0.25}Cu_{15}/Al_2O_3$ prepared by GR

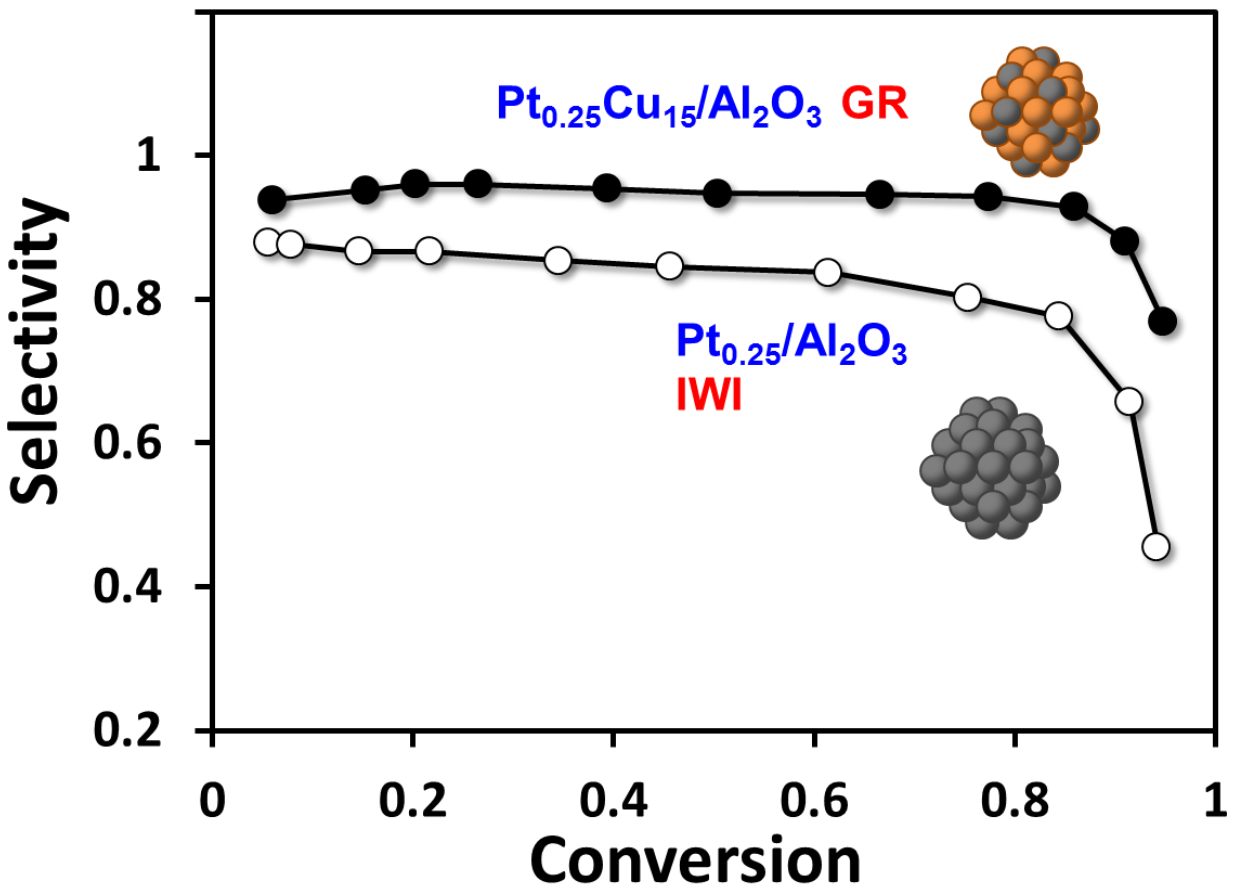

Figure 4.3 Time independent plot of styrene selectivity as a function of conversion for $Pt_{0.25}Cu_{15}/Al_2O_3$ and $Pt_{0.25}/Al_2O_3$

Sample	Initial Rates	Units	Selectivity	Conditions
Cu/Al_2O_3	0.00032	$\frac{mmol}{g_{cat} \cdot s}$	100%	P=100 psi, T=20 ^oC PA : m_c (10 : 1)
$Pt_{0.25}/Al_2O_3$	5.50	$\frac{mmol}{g_{Pt,surface} \cdot s}$	-	P=100 psi, T=45 ^oC PA : m_c (2 : 1)
$Pt_{0.25}/Al_2O_3$ [1]	5.00		48%[b]	
$Pt_{0.25}/Al_2O_3$	0.26		31%[a]	P=100 psi, T=20 ^oC PA : m_c (2 : 1)
$Pt_{0.25}Cu_{15}/Al_2O_3$	0.03		77%[a]	
$Pd_{0.18}/Al_2O_3$	7.75	$\frac{mmol}{g_{Pd} \cdot s}$	62%[c]	P=100 psi, T=20 ^oC PA : m_c (10 : 1)
$Pd_{0.18}Cu_{15}/Al_2O_3$	4.34		94%[c]	
$Pd_{0.90}/C$ [2]	13.56		~83%[c]	P=29 psi, T=20 ^oC PA : m_c (~10 : 1)
$Pd_{0.6}Cu_{0.05}$/pumice [4]	6.20			P=14.7 psi, T=25 ^oC PA_{mol}:Pd_{atoms} = 1000

Table 4.1 Summarized results of the rate and selectivity data for the different catalysts prepared in this work and from other literature

(a) Selectivity at peak value of styrene formation
(b) Selectivity at 95% conversion
(c) Selectivity at 90% conversion

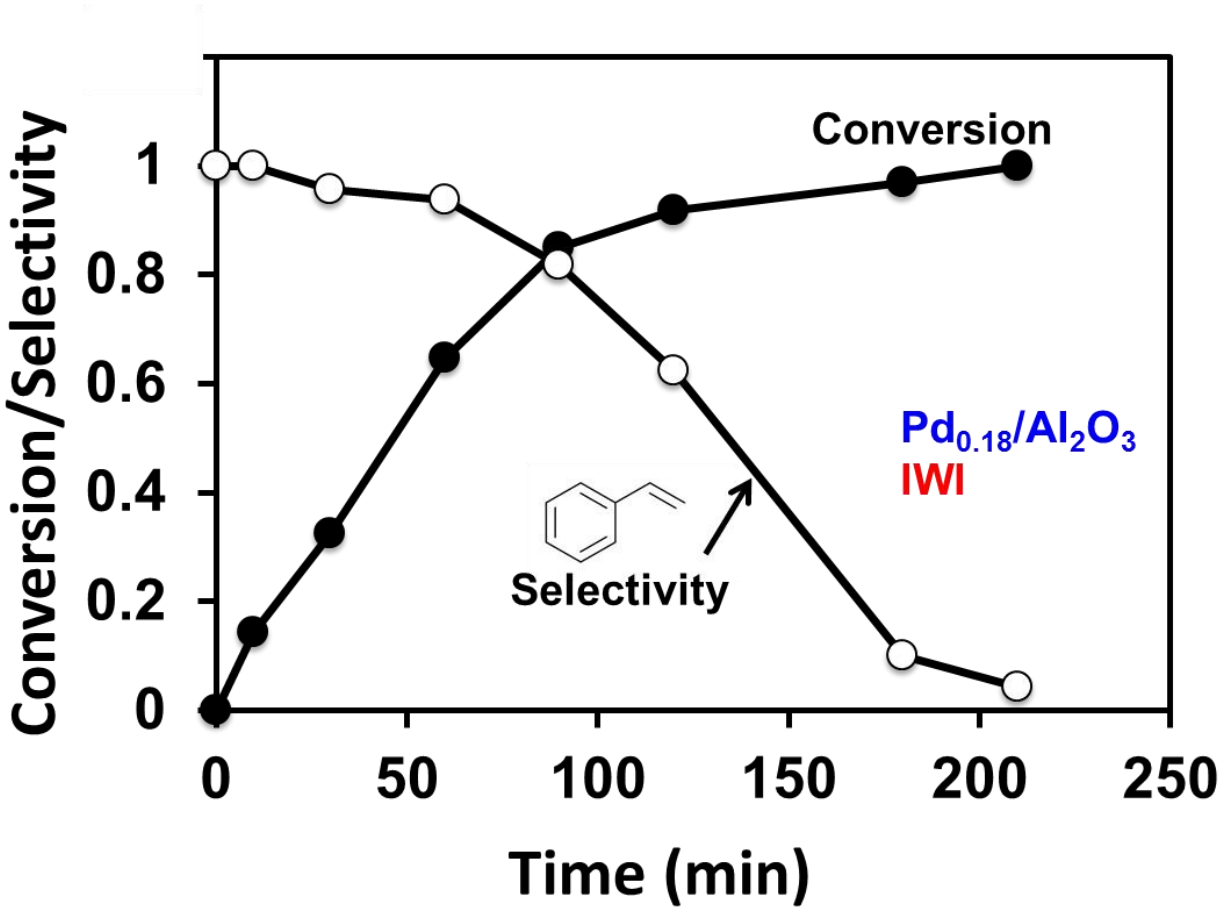

Figure 4.4 Time resolved batch reactor data at 20 ^{o}C for phenylacetylene hydrogenation on $Pd_{0.18}/Al_2O_3$ prepared by GR

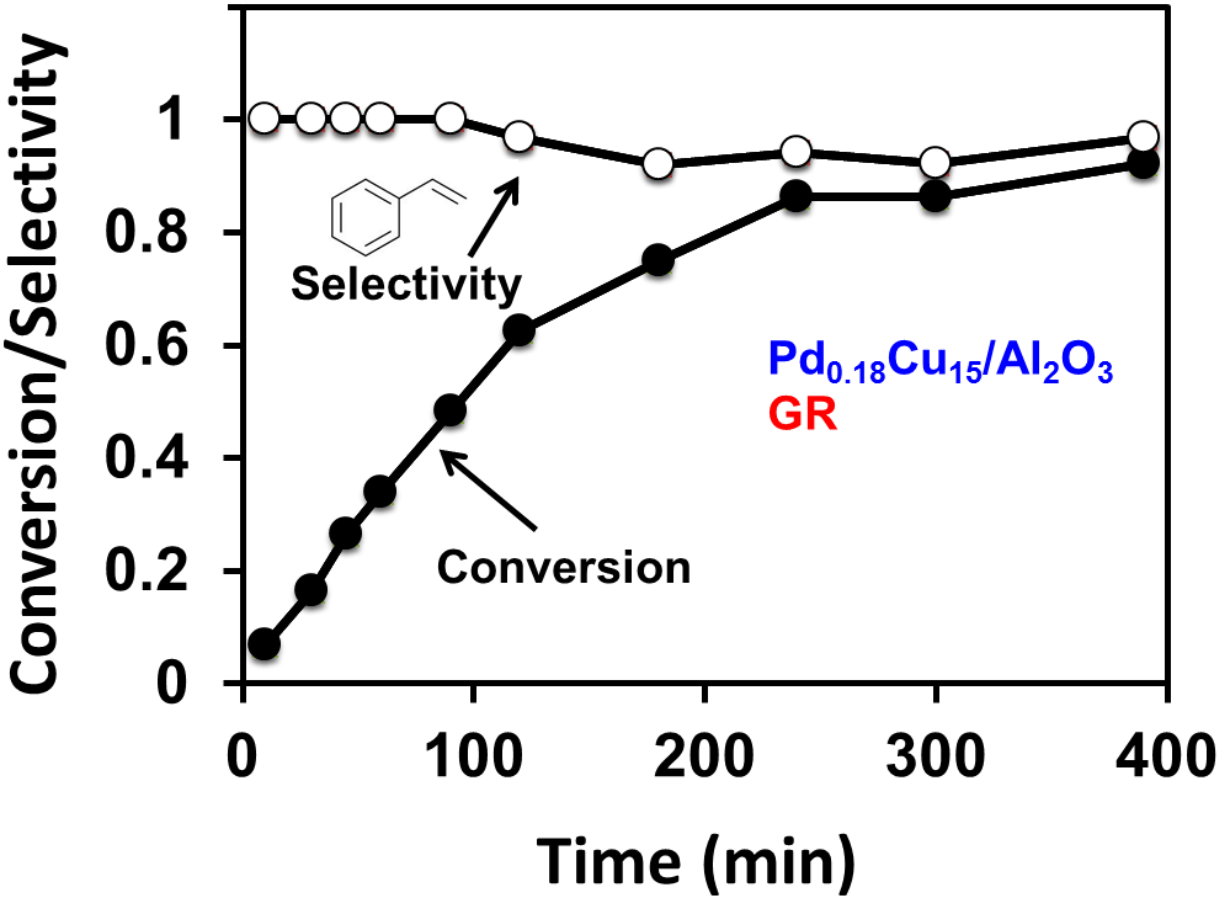

Figure 4.5 Time resolved batch reactor data at 20 ^{o}C for phenylacetylene hydrogenation on $Pd_{0.18}Cu_{15}/Al_2O_3$ prepared by GR

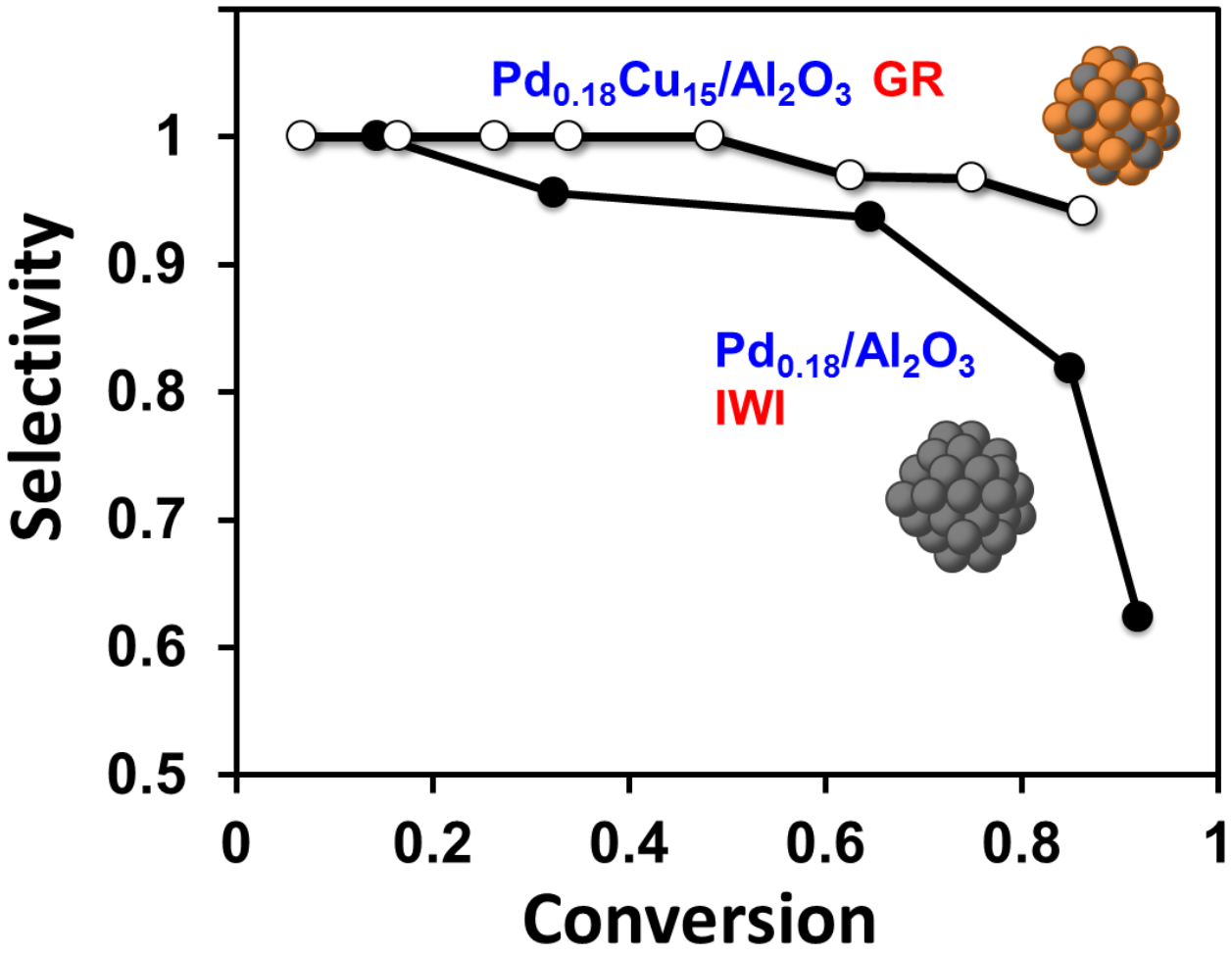

Figure 4.6 Time independent plot of styrene selectivity as a function of conversion for $Pd_{0.18}Cu_{15}/Al_2O_3$ and $Pd_{0.18}/Al_2O_3$

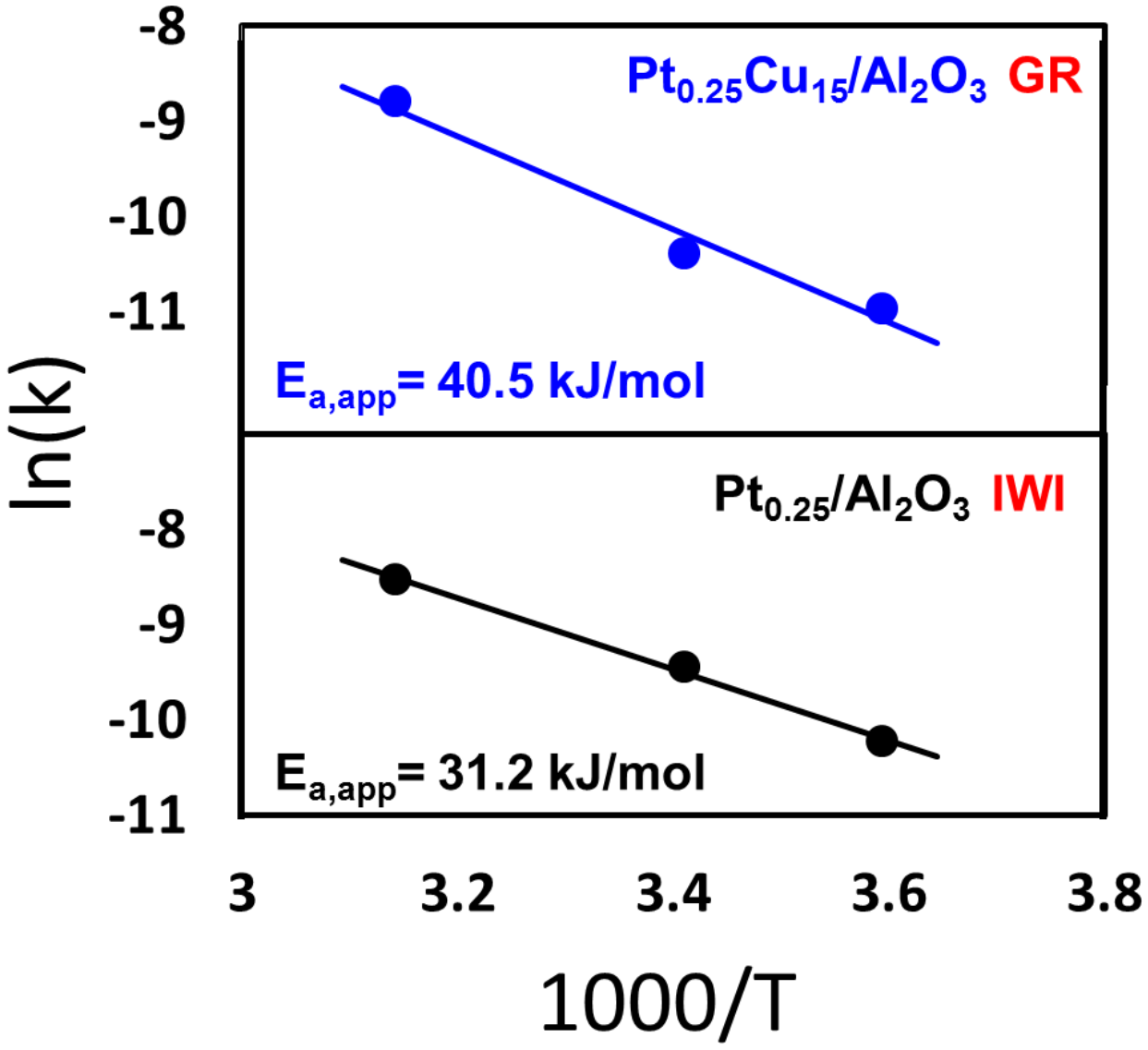

Figure 4.7 Plot of ln(k) vs 1000/T where the activation energy is calculated from the slope of the fitted line for $Pt_{0.25}Cu_{15}/Al_2O_3$ and $Pt_{0.25}/Al_2O_3$

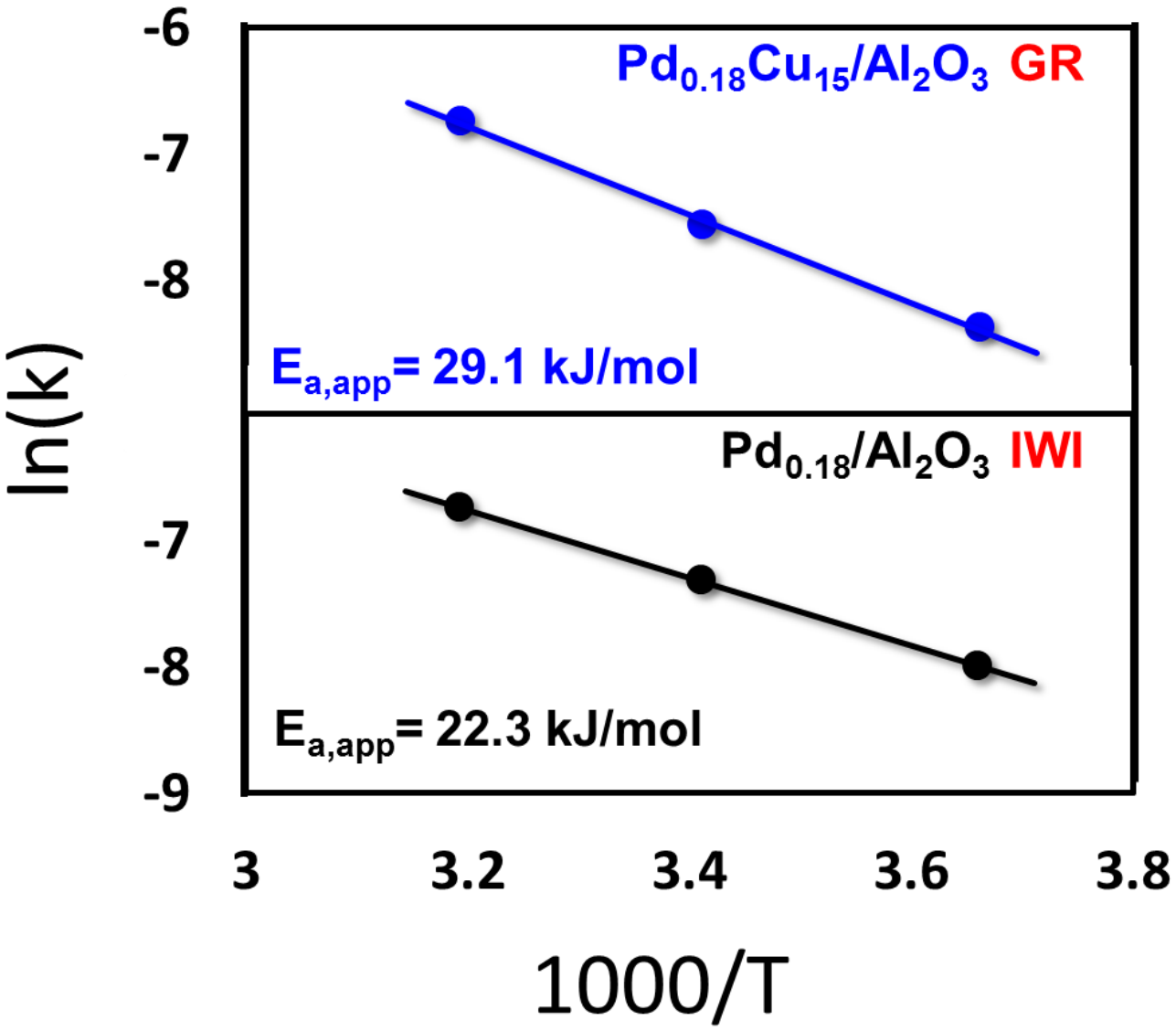

Figure 4.8 Plot of ln(k) vs 1000/T where the activation energy is calculated from the slope of the fitted line for $Pd_{0.18}Cu_{15}/Al_2O_3$ and $Pd_{0.18}/Al_2O_3$

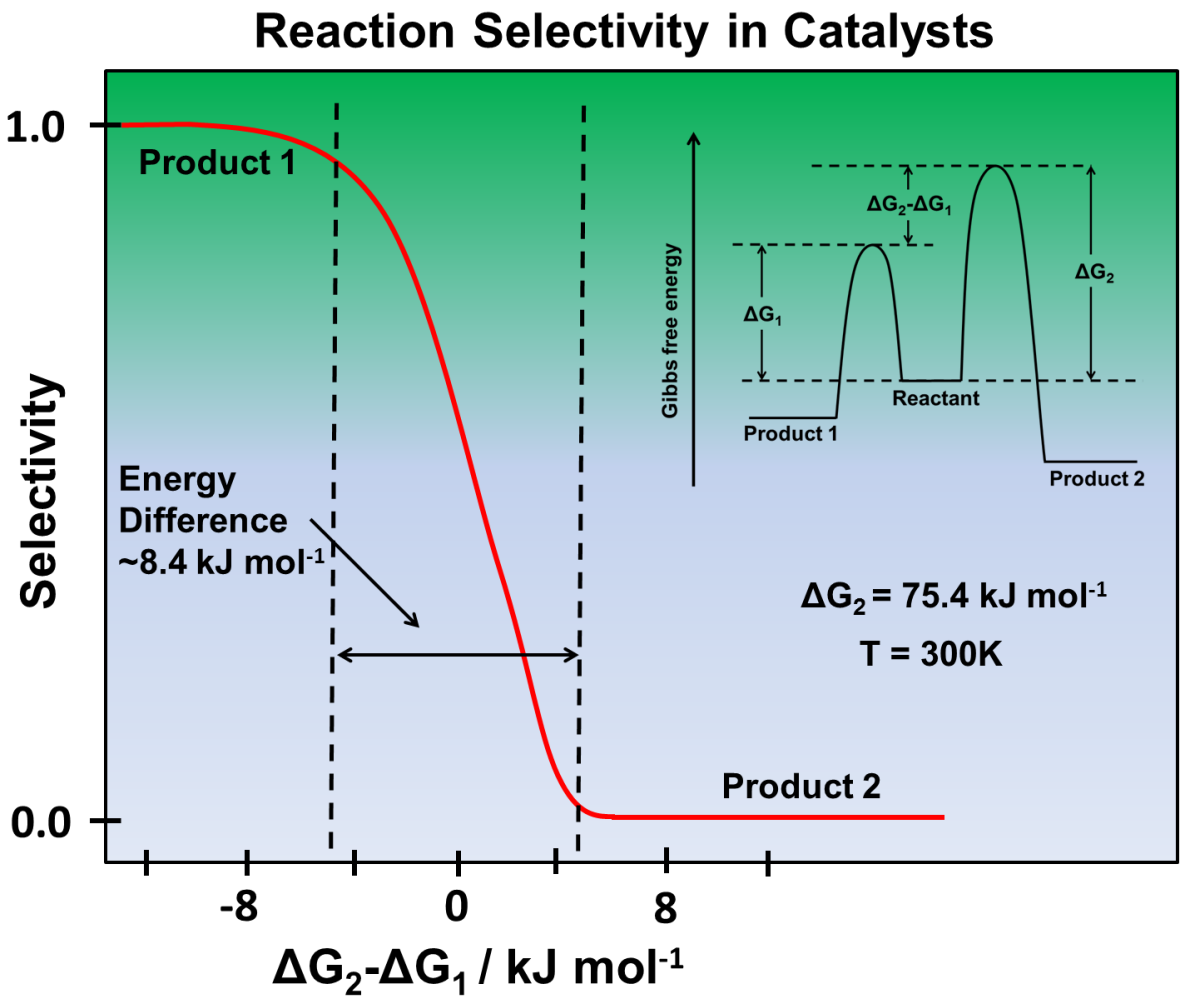

Figure 4.9 Potential energy plot illustrating how the activation barriers for different reactions determine the selectivity of a catalytic process.

Used from Reference [14]

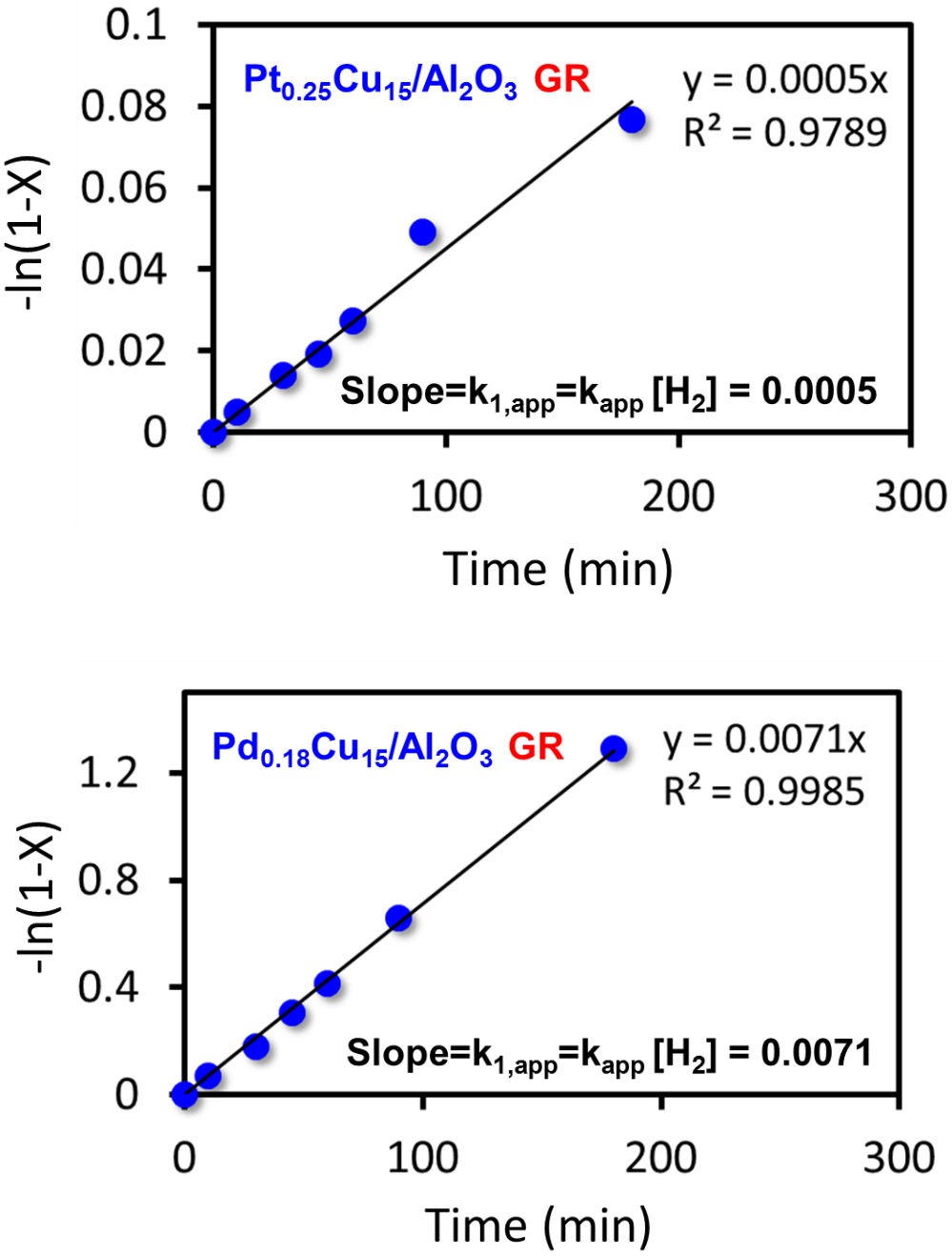

Figure 4.10 Initial guess for estimation of k_{app} by using power law regression for both $Pt_{0.25}Cu_{15}/Al_2O_3$ and $Pd_{0.18}Cu_{15}/Al_2O_3$

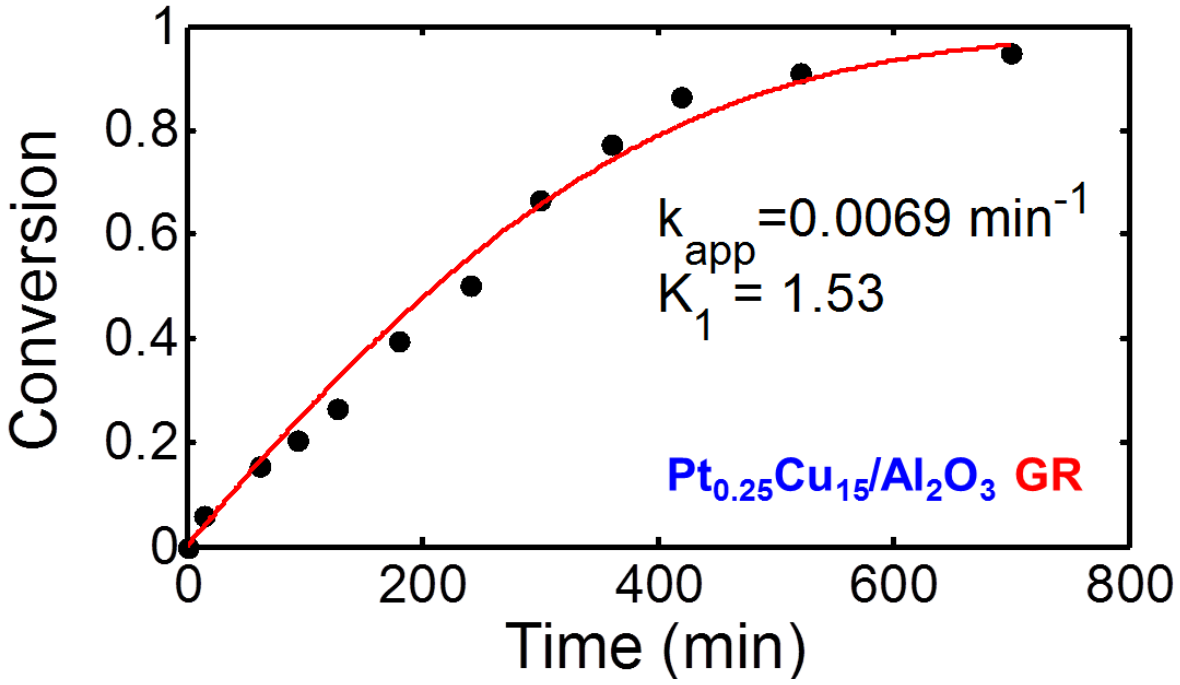

Figure 4.11 Simulated fit and parameter estimation for the experimental data of $Pt_{0.25}Cu_{15}/Al_2O_3$

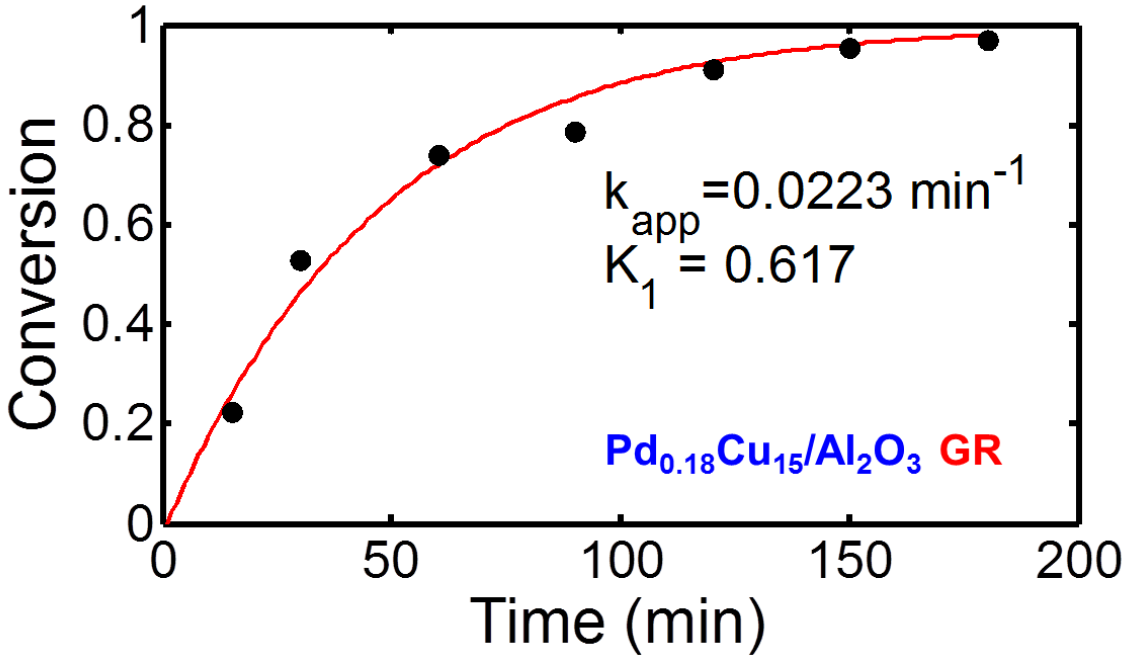

Figure 4.12 Simulated fit and parameter estimation for the experimental data of $Pd_{0.18}Cu_{15}/Al_2O_3$

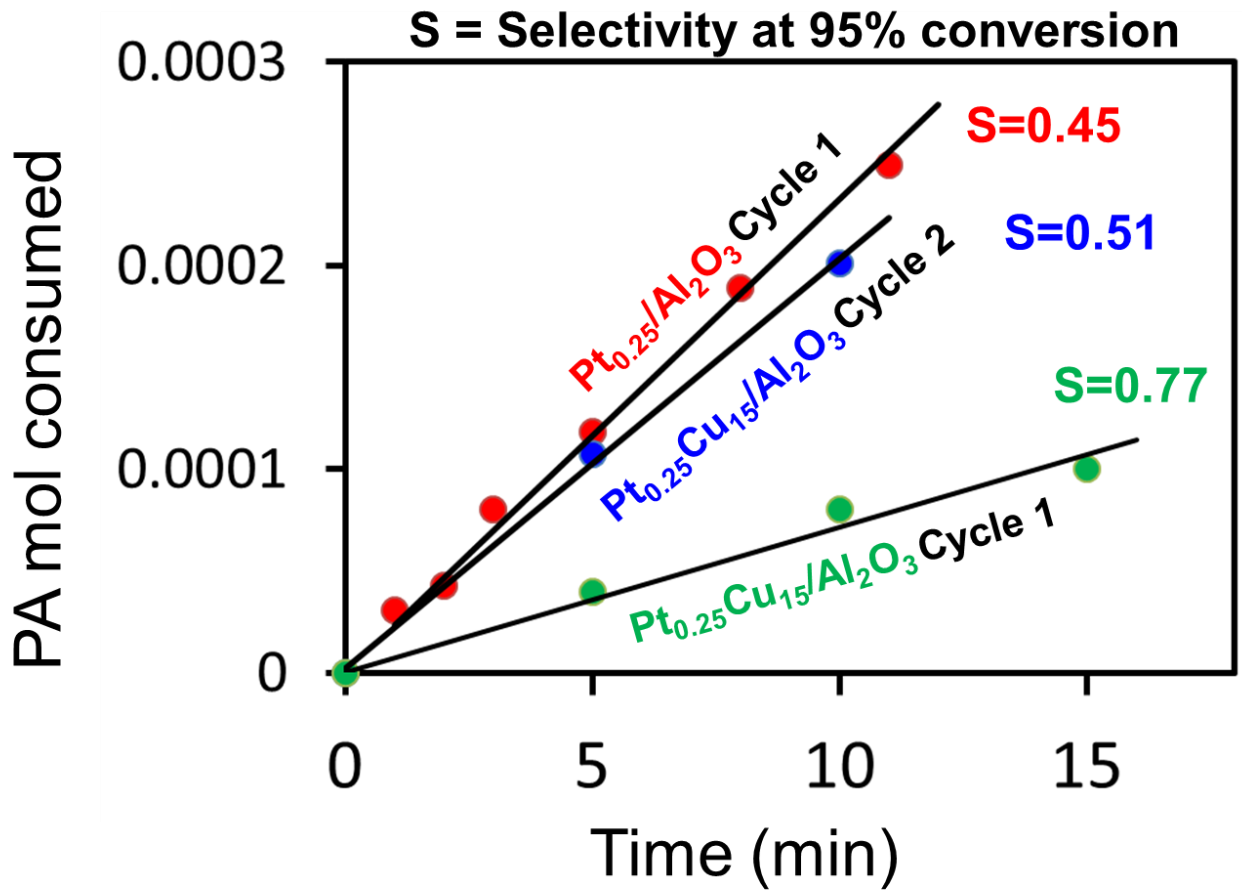

Figure 4.13 Reusability of $Pt_{0.25}Cu_{15}/Al_2O_3$ catalyst under the same pretreatment and reaction conditions at T=20 ^{o}C

Chapter 5 – Conclusions and Recommendations

5.1 Conclusions

The primarily target of this thesis was to extend the findings of selective hydrogenmation of a model single atom alloy Pd/Cu(111) to the design of a nanoparticle selective hydrogenation catalyst. To reiterate, the surface science study by our group done in UHV has demonstrated how Pd atoms on a Cu(111) surface serve as sites for hydrogen dissociation and spillover onto the Cu surface where the hydrogenation occurs. To begin with, a strategy was required to create a bimetallic catalyst which would have the desired properties. A colloidal nanoparticle preparation was chosen for the Cu in order to control the size, distribution and surface structure of the Cu nanoparticles. Synthesis of small Cu nanoparticles would also yield high area of Cu exposed for reaction. The prepared Cu nanoparticles were immobilized on γ-Al_2O_3 which also has a high surface area and is considered to be an inert support. This was important in order to avoid metal/metal oxide interactions which were not desirable in the study. After calcination of the alumina supported Cu nanoparticles, reduction treatment was necessary in order to form metallic Cu nanoparticles. These nanoparticles were characterized by HR-TEM and XRD and it was concluded that after reduction the surface of the Cu nanoparticles consisted primarily of Cu(111). The Scherrer equation was used on the diffractograms to estimate the size of the uncapped Cu particles and it was determined that they were approximately 14 nm which means that there was particle sintering after the heat treatments. Galvanic replacement was chosen as the method to prepare the bimetallic nanoparticles. This method is based on the difference in reduction potential of the host metal and metal ion in solution. It allowed for selective deposition of the

Pt/Pd on the Cu surface and not onto the alumina support and for control over the surface composition of the bimetallic catalyst. The GR was monitored by UV-Vis and it was deemed that the technique was successful, since complete uptake of the Pt/Pd species was observed by the disappearance of the corresponding peaks and Cu^{2+} was released in the filtrate solution indicating the exchange reaction occuring. To further characterize the surface of the bimetallic nanoparticles, XPS characterization was obtained for the samples. The XPS spectra showed certain energy shifts in the bimetallic samples compared to those of the monometallic which led to the conclusion that both the Pt and Pd are alloyed into the Cu. Furthermore, by utilizing the surface composition of the metals from the XPS survey scan, the relative ratio of the two metals was calculated and used to prove that all of the precious metal species was present on the catalyst surface. Finally, it was concluded that the bimetallic nanoparticle catalysts could be characterized as Cu nanoparticles with a surface of Cu(111) phase with Pt/Pd species well-dispersed and alloyed into the surface of the Cu.

Once the bimetallic catalysts were prepared they were used for the liquid phase hydrogenation of phenylacetylene. In both cases, the bimetallic catalysts show a marked improved selectivity to styrene compared to their monometallic counterparts which is accompanied by a slight decrease in the overall rate of reaction. The activation energies are also calculated for the mono- and bimetallic catalyst samples. The trend of the activation energies is in line with the rate data; the monometallic samples have a lower activation energy than the bimetallic samples. These results lead to the conclusion that there is a change in active site which is believed to be related to hydrogen spillover on the Cu surface where the hydrogenation reaction occurs. In order to further justify this hypothesis, a Langmuir-Hinshelwood model was developed for the competitive adsorption phenylacetylene and styrene onto the Cu surface.

Certain assumptions were made which were believed to describe the behavior of the system and the resulting model was used to fit the experimental data with Matlab. The fits yield the apparent rate constants and the adsorption coefficient of phenylacetylene on Cu. Based on the fits and values of the parameters, it can be concluded that the assumptions describe the system behavior satisfactorily, providing further evidence of the H_2 spillover mechanism. Finally, experiments were run with a used sample to examine the reusability of the catalyst. It seems that there is an increase in rate and decrease in selectivity which resembles the behavior of the monometallic samples. This is attributed to Pt sintering as a result of the reduction heat treatments.

Overall, this study has demonstrated the use of a catalyst design strategy stemming from model catalytic studies in UHV and the application in nanoparticle catalysis. Furthermore, it was demonstrated how this same idea can be used with a different hydrogen dissociation metal Pt instead of Pd, which can further support this work. The Pt-Cu and Pd-Cu alloy nanoparticles where trace amounts of precious metals were present and deposited exclusively onto the Cu showed an improvement in maintaining the selectivity of the reaction to styrene. It is proposed that this high selectivity of the bimetallic single atom surface alloys is due to hydrogen spillover on the Cu surface where the hydrogenation reaction occurs. In other words, it is demonstrated that Cu can be used as a selective hydrogenation catalyst with addition of trace amounts of a precious metal with a lower barrier for hydrogen dissociation. The cooperative use of surface science and heterogeneous catalysis techniques in this study has broader impact for “bridging the gap” between these two fields.

5.2 Recommendations for Future Study

5.2.1 Unsupported Nanoparticles

The preparation of unsupported CuPd or CuPt particles is of interest to ensure that there is no effect of the support with the reaction. This could also ensure that the reacting nanoparticles are better suspended in solution and potentially be more stable. A synthesis technique in order to employ this method would be based on the aqueous phase preparation of the bimetallic nanoparticles which could be transferred into the organic phase by using a non-polar capping agent such as octadecylamine (ODA) in hexane. A similar preparation has been employed by Kumar et al.[1] where the aqueous phase colloidal Pt nanoparticles were in contact with ODA in hexane and shaken vigorously. During the shaking of the biphasic mixture (Pt-in-water/ODA in hexane) results in the rapid interaction of ODA with Pt yielding ODA-stabilized Pt nanoparticles in the organic phase. The resulting nanoparticles are extremely stable and can be easily precipitated out of solution and re-dissolved in other organic solvents.

5.2.2 Substitute Cu with Au as a substrate

Another approach could be to prepare Au nanoparticles with trace amounts of Pt or Pd on the surface. This would be of interest since Au is typically not associated with hydrogenation reactions nor does it have a low dissociation barrier for hydrogen. For these reasons the same principles could apply for this system yielding a highly selective hydrogenation catalyst. Also, it previous studies have demonstrated that there is electronic restructuring in these types of alloys which also might have an effect on this reaction.

5.2.3 Recycle Reactor studies

[1] J. Chem. Sci., Vol. 116, No. 5, September 2004, pp. 293–300

Using the results and catalysts generated from this work, a steady state recycle reactor could be designed. This is important since it would be more relevant to industry since it would operate continuously and the catalysts from this study could be applied there to investigate their selectivity and stability over time. By using the rates and conversion from this work the space/time of the recycle reactor can be calculated and designed.